FINITE DEFLECTIONS AND BUCKLING OF SLIGHTLY CURVED BEAMS AND SHALLOW SPHERICAL SHELLS UNDER LATERAL LOADS

Thesis by

Abner Kaplan

In Partial Fulfillment of the Requirements

for the Degree of

Doctor of Philosophy

California Institute of Technology

Pasadena, California

1954

ACKNOWLEDGEMENTS

The author would like to express his very great thanks to Dr. Yuan-Cheng Fung for suggesting this problem and for his help and encouragement in carrying it through.

In addition he would like to express his appreciation to Dr. Ernest Sechler for his suggestions on designing the experimental equipment; to Mr. Beverly Morant, Mr. Carroll Bartsch and Mr. Milton Wood for their assistance in building and assembling the equipment; to Mrs. Dorothy Eaton and Miss Joan Benson for the work on the never ending numerical calculations; to Mrs. Betty Wood and Mrs. Virginia Boughton for their efforts in producing the manuscript, and finally to the National Advisory Committee for Aeronautics for sponsoring the research.

ABSTRACT

This research consists in the experimental and theoretical investigation of the finite deflection and buckling of two similar structures; the low arch or slightly curved beam and the shallow spherical dome, both subjected to lateral loads. These structures are of interest because the large interaction between bending and axial forces causes their load-deflection behavior to become non-linear at very low values of the deflection. Due to the wide difference in the methods of solution of these two problems they are separated into two parts, each having its own abstract.

TABLE OF CONTENTS

PART I

BUCKLING OF LOW ARCHES OR CURVED BEAMS

OF SMALL CURVATURE

TABLE OF CONTENTS

PART II

A NONLINEAR THEORY OF BENDING AND

BUCKLING OF THIN ELASTIC SHALLOW SPHERICAL SHELLS

NATIONAL ADVISORY COMMITTEE FOR AERONAUTICS

TECHNICAL NOTE 2840

BUCKLING OF LOW ARCHES OR CURVED BEAMS OF SMALL CURVATURE

By Y. C. Fung and A. Kaplan

California Institute of Technology

Washington
November 1952

NATIONAL ADVISORY COMMITTEE FOR AERONAUTICS

TECHNICAL NOTE 2840

BUCKLING OF LOW ARCHES OR CURVED BEAMS OF SMALL CURVATURE

By Y. C. Fung and A. Kaplan

SUMMARY

When a low arch (a thin curved beam of small curvature) is subjected to a lateral loading acting toward the center of curvature, the axial thrust induced by the bending of the arch may cause the arch to buckle so that the curvature becomes suddenly reversed. The critical lateral loading depends on the dimensions and rigidity of the arch, the elasticity of the end fixation, the type of load distribution, and the initial curvature of the arch. A general solution of the problem is given in this paper, using the classical buckling criterion which is based on the stability with respect to infinitesimal displacements about the equilibrium positions.

For a sinusoidal arch under sinusoidal loading, the critical load can be expressed exactly as a simple function of the beam dimension parameters. For other arch shapes and load distributions, approximate values of the critical load can be obtained by summing a few terms of a rapidly converging Fourier series. The effects of initial end thrust and axial and lateral elastic support are discussed.

The buckling load based on the energy criterion of Kármán and Tsien is also calculated. The results for both the classical and the energy criteria are compared with experiments made on a series of centrally loaded, pin-ended arches. For larger values of a dimensionless parameter λ_1, which is proportional to the ratio of the arch rise to the arch thickness, the experimental critical buckling loads agreed quite well with the classical criterion, but, for smaller values of λ_1, the experimental critical loads were appreciably below those calculated from the classical criterion, although they were always above those obtained from the energy criterion.

INTRODUCTION

An arch subjected to lateral loads may become elastically unstable. Generally speaking, there are two possibilities of buckling:

(1) If the rise of the arch (a in fig. 1) is of the same order as the span of the arch, then it is possible for the arch to buckle at the critical pressure in the mode indicated by the dashed curve in figure 1. Buckling of this type can be safely assumed to be "inextensional," as suggested by Lord Rayleigh, and, as such, has been discussed by E. Hurlbrink, E. Chwalla, R. Mayer, E. Gaber, E. L. Nicolai, and S. Timoshenko. (See Timoshenko's book, reference 1, for references to original papers.) In all these studies, circular arches under uniformly distributed lateral loading are assumed, with various types of end fixations.

(2) If the rise a of the arch is much smaller than the span L, (fig. 2), then the induced axial thrust plays an important role in the elastic stability. The beam may become unstable and suddenly reverse its curvature, jumping, for example, from the solid-line position in figure 2 to the dashed-line position.

It is the object of the present paper to treat arches of small rise; therefore, the buckling deformation will be "extensional" rather than "inextensional." It will be shown that the variation in the initial curvature of the beam has a very important effect on the critical load. Furthermore, with a view to possible applications to thin-wing design problems, beams acted on by initial thrust and those with elastic supports will be discussed.

The same problem has been treated before by Biezeno (reference 2), Marguerre (references 3 and 4), Timoshenko (reference 1), and Friedrichs (reference 5).[1] Biezeno and Timoshenko derived the fundamental differential equation in the same manner as this paper, while Marguerre and Friedrichs derived their equations by variational principles. The resulting equations are the same. Biezeno treated a circular arch under a concentrated load at the center and Marguerre and Friedrichs, a circular arch under uniformly distributed pressure; all arrived at the main features of the buckling problem, but the calculations are rather involved. Timoshenko assumed that the center line of the deflected beam as well as the initial shape is a half wave of a sine curve and arrived at a very simple solution. The restriction of the buckling mode to the symmetrical one, however, sometimes gives the critical buckling load manyfold too high in a certain range of arch rise.

The buckling criterion used by the authors of references 1 to 5 is the classical one which is based on the stability with respect to

---

[1]After completion of the present work, it was learned that Hoff and Bruce (reference 6) treated a similar problem from the point of view of dynamic stability. Part of Hoff and Bruce's work coincides almost identically with the present report.

infinitesimal displacements about the equilibrium positions. But Friedrichs, in reference 5, also calculated the buckling load on the basis of Tsien's energy criterion, which is based on finite displacements. The energy criterion yields a buckling load much lower than that obtained from the classical criterion. It is not evident which of these two criteria corresponds to the real practical situation. Therefore in this paper, both criteria will be used and the results will be compared with experiments.

This work was conducted at the California Institute of Technology under the sponsorship and with the financial assistance of the National Advisory Committee for Aeronautics.

SYMBOLS

A cross-sectional area of beam

a rise of arch

E Young's modulus

F dead-weight load (in section "Buckling Load Based on Kármán and Tsien's Energy Criterion")

H axial compression at ends of beam

H_o initial thrust in beam

I moment of inertia (or second moment) of cross section of beam

$K = \pi^4 EI^2/AL^3$

$$k = \frac{1}{36}\left[\frac{\lambda_1 + \sqrt{\frac{4}{27}\left(\lambda_1^2 - 1 - k\right)^3}}{\lambda_1^2 - 13}\right]^2$$

L span of beam

M bending moment; positive when it tends to put upper side of beam in compression

M_o bending moment due to lateral forces alone

Q shearing force in beam; positive when $\int_{\Delta x} Q\,dx$ produces positive moment

q lateral pressure per unit length of beam; positive downward (in negative y-direction)

q_o characteristic lateral pressure per unit length of beam

t thickness of beam

U strain energy

V change in thrust in lateral support

W total load beam can sustain without buckling

y, y_o actual and initial curve of center line of beam, respectively

α spring constant of arch support

α' spring constant of lateral support

Δ distance spring-supported end of beam is displaced

δ deviation ratio $\left(a_m/a_1\right)$

ρ_o radius of circular-arc arch

σ_b bending stress in beam

σ_c axial stress in beam

$\sigma_p = \left(\pi^2 EI/L^2\right)/A$

ϕ total energy for dead-weight loading

Subscripts:

class classical criterion

conc concentrated loading

cr critical

energy	energy criterion
exp	experimental
max	maximum
sine	sinusoidal loading
unif	uniform loading

Nondimensional coefficients:

Let

$$y_o = \sum_{m=1}^{\infty} a_m L \sin \frac{m\pi x}{L}$$

$$y = \sum_{m=1}^{\infty} b_m L \sin \frac{m\pi x}{L}$$

$$q = q_o f(x)$$

Then

$$\lambda_m = \frac{a_m L}{2}\sqrt{\frac{A}{I}} \qquad (m = 1, 2, 3, \ldots)$$

$$B_m = \frac{b_m L}{2}\sqrt{\frac{A}{I}} \qquad (m = 1, 2, 3, \ldots)$$

$$R = \frac{q_o L^4}{2\pi^4 EI}\sqrt{\frac{A}{I}}$$

$$S = \frac{H_o L^2}{\pi^2 EI}$$

$$\beta = \frac{\alpha}{\alpha + \frac{EA}{L}}$$

$$\mu = \frac{2\alpha' L^3}{\pi^4 EI}$$

GENERAL ANALYSIS

Consider a thin curved beam of small curvature, one end of which is hinged, that is, it is free to rotate but is fixed in position, while the other end of the beam is attached to a spring, with a spring constant α. When the spring-supported end is displaced by a distance Δ, the thrust induced in the spring will be

$$H = H_o + \alpha\Delta \tag{1}$$

where H_o is the initial thrust built in the beam.[2] (See fig. 3.) Before the application of the lateral load $q(x)$, the axial load in the beam is H_o and the beam center line is represented by the following Fourier series:

$$y_o = \sum_{m=1}^{\infty} a_m L \sin \frac{m\pi x}{L} \tag{2}$$

Under the lateral load q, the displaced center line can be written as

$$y = \sum_{m=1}^{\infty} b_m L \sin \frac{m\pi x}{L} \tag{3}$$

Assume that $|y_o|$ and $|y|$ are much smaller than L, and hence $|a_m|$ and $|b_m|$ are much smaller than 1; that the beam is made of homogeneous material, of constant cross section, and with small curvature so that $(dy/dx)^2$ is negligible in comparison with 1; and that the thickness of the beam is much smaller than the radius of curvature of the beam. Then the usual beam theory gives

$$EI\left(\frac{d^2y}{dx^2} - \frac{d^2y_o}{dx^2}\right) = M \tag{4}$$

---

[2]No generality is lost by treating this case of one end spring instead of the case with both ends of the beam elastically supported because the springs at both ends can be replaced by a single spring at one end.

where M is the increase in bending moment due to the application of $q(x)$. From statics,

$$M = \int_0^x Q\,dx - (Hy - H_o y_o) \tag{5}$$

Substituting equation (5) into equation (4) and differentiating twice, remembering that $\frac{dQ}{dx} = -q$ and that the axial thrust in the beam H can be regarded as constant by the assumption of small curvature, the equation of equilibrium is obtained:

$$EI\frac{d^4(y - y_o)}{dx^4} + H\frac{d^2y}{dx^2} - H_o\frac{d^2y_o}{dx^2} = -q \tag{6}$$

To find the thrust H, it is noted that the shortening of the center line of the beam is

$$\Delta L \doteq \frac{1}{2}\int_0^L \left[\left(\frac{dy_o}{dx}\right)^2 - \left(\frac{dy}{dx}\right)^2\right] dx - \Delta \tag{7}$$

where small quantities of higher orders are neglected. It is assumed that the end support spring is rather strong, so that Δ is very small compared with L. (Otherwise the problem becomes one of a simple bending, with no possible difficulty.) Hence

$$H = H_o + \frac{EA(\Delta L)}{L}$$

$$= H_o + \frac{EA}{2L}\int_0^L \left[\left(\frac{dy_o}{dx}\right)^2 - \left(\frac{dy}{dx}\right)^2\right] dx - \frac{EA}{L}\Delta \tag{8}$$

On the other hand, the deflection Δ is connected with the spring constant α by equation (1). Eliminating Δ between equations (1) and (8), substituting equations (2) and (3) for y and y_o into the result, and integrating, there is obtained

$$H = H_o + \beta \frac{\pi^2 EA}{4} \sum_m m^2 \left(a_m^2 - b_m^2\right) \tag{9}$$

where

$$\beta = \frac{\alpha}{\alpha + \frac{EA}{L}} \tag{10}$$

Substituting equations (2) and (3) again into equation (6) and using equation (9), there is obtained now the equation of equilibrium expressed in terms of the Fourier coefficients:

$$-q = \frac{\pi^4 EI}{L^3} \sum_m m^4 (b_m - a_m) \sin \frac{m\pi x}{L} + \frac{H_o \pi^2}{L} \sum_m m^2 (a_m - b_m) \sin \frac{m\pi x}{L} -$$

$$3 \frac{\pi^4 EA}{4L} \left[\sum_m m^2 \left(a_m^2 - b_m^2\right) \right] \sum_m m^2 b_m \sin \frac{m\pi x}{L} \tag{11}$$

The boundary conditions are already satisfied.

Expand $q = q_o f(x)$ into a Fourier series:

$$q = q_o f(x) = q_o \sum_m k_m \sin \frac{m\pi x}{L} \tag{12}$$

where

$$k_m = \frac{2}{L} \int_0^L f(x) \sin \frac{m\pi x}{L} \, dx$$

On equating the coefficients of the corresponding terms in the right-hand sides of equations (11) and (12), there is obtained a set of an infinite number of simultaneous equations:

$$\beta \frac{\pi^4 EA}{4L}\left[\sum_{n=1}^{\infty} n^2\left(b_n^2 - a_n^2\right)\right] m^2 b_m + \left(\frac{\pi^4 EIm^4}{L^3} - \frac{H_o \pi^2 m^2}{L}\right)(b_m - a_m) = -k_m$$

$$(m = 1, 2, 3, \ldots) \quad (13)$$

To simplify the expressions, introduce the following notations:

$$\left.\begin{aligned} \lambda_m &= \frac{a_m L}{2}\sqrt{\frac{A}{I}} & B_m &= \frac{b_m L}{2}\sqrt{\frac{A}{I}} \\ R &= \frac{q_o L^4}{2\pi^4 EI}\sqrt{\frac{A}{I}} & S &= \frac{H_o L^2}{\pi^2 EI} \end{aligned}\right\} \quad (14)$$

Then equations (13) become

$$B_m\left(\beta \sum_{n=1}^{\infty} n^2 B_n^2 - \beta \sum_{n=1}^{\infty} n^2 \lambda_n^2 + m^2 - S\right) = -\frac{R}{m^2} k_m + \lambda_m(m^2 - S)$$

$$(m = 1, 2, 3, \ldots) \quad (15)$$

Here λ_m and B_m represent the rise of the arch, being half the ratio of the amplitude of the mth harmonic in the initial and the deflected curve to the radius of gyration of the beam cross section; R is a dimensionless quantity specifying the lateral loading; and S is the ratio of the initial axial compression to the Euler column buckling load of the beam. Now $f(x)$, λ_n, and S are known in the problem; it remains to find the relation between R and B_m, from which the correspondence between the load and deflection can be traced and the stability of the beam determined.

Sometimes the Fourier series of the moment curve converges much faster than that of the loading itself. In such cases it is advantageous to use equations (4) and (5) directly instead of equation (6). Let the static bending moment of the lateral loading alone be written as M_o:

$$M_o = q_o L^2 F(x) \tag{16}$$

where q_o is a characteristic lateral pressure with the physical dimensions of force per unit length of the beam. Let $F(x)$ be expanded into a Fourier series, so that

$$M_o = q_o L^2 \sum_{m=1}^{\infty} K_m \sin \frac{m\pi x}{L} \tag{17}$$

where

$$K_m = \frac{2}{L} \int_0^L F(\xi) \sin \frac{m\pi \xi}{L} \, d\xi$$

Following the same reasoning as before, one arrives at the equations:

$$B_m \left(\beta \sum_{n=1}^{\infty} n^2 B_n^2 - \beta \sum_{n=1}^{\infty} n^2 \lambda_n^2 + m^2 - S \right) = -\pi^2 K_m R + \lambda_m (m^2 - S)$$

$$(m = 1, 2, 3, \ldots) \tag{18}$$

Both equations (15) and (18) will be used later. They are a system of an infinite number of simultaneous equations for which a general treatment is not known. However, there are many important cases where the number of equations can be reduced into a finite number; then a complete discussion is possible. Several examples will be given below.

Equations (4) and (5) may be written as

$$\frac{d^2 y}{dx^2} + \frac{H}{EI} y = \frac{d^2 y_o}{dx^2} + \frac{M_o(x)}{EI} + \frac{H_o}{EI} y_o$$

$$= G(x) \tag{19}$$

where $G(x)$ is a known function. The general solution is

$$y = C_1 \cos \nu x + C_2 \sin \nu x + \frac{1}{\mu} \int_0^x G(t) \sin \nu(x - t)\, dt \qquad (20)$$

where

$$\nu = \sqrt{\frac{H}{EI}}$$

The constants C_1 and C_2 must be determined according to the boundary conditions at the ends $y = 0$ for $x = 0$ and L. The solution $y(x)$ can then be substituted into equation (8) and ν computed. This gives a relation between ν and the external load. Biezeno and Friedrichs based their calculations on this relationship. Marguerre, on the other hand, used the energy principle and the methods of Ritz and Galerkin to obtain approximate solutions. The method of the present paper, based on the Fourier analysis, is due to the work of Y. S. Huang.[3] Recently, the same method was used by Hoff and Bruce (reference 6).

It is clear from equation (20) that the deflection and the critical load are continuous functionals of $y_o(x)$ and $M_o(x)$. Hence infinitesimal changes in $y_o(x)$ and $M_o(x)$ would always cause an infinitesimal change in the critical load.

SINUSOIDAL ARCH UNDER SINUSOIDAL LOADING

Consider the simplest case of a low sinusoidal arch subjected to a sinusoidal load distribution:

$$\left.\begin{aligned} y_o &= a_1 L \sin \frac{\pi x}{L} \qquad (0 < a_1 \ll 1) \\ q &= q_o \sin \frac{\pi x}{L} \end{aligned}\right\} \qquad (21)$$

[3] Professor of Aeronautics, Central University, Nanking, China.

The general equations of equilibrium (15) then become, in this particular case,

$$\left.\begin{aligned}
&B_1\left(\beta \sum_{n=1}^{\infty} n^2B_n{}^2 - \beta\lambda_1{}^2 + 1 - S\right) = -R + \lambda_1(1 - S) \\
&B_2\left(\beta \sum_{n=1}^{\infty} n^2B_n{}^2 - \beta\lambda_1{}^2 + 4 - S\right) = 0 \\
&\cdots\cdots\cdots\cdots\cdots\cdots\cdots \\
&B_m\left(\beta \sum_{n=1}^{\infty} n^2B_n{}^2 - \beta\lambda_1{}^2 + m^2 - S\right) = 0 \\
&\cdots\cdots\cdots\cdots\cdots\cdots\cdots
\end{aligned}\right\} \tag{22}$$

This set of equations must be solved for B_m. In order to get a qualitative investigation into the nature of the solution, first consider the simplest case of an arch rigidly hinged at both ends, so that $\alpha = \infty$ or $\beta = 1$, and with zero initial axial thrust $S = H_o = 0$. The more general case will be considered later.

An obvious set of solutions of equations (22) is

$$\left.\begin{aligned}
&B_2 = B_3 = \ldots = 0 \\
&B_1{}^3 - B_1\left(\lambda_1{}^2 - 1\right) = \lambda_1 - R
\end{aligned}\right\} \tag{23}$$

If the relation between B_1 and R is plotted, the curves in figure 4 are obtained. Depending upon the values of λ_1, there are several possibilities: (1) If $\lambda_1 \leqq 1$, the curves have monotonic slope; consequently, they determine the load-deflection curve uniquely. There is no question of instability. (2) If $\lambda_1 > 1$, then there are two real extremes and, for values of R in between these extremes, every loading may have three possible positions of equilibrium. Following, for example, curve IV in figure 4, the deformation of the beam can be traced as follows: When the lateral loading is gradually increased from the starting point a, the deflection gradually increases according to curve IV (the rise of the

arch decreases). When the point M is reached, any further increase of loading will make the beam jump to the configuration corresponding to the point N and then follow the right-hand branch of the curve. In between M and N, any increase in deformation needs no addition of loading and therefore is unstable. Hence M is the critical point, with the critical condition given by

$$\left.\begin{aligned} \frac{dR}{dB_1} &= 0 \\ \frac{d^2R}{dB_1^2} &< 0 \end{aligned}\right\} \tag{24}$$

From equations (23) and (24), the critical values of B_1 and R can be obtained:

$$\left.\begin{aligned} \left(B_1\right)_{cr} &= \sqrt{\frac{\lambda_1^2 - 1}{3}} \\ R_{cr} &= \lambda_1 + \sqrt{\frac{4}{27}\left(\lambda_1^2 - 1\right)^3} \end{aligned}\right\} \tag{25}$$

If $\lambda_1 < 1$, R_{cr} is imaginary; hence no instability will occur. This checks with the former discussion based on the uniqueness of the load-deflection curve.

The above solution, equations (23), however, is not unique. Equations (22) can allow a solution with one B_n, in addition to B_1, to be different from zero.[4] In this case

$$\left.\begin{aligned} B_1\left(B_1^2 + n^2B_n^2\right) - \left(\lambda_1^2 - 1\right)B_1 &= \lambda_1 - R \\ B_1^2 + n^2B_n^2 &= \lambda_1^2 - n^2 \end{aligned}\right\} \tag{26}$$

[4]These two cases exhaust the possibilities, as can be seen by writing down the rest of the set of equations (22), which gave the result that all other B's must vanish.

have the solution

$$\left.\begin{aligned} B_1 &= \frac{R - \lambda_1}{n^2 - 1} \\ n^2 B_n^2 &= \lambda_1^2 - n^2 - \left(\frac{R - \lambda_1}{n^2 - 1}\right)^2 \end{aligned}\right\} \tag{27}$$

Equations (27) indicate that B_n can exist (with real value) only in a definite range of R. The deformation history of a beam subjected to gradually increasing lateral loading can now be traced as in figure 5: Along ab, $B_n = 0$, the curve is that of equations (23). Along bc, $B_n \neq 0$, the deflection curve becomes

$$y = b_1 L \sin \frac{\pi x}{L} + b_n L \sin \frac{n\pi x}{L} \tag{28}$$

If the point b is real and lower than M, then it is the critical point where the beam will have a tendency to buckle. The point b is given by

$$\left.\begin{aligned} B_1 &= \sqrt{\lambda_1^2 - n^2} \\ B_n &= 0 \\ R &= \lambda_1 - (n^2 - 1)\sqrt{\lambda_1^2 - n^2} \end{aligned}\right\} \tag{29}$$

Equations (29) will yield the lowest critical value if the following conditions are satisfied:

(1) R, B_1, and B_n are real

(2) The R given by equations (29) is less than the R given by equations (25)

(3) The B_1 given by equations (29) must be greater than that given by equations (25); otherwise, the beam will buckle in the first mode, at point M

(4) The particular number n is so chosen that the corresponding R_{cr} is a minimum

Conditions (1), (2), and (3) are satisfied if and only if

$$\lambda_1^2 \geqq \frac{3}{2}\left(n^2 - \frac{1}{3}\right) \tag{30}$$

Condition (4) is satisfied only if $n = 2$. Hence the complete expression for the critical loading is obtained:

$$\left.\begin{aligned} R_{cr} &= \lambda_1 + \sqrt{\frac{4}{27}\left(\lambda_1^2 - 1\right)^3} \qquad (1 \leqq \lambda_1 < \sqrt{5.5}) \\ R_{cr} &= \lambda_1 + 3\sqrt{\lambda_1^2 - 4} \qquad (\lambda_1 \geqq \sqrt{5.5}) \end{aligned}\right\} \tag{31}$$

The relation between the critical loading and the beam-rise ratio is illustrated in figure 6. The solid lines are the actual critical conditions. The dashed lines are either imaginary or not the lowest critical load.

It is interesting to note here that for $\lambda_1 < \sqrt{5.5} \approx 2.345$ the buckling mode of a low sinusoidal arch is symmetrical but for $\lambda_1 > \sqrt{5.5}$ the buckling mode imitates that of a high arch, for which the deformation is essentially inextensional. As illustrated in figure 7, the arch deflects (flattens) at first under the increasing lateral loading from the initial position I to the state II, when the second mode B_2 starts entering into the picture. The mode of the beam during buckling, when it jumps from the upper to the lower side, is a curve like III in figure 7.

EFFECT OF INITIAL AXIAL COMPRESSION

Still restricting this discussion to the simple case of a sinusoidal arch under a sinusoidal loading and with fixed hinged supports at both ends, let an initial compressive force H_o act on the beam, so that

$$S = \frac{H_o L^2}{\pi^2 EI}$$

is different from zero, S being the ratio of the initial axial compression to the Euler column buckling load of the beam. The equation of equilibrium is given by equations (22) with $\beta = 1$. The solution of this set of equations is again either

$$B_1 \neq 0, \quad B_2 = B_3 = \ldots = 0$$

or

$$B_1 \neq 0, \quad B_n \neq 0, \quad \text{all the other } B_m\text{'s vanish}$$

One is led to the following conclusions:

$$\left.\begin{aligned} &\text{For } \sqrt{1 - S} < \lambda_1 \leq \sqrt{5.5 - S}, \\ &\qquad R_{cr} = (1 - S)\lambda_1 + \sqrt{\frac{4}{27}\left(\lambda_1^2 + S - 1\right)^3} \\ &\text{and for } \lambda_1 > \sqrt{5.5 - S}, \\ &\qquad R_{cr} = (1 - S)\lambda_1 + 3\sqrt{\lambda_1^2 + S - 4} \end{aligned}\right\} \tag{32}$$

The effect of the initial axial compression is included in this formula. As expected, the increase of the initial axial compression will decrease the critical load, as can be easily verified by the fact that

$$\frac{\partial R_{cr}}{\partial S} < 0 \tag{33}$$

for the full range of S, $0 \leq S \leq 1$ (S cannot exceed 1). Furthermore, the lower limit for instability is now

$$\lambda_1 = \sqrt{1 - S} \tag{34}$$

For λ_1 smaller than this value, the bar is stable; no buckling is possible. This lower limit decreases with increasing S until $S = 1$, when the beam will fail as a simple Euler column, R_{cr} becoming zero.

The values of the critical load R_{cr} as a function of λ_1, with values of S as parameters, are given in figure 6 and table I. A clearer presentation of the effect of S is a curve of the change in the critical load $(\Delta R_{cr})_S$ against λ_1, where

$$(\Delta R_{cr})_S = (R_{cr})_{S=0} - (R_{cr})_{S=S} \tag{35}$$

This is given in figure 8.

From equations (32), it is seen that when λ_1 is large, say, with magnitude of the order of 2.5 or larger, $(\Delta R_{cr})_S$ is almost linearly proportional to S. As a crude approximation, one may take

$$(\Delta R_{cr})_S = S \frac{(R_{cr})_{S=0}}{4} \tag{36}$$

INITIAL SHAPE OF ARCH OTHER THAN SINUSOIDAL

In order to find the effect of the irregularities in the initial shape of the arch on the buckling load, some simple cases of low arches whose center lines are nonsinusoidal will be considered. By comparing such solutions with the previous one, the significance of such variations in form can be estimated. Let the initial shape of the center line of the arch be given by the equation:

$$y_o = a_1 L \sin \frac{\pi x}{L} + a_m L \sin \frac{m\pi x}{L} \tag{37}$$

(A few examples are shown in fig. 9.) Assume again for simplicity that the lateral loading q is sinusoidal, given by equation (20), and that the ends of the arch are hinged and without initial thrust, so that $H_o = S = 0$ and $\beta = 1$. The fundamental equations (15) become

$$\left.\begin{aligned} B_1\left(\sum_n n^2B_n^2 - \lambda_1^2 - m^2\lambda_m^2 + 1\right) &= -R + \lambda_1 \\ B_m\left(\sum_n n^2B_n^2 - \lambda_1^2 - m^2\lambda_m^2 + m^2\right) &= m^2\lambda_m \\ B_k\left(\sum_n n^2B_n^2 - \lambda_1^2 - m^2\lambda_m^2 + k^2\right) &= 0 \qquad (\text{for all } k \neq 1, m) \end{aligned}\right\} \tag{38}$$

Again two possibilities exist: (1) A solution consists of $B_1 \neq 0$ and $B_m \neq 0$, but with all other B's vanishing; (2) a solution with <u>one</u> B_k, other than B_1 and B_m, different from zero. They must be discussed separately.

In the first case, B_m and R may be regarded as functions of B_1 and the second of equations (38) differentiated to determine dB_m/dB_1. From the sign of dB_m/dB_1 it can be observed that, when the load R is gradually increasing, the amplitude of B_m $(\text{i.e., } |B_m|)$ will increase irrespective of the initial sign of λ_m. Furthermore, by differentiating the first of equations (38) to obtain dR/dB_1, it can be observed that, in the prebuckling stage, the amplitude B_1 will decrease when the load R increases. Hence the critical condition is given by

$$\frac{dR}{dB_1} = 0 \tag{39}$$

Carrying out the differentiation and reducing, the equation governing B_m at the critical condition is obtained:

$$B_m^4 + cB_m + d = 0 \tag{40}$$

where

$$c = -\frac{2\lambda_1^2 + 2m^2\lambda_m^2 - 3m^2 + 1}{2(m^2 - 1)}\lambda_m$$

$$d = -\frac{3m^2\lambda_m^2}{2(m^2 - 1)}$$

Equation (40) can have at most two real roots. If the two real roots are different, then the one nearer to λ_m is the true critical value provided that the corresponding $(B_1)_{cr}$ and R_{cr} are also real. If equation (40) has no real root, then there is no critical load and the beam is stable.

With the critical value of B_m so determined, the critical values of B_1 and R can be obtained from equations (38) as follows:

$$\left.\begin{aligned} (B_1)_{cr}^2 &= \frac{m^2\lambda_m}{(B_m)_{cr}} + \lambda_1^2 - m^2\left[(B_m)_{cr}^2 - \lambda_m^2 + 1\right] \\ R_{cr} &= \lambda_1 + (m^2 - 1)(B_1)_{cr} - m^2\frac{\lambda_m}{(B_m)_{cr}}(B_1)_{cr} \end{aligned}\right\} \tag{41}$$

It is interesting to note here that the critical load is independent of the sign of λ_m. This is so because a change in sign of λ_m changes the sign of the roots $(B_m)_{cr}$ of equation (40). But since $(B_m)_{cr}/\lambda_m$ does not change sign, $(B_1)_{cr}$ from the first of equations (41) is not affected by the change in sign of λ_m. Hence the conclusion follows from the second of equations (41). This is rather unexpected. It shows that under sinusoidal loading the two apparently different curved beams in figures 9(b) and 9(c) have exactly the same critical load.

Equation (40) can be solved graphically or numerically. The results of such calculations for the cases $m = 2$ and 3 are given in figures 10(a) and 10(b). The magnification of the amplitude of the higher harmonic, initially at λ_m, into $(B_m)_{cr}$ at the critical point, is clearly seen from figure 10. The reduction of the critical load due to the presence of λ_m will be discussed later when the second possible solution is obtained. The parameter used in the curves of figure 10 is not λ_m but the deviation ratio:

$$\delta = \frac{\lambda_m}{\lambda_1} = \frac{a_m}{a_1} \tag{42}$$

This ratio indicates the deviation from a sinusoidal form better than the parameter λ_m itself.

It remains to discuss the second possible solution which includes one nonvanishing B_k $(k \neq 1, m)$. In this case the solution of equations (38) is

$$\left.\begin{aligned} B_1 &= \frac{R - \lambda_1}{k^2 - 1} \\ B_m &= \frac{-m^2\lambda_m}{k^2 - m^2} \\ k^2 B_k^2 &= \lambda_1^2 + m^2\lambda_m^2 - k^2 - \frac{m^6\lambda_m^2}{(k^2 - m^2)^2} - \frac{(R - \lambda_1)^2}{(k^2 - 1)^2} \end{aligned}\right\} \tag{43}$$

The relation between B_k and R is again an ellipse of a similar nature to that for a sinusoidal arch under sinusoidal loading. The instant when B_k will appear is the critical point. Hence the condition $B_k = 0$ leads to

$$R_{cr} = \lambda_1 + (k^2 - 1)\sqrt{\lambda_1^2 - k^2 + m^2\lambda_m^2\left[1 - \frac{m^4}{(k^2 - m^2)^2}\right]} \tag{44}$$

This will lead to a fundamental critical value if the four conditions enumerated under equations (29) are satisfied. Whether equations (41) or equation (44) gives the critical load depends on the initial shape of the beam.

If $m = 2$, equation (44) always gives a higher R_{cr} than equations (41). Hence the critical load is determined by equations (41). No B_3, B_4, and so forth can appear during buckling.

If $m \geq 3$, equation (44) with $k = 2$ gives the lowest R_{cr} provided that λ_1 is greater than a certain constant, say $(\lambda_1)_o$. For λ_1 less than $(\lambda_1)_o$, equations (41) give the lowest R_{cr}. The point $(\lambda_1)_o$ is the point of tangency of the curves of R_{cr} against λ_1 computed according to equations (41) and (44), respectively.

Again it is evident from equation (44) that the critical load is independent of the sign of λ_m.

The combined results of equations (41) and (44) are shown in figure 11, and the numerical results are given in tables II and III. In table II, $(B_m)_{cr}$ and R_{cr} computed according to equations (40) and (41) are listed. Comparing tables II and III, it is seen that in certain ranges of λ_1, equations (41) give the lower R_{cr}, while in another range equation (44) gives the lower R_{cr}. Furthermore, at smaller values of λ_1, even if $\lambda_1 > 1$, $(B_1)_{cr}$ and R_{cr} may become imaginary, as shown in table II. The physical meaning of this is that the process is then a continuous one. There is no sudden change of configurations. The beam, under bending, simply yields continuously to the increasing external load.

These examples illustrate the serious nature of the effect of the λ_m terms. When the loading is symmetrical, a very slight component of unsymmetry in the curved beam lowers the critical load considerably. For example, in case of a sinusoidal loading acting on a sinusoidal beam, an unsymmetrical second harmonic in the initial curve with an amplitude ratio of 1 percent in the initial form lowers the critical load by approximately 10 percent. The buckling mode is always unsymmetrical if the initial shape of the arch contains unsymmetrical modes.

On the other hand, for a symmetric loading, the effect of higher harmonics that are symmetrical is much less pronounced. A similar effect should be expected when the beam is sinusoidal but the lateral loading deviates from a sinusoidal distribution.

An important special arch form is a circular arc with a radius ρ_o. Within the present approximation, there may be written

$$y_o = \frac{1}{2\rho_o} x(L - x) = \frac{4L^2}{\pi^3 \rho_o} \sum_{n=1,3,5,\ldots} \frac{1}{n^3} \sin \frac{n\pi x}{L} \tag{45}$$

This corresponds to an arch rise of $L^2/8\rho_o$ at the center. The coefficients λ_m form a rapidly decreasing sequence. In fact,

$$a_1 = \frac{4L^2}{\pi^3 \rho_o} \qquad a_{2n} = 0$$

$$a_2 = 0 \qquad a_{2n+1} = \frac{1}{(2n+1)^3} a_1$$

$$a_3 = \frac{1}{27} a_1$$

The effect of the higher harmonics is negligible. If a_5, a_7, and so forth are neglected, then the R_{cr} (sinusoidal loading) of a circular arch can be found from figure 11(b) or table III (m = 3) by taking

$$\delta \doteq \frac{\lambda_3}{\lambda_1} = \frac{1}{27}$$

The difference in R_{cr} is readily seen to be small.

To illustrate the fact that a_5, a_7, and so forth may be neglected without causing appreciable error, the case of the unsymmetrical buckling mode will be considered. Equations (43) should be modified, when k = 2, into

$$\sum_n n^2 B_n^2 = \sum_n n^2 \lambda_n^2 - 4$$

$$B_1 = \frac{R - \lambda_1}{3}$$

$$B_m = \frac{\lambda_1}{m(m^2 - 4)}$$

Now

$$\sum_{n=1,3,5,\ldots} n^2 \lambda_n^2 = \lambda_1 \sum_{n=1,3,5,\ldots} \frac{1}{n^4} = (1 + \epsilon_1)\lambda_1^2$$

$$\sum_{m=3,5,7,\ldots} m^2 B_m^2 = \sum_{m=3,5,7,\ldots} \frac{\lambda_1^2}{(m^2 - 4)^2} = \frac{\lambda_1^2}{25}(1 + \epsilon_2)$$

where

$$\epsilon_1 \doteq 0.01436$$

$$\epsilon_2 \doteq 0.07325$$

The critical load is given by the equation:

$$\left(\frac{R - \lambda_1}{3}\right)^2 + (1 + \epsilon_2)\frac{\lambda_1^2}{25} = (1 + \epsilon_1)\lambda_1^2 - 4$$

Neglecting the effect of λ_5, λ_7, and so forth on R_{cr} is to neglect the effect of ϵ_1 and ϵ_2 on the root R of this equation. It is clearly justifiable.

UNIFORMLY DISTRIBUTED PRESSURE

In this section the critical load of a sinusoidal arch under uniformly distributed pressure will be discussed. From the results of the preceding sections, it is expected that the deflected curve of the arch would not remain sinusoidal and that an unsymmetrical component would in general enter into the buckling mode. For simplicity, again consider a simple sinusoidal arch, with ends hinged and without initial end thrust, so that $\beta = 1$, $\lambda_2 = \lambda_3 = \ldots = 0$, and $S = 0$. The lateral pressure is denoted by q_o per unit length of the span. Hence the bending moment in the beam, due to the lateral forces alone, without counting the contribution of the axial thrust, is

$$M_o = \frac{1}{2} q_o x(L - x)$$

$$= q_o \frac{4L^2}{\pi^3} \sum_{n=1,3,5,\ldots} \frac{1}{n^3} \sin \frac{n\pi x}{L} \tag{46}$$

It is convenient here to use equations (18) because the Fourier series of M_o converges much faster than that of the lateral loading itself. From equations (18), there can be obtained

$$\left.\begin{aligned} B_m\left(\sum_n n^2 B_n^2 - \lambda_1^2 + m^2\right) &= -\frac{4}{\pi m^3} R + \delta_{1m}\lambda_1 \qquad (m = 1, 3, 5, \ldots) \\ B_m\left(\sum_n n^2 B_n^2 - \lambda_1^2 + m^2\right) &= 0 \qquad\qquad\qquad\quad (m = 2, 4, 6, \ldots) \end{aligned}\right\} \tag{47}$$

where $\delta_{1m} = 1$ if $m = 1$; $\delta_{1m} = 0$ if $m \neq 1$.

It is evident that when the load is applied, $R \neq 0$, all the B's with an odd subscript would in general differ from zero. It is also clear from the second of equations (47) that only one of the B's with an even subscript can differ from zero, because $\sum n^2 B_n^2$ cannot be equal to two different values of $\lambda_1^2 - m^2$. As before, these two cases would be separately treated.

Consider first the simpler case in which one of the B's with an even subscript is different from zero. In this case the deflection curve of the beam is unsymmetrical. Let the nonvanishing B be B_{2k}, where k is an integer. From the second of equations (47), then

$$\sum_n n^2 B_n^2 = \lambda_1^2 - 4k^2 \tag{48}$$

Hence from the first of equations (47),

$$B_m = \frac{1}{m^2 - 4k^2}\left(-\frac{4}{\pi m^3} R + \delta_{1m}\lambda_1\right) \qquad (m = 1, 3, 5, \ldots) \tag{49}$$

Squaring B_m, multiplying by m^2, and summing, there is obtained

$$\sum_n n^2 B_n^2 = \frac{1}{\left(1 - 4k^2\right)^2}\left(\lambda_1 - \frac{4}{\pi} R\right)^2 +$$

$$\frac{16R^2}{\pi^2} \sum_{m=3,5,\ldots} \frac{1}{m^4\left(m^2 - 4k^2\right)^2} + 4k^2 B_{2k}^2 \tag{50}$$

Equating this to $\lambda_1^2 - 4k^2$ according to equation (48), an equation is obtained relating B_{2k} with R. This relation is an ellipse, as in the section "Sinusoidal Arch under Sinusoidal Loading." The critical condition is reached when

$$\frac{dR}{dB_{2k}} = 0$$

which implies that

$$B_{2k} = 0 \tag{51}$$

With condition (51), the critical load R_{cr} is given by the following equation derived from equations (48) and (50):

$$\frac{16}{\pi^2} R^2 \sum_{m=1,3,5,\ldots} \frac{1}{m^4\left(m^2 - 4k^2\right)^2} - \frac{8\lambda_1 R}{\pi\left(1 - 4k^2\right)^2} = \left[1 - \frac{1}{\left(1 - 4k^2\right)^2}\right]\lambda_1^2 - 4k^2 \tag{52}$$

The series in the coefficient of R^2 converges very fast. If all terms except the first one are neglected, the error is less than 1/2 percent. Hence equation (52) is essentially equivalent to

$$\left(\frac{4}{\pi} R - \lambda_1\right)^2 = \left(4k^2 - 1\right)^2\left(\lambda_1^2 - 4k^2\right) \tag{53}$$

Comparing this equation with equations (29) for the case of a sinusoidal arch under sinusoidal loading, it can be seen that they are almost identical except that R in equations (29) is replaced by $\frac{4}{\pi} R$ and n is written here as $2k$. One of the roots of equation (53) which would represent the critical load on the beam must satisfy the four conditions stated below equations (29). In a manner completely analogous to the treatment of sinusoidal loading under equations (29), one concludes that k must be equal to 1 and that the solution exists only when λ_1 is equal to or greater than $\sqrt{5.5}$. The critical load is then

$$R_{cr} \doteq \frac{\pi}{4}\left(\lambda_1 + 3\sqrt{\lambda_1^2 - 4}\right) = \frac{\pi}{4}\left(R_{cr}\right)_{sine} \qquad \left(\lambda_1 \geq \sqrt{5.5}\right) \tag{54}$$

where $\left(R_{cr}\right)_{sine}$ means the critical R of a sinusoidally distributed lateral pressure.

If the full series in the coefficient of R^2 in equation (52) were taken, then, since $k = 1$, and

$$\sum_{m=3,5,7,\ldots} \frac{1}{m^4\left(m^2 - 4\right)^2} \doteq 4.977 \times 10^{-4}$$

equation (54) is modified by a factor of approximately (1 - 0.005), or

$$R_{cr} \doteq 0.995 \frac{\pi}{4}\left(R_{cr}^{*}\right)_{sine} \qquad \left(\lambda_1 \geqq \sqrt{5.5}\right) \quad (55)$$

Turning now to the other possible solution, that all the B's with an even subscript vanish, one sees by analogy to the case of a sinusoidal arch under sinusoidal loading that this mode of deformation would lead to a critical buckling load only if λ_1 is sufficiently small. Let

$$\sum_{n=1,3,5,\ldots} n^2 B_n^2 = C \quad (56)$$

Then equations (47) give

$$B_m = \frac{1}{C - \lambda_1^2 + m^2}\left(-\frac{4}{\pi m^3} R + \delta_{1m}\lambda_1\right) \qquad (m = 1, 3, 5, \ldots) \quad (57)$$

From equations (57) compute $m^2 B_m^2$ and sum:

$$C = \sum_{m} m^2 B_m^2$$

$$= \frac{16}{\pi^2} R^2 \sum_{m=1,3,5,\ldots} \frac{1}{m^4\left(C - \lambda_1^2 + m^2\right)^2} -$$

$$\frac{8}{\pi} R\lambda_1 \frac{1}{C - \lambda_1^2 + 1} + \frac{\lambda_1^2}{C - \lambda_1^2 + 1} \quad (58)$$

This gives a relation between C and R but is rather useless because of its complexity. A more practical solution can be obtained by successive approximation. According to equations (57), for a given R, B_m decreases rapidly with increasing m. As a first approximation, then, neglect the effect of B_3, B_5, . . . and obtain from equations (47), m = 1, the equation of equilibrium:

$$B_1^3 - \left(\lambda_1^2 - 1\right)B_1 = -\frac{4}{\pi} R + \lambda_1$$

which is again almost identical with equations (22) for the case of a sinusoidal arch under sinusoidal loading, except that R in equations (22) is now replaced by $\frac{4}{\pi} R$. Hence analogously,

$$\left.\begin{aligned} (B_1)_{cr} &\doteq \sqrt{\frac{\lambda_1^2 - 1}{3}} \\ R_{cr} &\doteq \frac{\pi}{4}\left[\lambda_1 + \sqrt{\frac{4}{27}(\lambda_1^2 - 1)^3}\right] \\ &= \frac{\pi}{4}(R_{cr})_{sine} \qquad \left(1 \leqq \lambda_1 \leqq \sqrt{5.5}\right) \end{aligned}\right\} \tag{59}$$

For the second approximation, neglect the effect of B_5, B_7, and so forth, but consider B_3. Now equations (47) may be written as

$$\left.\begin{aligned} B_1\left(\sum_n n^2 B_n^2 - \lambda_1^2 + 9\right) &= -\frac{4}{\pi} R + \lambda_1 + 8B_1 \\ B_3\left(\sum_n n^2 B_n^2 - \lambda_1^2 + 9\right) &= -\frac{4}{27\pi} R \end{aligned}\right\} \tag{60}$$

Hence at the buckling point,

$$\left(\frac{B_3}{B_1}\right)_{cr} = \frac{-\frac{1}{27}\frac{4}{\pi} R_{cr}}{-\frac{4}{\pi} R_{cr} + \lambda_1 + 8(B_1)_{cr}} = \frac{\lambda_1 + \sqrt{\frac{4}{27}(\lambda_1^2 - 1)^3}}{(18\lambda_1^2 - 234)(B_1)_{cr}}$$

Substituting into equations (60), which now become a relation combining B_1 and R, and using the criterion $dR/dB_1 = 0$ for buckling, there is obtained

$$\left.\begin{aligned} (B_1)_{cr} &= \sqrt{\frac{1}{3}\left(\lambda_1^2 - 1 - k\right)} \\ R_{cr} &= \frac{\pi}{4}\left[\lambda_1 + \sqrt{\frac{4}{27}\left(\lambda_1^2 - 1 - k\right)^3}\right] \qquad \left(\lambda_1 < \sqrt{5.5}\right) \end{aligned}\right\} \tag{61}$$

where

$$k = \frac{1}{36}\left[\frac{\lambda_1 + \sqrt{\frac{4}{27}\left(\lambda_1^2 - 1 - k\right)^3}}{\lambda_1^2 - 13}\right]^2 \tag{62}$$

Since k is always positive, the critical load R_{cr} given by equations (61) is always smaller than the first approximation given by equations (59). But the difference is really very small because $k \ll 1$. Values of k are given as a function of λ_1 in table IV.

Since $(B_m)_{cr}$ decreases very fast with increasing m, the convergence of the successive approximation is very good. From a comparison of equations (62) and (59), there appears no need for further approximations.

It can be concluded that, with an error less than 1/2 percent, the critical value of R for a uniformly distributed loading is equal to $\pi/4$ times that of a sinusoidal loading.

Interpreting the result somewhat differently, compare the total load that an arch can carry when the load is distributed first uniformly and then sinusoidally. Let W be the total load. Then since

$$W_{unif} = q_o L$$

and

$$W_{sine} = \frac{2}{\pi} q_o L$$

and since R_{cr} is based on q_o,

$$\frac{(W_{cr})_{sine}}{(W_{cr})_{unif}} = \frac{\frac{2}{\pi}(R_{cr})_{sine}}{(R_{cr})_{unif}} = \frac{2/\pi}{\pi/4} = \frac{8}{\pi^2} \tag{63}$$

Expressed in words, if W is the total lateral load an arch can sustain without buckling when the load is distributed uniformly over the span, then the same arch can sustain only a total load of $\frac{8}{\pi^2} W$ if that load is distributed sinusoidally. Thus concentrating a load toward the center of the arch lowers the critical buckling load.

CENTRAL CONCENTRATED LOAD ON A SINUSOIDAL ARCH

The case of a concentrated load acting at the midpoint of the span can be analyzed in the same manner as for the case in the preceding section. Only a very brief explanation will be given below.

Assume again that the arch is initially sinusoidal, rigidly hinged at both ends and without initial end thrust, so that $\beta = 1$, $\lambda_2 = \lambda_3 = \ldots = 0$, and $S = 0$. The lateral load is written as

$$W = q_o L \tag{64}$$

The bending moment due to the lateral forces alone is

$$M_o = \begin{cases} \frac{1}{2} Wx & \text{for } \left(0 \leqq x \leqq \frac{L}{2}\right) \\ \frac{1}{2} W(L - x) & \text{for } \left(\frac{L}{2} \leqq x \leqq L\right) \end{cases} = 2 \frac{WL}{\pi^2} \sum_{m=1,3,5,\ldots} (-1)^{\frac{m-1}{2}} \frac{1}{m^2} \sin \frac{m\pi x}{L} \tag{65}$$

The equations of equilibrium are

$$B_m \left(\sum_n n^2 B_n^2 - \lambda_1^2 + m^2 \right) = -\sin \frac{m\pi}{2} \frac{2}{m^2} R + \delta_{1m} \lambda_1$$

$$(m = 1, 2, 3, \ldots) \tag{66}$$

For the unsymmetric mode of buckling, if this mode is possible, the lowest R_{cr} occurs when $B_2 \neq 0$, which implies that

$$\sum_n n^2 B_n^2 = \lambda_1^2 - 4$$

and the critical load is given by the smallest positive root of the equation:

$$4R^2 \sum_{m=1,3,5,\ldots} \frac{1}{m^2(m^2 - 4)^2} - \frac{4\lambda_1}{9} R - \frac{8}{9} \lambda_1{}^2 + 4 = 0$$

Letting

$$\sum_{m=1,3,5,\ldots} \frac{1}{m^2(m^2 - 4)^2} = \frac{1 + \epsilon}{9}$$

where ϵ is approximately 0.0409,

$$R_{cr} = \frac{1}{2(1 + \epsilon)} \left[\lambda_1 + 3\sqrt{\lambda_1 - 4 + \left(\frac{8}{9} \lambda_1{}^2 - 4 \right) \epsilon} \right] \tag{67}$$

or

$$R_{cr} \doteq \frac{1}{2} (R_{cr})_{sine}$$

The numerical results of equation (67) which are used in the testing program are tabulated in table V and compared with $\frac{1}{2}(R_{cr})_{sine}$ in figure 12. For the symmetrical mode of buckling, steps analogous to those in the preceding section lead to

$$R_{cr} = \frac{1}{2} \left[\lambda_1 + \sqrt{\frac{4}{27} \left(\lambda_1{}^2 - 1 - k' \right)^3} \right] \qquad \left(\lambda_1 < \sqrt{5.5} \right) \tag{68}$$

where

$$k' = 9k$$

k being the constant given by equation (62) and table IV.

Hence R_{cr} for a concentrated load is approximately equal to one-half of R_{cr} for a sinusoidally distributed load.

As in the preceding section compare the load carrying capacity of a low arch with respect to various distributions of the loading. Thus

$$\left.\begin{aligned} \frac{(W_{cr})_{conc}}{(W_{cr})_{sine}} &\doteq \frac{1/2}{2/\pi} = \frac{\pi}{4} \\ \frac{(W_{cr})_{sine}}{(W_{cr})_{unif}} &\doteq \frac{8}{\pi^2} \\ \frac{(W_{cr})_{conc}}{(W_{cr})_{unif}} &\doteq \frac{8}{\pi^2} \times \frac{\pi}{4} = \frac{2}{\pi} \end{aligned}\right\} \qquad (69)$$

These ratios are within 2 percent of the corresponding ratios of the total loads causing equal center deflections of a simply supported beam under the three load distributions. This indicates that, for any symmetrical load distribution, the buckling load W_{cr} is proportional to the total load (of the specified distribution) which causes unit center deflection of a straight simply supported beam.[5]

CENTRAL CONCENTRATED LOAD ON A NONSINUSOIDAL ARCH

Because the experiments to be described were carried out on a series of approximately sinusoidal arches with a central concentrated load, a more complete investigation of this case will be made. First the case $\lambda_1 \neq 0$ and $\lambda_3 \neq 0$ will be studied and the difference in the influence of λ_3 on R_{cr} for sinusoidal load and R_{cr} for a central load will be shown. Then the case in which $\lambda_1 \neq 0$, $\lambda_2 \neq 0$, and $\lambda_3 \neq 0$ will be investigated. The results of the second case are more complicated and are used principally to show when the simple superposition of the effects of λ_2 and λ_3 is not possible.

---

[5]This result was previously shown by Timoshenko (reference 1) for the case of symmetrical buckling mode.

For a pin-ended arch without initial thrust ($\beta = 1$, $S = 0$), the equation of equilibrium for a concentrated center load is

$$B_m\left[\sum_n n^2\left(\lambda_n^2 - B_n^2\right) - m^2\right] = \frac{2R}{m^2}\sin\frac{m\pi}{2} - m^2\lambda_m$$

$$(m = 1, 2, 3, \ldots) \quad (70)$$

If only $\lambda_1 \neq 0$ and $\lambda_3 \neq 0$, equations (70) become

$$\left.\begin{aligned} B_1\left(\lambda_1^2 + 9\lambda_3^2 - \sum_n n^2B_n^2 - 1\right) &= 2R - \lambda_1 \\ B_2\left(\lambda_1^2 + 9\lambda_3^2 - \sum_n n^2B_n^2 - 4\right) &= 0 \\ B_3\left(\lambda_1^2 + 9\lambda_3^2 - \sum_n n^2B_n^2 - 9\right) &= -\frac{2}{9}R - 9\lambda_3 \end{aligned}\right\} \quad (71)$$

For the case of buckling in the unsymmetric second mode one can solve for $\sum_n n^2B_n^2$ from the second of equations (71). Substituting this into the other two of equations (71), solving the resulting equations for B_1 and B_3, and again forming the sum $\sum_n n^2B_n^2$ an equation is obtained connecting R, λ_1, λ_3, and B_2. At the critical condition B_2 vanishes. Thus one arrives at an equation governing the critical load:

$$4R^2 \sum_{n=1,3,5,\ldots} \frac{1}{n^2(n^2 - 4)^2} + R\left(-\frac{4}{9}\lambda_1 + \frac{36}{25}\lambda_3\right) - \frac{8}{9}\lambda_1^2 + \frac{504}{25}\lambda_3^2 + 4 = 0$$

Letting

$$\sum_{n=1,3,5,\ldots} \frac{1}{n^2(n^2 - 4)^2} = \frac{k}{9}$$

$$k \doteq 1.0409$$

there is obtained

$$R_{cr} = \frac{1}{2k}\left[\lambda_1 - \frac{81}{25}\lambda_3 + \sqrt{\left(\lambda_1 - \frac{81}{25}\lambda_3\right)^2 + 4k\left(2\lambda_1^2 - \frac{1134}{25}\lambda_3^2 - 9\right)}\right] \qquad (72)$$

It is interesting to note that in contrast with the sinusoidal load case, the sign of λ_3 is important, and $(R_{cr})_{conc}$ no longer approaches $\frac{1}{2}(R_{cr})_{sine}$ unless $\frac{81}{25}\lambda_3 \ll \lambda_1$. In fact, the effect of λ_3 on the ratio $(R_{cr})_{conc}/(R_{cr})_{sine}$ can be appreciable.

The $\frac{81}{25}\lambda_3$ terms in equation (72) arise from the cross product in the squaring of the right-hand side of the last equation of equations (71) to obtain B_3^2. If the case is considered in which only λ_1 and λ_2 are different from zero, there is no corresponding cross product and therefore it can be expected that λ_2 will have the same proportional effect on R_{cr} for a centrally loaded arch as for a sinusoidally loaded arch. Physically this difference in the effect of λ_2 and λ_3 seems reasonable since the central load occurs at the maximum amplitude of the λ_3 wave, but at a node of the λ_2 wave.

For the case in which λ_1, λ_2, and λ_3 differ from zero it is known from the section "Initial Shape of Arch Other Than Sinusoidal" that buckling always occurs in the second mode and that the influence of the higher modes is small. Therefore all B_m's with $m > 3$ will be neglected. Letting $\beta = 1$ and $S = 0$, the equations of equilibrium are

$$B_1\left(\sum_1^3 n^2\lambda_n^2 - B_1^2 - 4B_2^2 - 9B_3^2 - 1\right) = 2R - \lambda_1 \tag{73a}$$

$$B_2\left(\sum_1^3 n^2\lambda_n^2 - B_1^2 - 4B_2^2 - 9B_3^2 - 4\right) = -4\lambda_2 \tag{73b}$$

$$B_3\left(\sum_1^3 n^2\lambda_n^2 - B_1^2 - 4B_2^2 - 9B_3^2 - 9\right) = -\frac{2}{9}R - 9\lambda_3 \tag{73c}$$

These equations are to be solved for the critical values of B_1, B_2, B_3, and R under the critical condition $\partial R/\partial B_1 = 0$. The solution can be effected in the following steps:

(1) Eliminate R between equations (73a) and (73c) and use equation (73b) to obtain an equation connecting B_1 and B_2:

$$\left[\left(3 - 4\frac{\lambda_2}{B_2}\right)^2 + 9\left(5 + 4\frac{\lambda_2}{B_2}\right)^2\right]B_1^2 + 2\left(3 - 4\frac{\lambda_2}{B_2}\right)\left(\lambda_1 + 81\lambda_3\right)B_1 -$$

$$9\left(5 + 4\frac{\lambda_2}{B_2}\right)^2\left(\frac{4\lambda_2}{B_2} - 4B_2^2 + \sum n^2\lambda_n^2 - 4\right) + \left(\lambda_1 + 81\lambda_3\right)^2 = 0 \tag{74}$$

(2) Differentiate equations (73a) and (73b) with respect to B_1 and use the critical condition $\partial R/\partial B_1 = 0$ and equation (73b) to obtain $\partial B_2/\partial B_1$ and $\partial B_3/\partial B_1$ at the critical point. The results are expressed in terms of B_1, B_2, and B_3.

(3) These expressions for $\left(\partial B_2/\partial B_1\right)_{cr}$ and $\left(\partial B_3/\partial B_1\right)_{cr}$ are substituted into equation (73a) after differentiating it with respect to B_1. Using the critical condition $\partial R/\partial B_1 = 0$ and eliminating B_3 through equation (73b), an equation for $\left(B_1\right)_{cr}$ in terms of $\left(B_2\right)_{cr}$ is obtained:

$$(B_1)_{cr}^2 = \frac{1}{16}\left[3 - 4\frac{\lambda_2}{(B_2)_{cr}}\right]\left[12\frac{\lambda_2}{(B_2)_{cr}} + \frac{10}{\lambda_2}(B_2)_{cr}^2 - 3 + 2\sum_n n^2\lambda_n^2\right] \quad (75)$$

By plotting equations (74) and (75) a compatible solution can be found. This solution will not hold for $\lambda_2 = 0$, but it is valid for $\lambda_3 = 0$, although no simplification will result. The results for a series of arches with $\lambda_2/\lambda_1 = 0.005$ and $\lambda_3/\lambda_1 = 0.04$, which are representative of the test specimens to be described in the experimental section, are tabulated in table VI and plotted in figure 12. Comparing this with figure 11 it is seen that the combined influence of λ_2 and λ_3 is stronger than the sum of their separate influences for lower values of λ_1; but for higher values of $\lambda_1\left(\lambda_1^2 > 5.5\right)$ the principle of superposition can be used. This is not unexpected since for low values of λ_1 the presence of λ_2 causes the mode of buckling to change from symmetrical to unsymmetrical and thus changes the influence of λ_3 on R_{cr}.

In figure 13 the process of loading is pictured for two examples in the above sequence of arches, one below the dividing value of $\lambda_1 = \sqrt{5.5}$ and one above. The changes in amplitudes of the three modes $\lambda_1 - B_1$, $B_2 - \lambda_2$, and $B_3 - \lambda_3$ are plotted as functions of the load R for $\lambda_1 = 2$ and $\lambda_1 = 4$. It is to be noted that, for the lower value of λ_1, B_2 does not increase rapidly until just before buckling occurs, while, for $\lambda_1 = 4$, B_2 starts increasing rapidly at a point appreciably before the buckling point. For both cases B_3 increases at an almost constant rate until just at the point of buckling.

ELASTIC SUPPORTS AT ENDS

So far the ends of the arch have been considered as rigidly hinged. Since ideal rigid hinges cannot be realized in the testing machine, it is expected that some deviation in the experimental buckling load from the theoretical value may exist owing to the yielding of the supports. In order to obtain some quantitative measure of the effect of support displacement, an example of an arch with elastic supports will be considered.

Assume that the supports are perfectly elastic. Let α be the spring constant of the support so that a displacement Δ would produce a thrust of magnitude $\alpha\Delta$. Without loss of generality it can be assumed that one end is rigidly hinged, and the other is elastically supported, as shown in figure 3. The effect of the support rigidity on the

equilibrium is expressed by the parameter β, defined by equation (10). The equations of equilibrium are either equations (15) or (18).

As an example, consider a sinusoidal arch loaded laterally by a sinusoidally distributed load of intensity q per unit length:

$$y_o = a_1 L \sin \frac{\pi x}{L}$$

$$q = q_o \sin \frac{\pi x}{L}$$

The equation of equilibrium is given by equations (22). The solution obtainable in the same manner as in the section "Sinusoidal Arch under Sinusoidal Loading" is

$$\left.\begin{aligned} R_{cr} &= (1 - S)\lambda_1 + \sqrt{\frac{4}{27}\frac{\left(\beta\lambda_1^2 - 1 + S\right)^3}{\beta}} && \left(\frac{1}{\sqrt{\beta}} < \lambda_1 \leqq (\lambda_1)_o\right) \\ R_{cr} &= (1 - S)\lambda_1 + 3\sqrt{\frac{\beta\lambda_1^2 - 4 + S}{\beta}} && \left(\lambda_1 > (\lambda_1)_o\right) \end{aligned}\right\} \quad (76)$$

where $(\lambda_1)_o$ is the smallest positive real root of the equation:

$$\left(\beta\lambda_1^2 - 4 + S\right) = \frac{4}{243}\left(\beta\lambda_1^2 - 1 + S\right)^3 \quad (77)$$

The effect of the nonrigidity of the support ($\beta < 1$) is shown in figure 14 and table VII. The values of $(\lambda_1)_o$ as a function of β are also given in that figure and table. The limiting case, $\alpha \longrightarrow \infty$ and $\beta \longrightarrow 1$, checks with the results of the sections "Sinusoidal Arch under Sinusoidal Loading" and "Effect of Initial Axial Compression."

If the support offers no resistance to the axial thrust, that is, it is perfectly flexible, then $\alpha = 0$ and $\beta = 0$. In this case there is no critical buckling load; the arch deflects continuously because the lower limit of λ_1, $1/\sqrt{\beta}$, below which no buckling can occur, now tends to infinity.

Similarly other loading conditions may be treated. For example, if β differs from 1, the ratios of R_{cr} for a uniformly distributed load, a sinusoidally distributed load, and a concentrated load at the center are again, respectively, $\pi/4$, 1, and 1/2.

LATERAL ELASTIC SUPPORTS

In application to certain wing design problems, it is desired to investigate the effect of lateral elastic supports on the buckling load of the arch. As an example, consider an arch having an elastic support at the center, as shown in figure 3. Let α' be the spring constant of the support. Then the change in thrust in the spring is

$$V = \alpha'\left[\Delta' - (\Delta')_o\right] \tag{78}$$

where $\Delta' - (\Delta')_o$ is the change in the deflection at the midspan. No generality is lost by assuming $(\Delta')_o$ to be zero, if initial thrust in the spring is counted as a lateral force.

Now when the deflection curve of the arch is given by equations (2) and (3),

$$\Delta' - (\Delta')_o = \sum_{m=1,3,5,\ldots} (-1)^{\frac{m-1}{2}} (a_m - b_m)L \tag{79}$$

The moment contributed by V is then (cf. equation (65))

$$(M_o)_V = -\frac{2VL}{\pi^2} \sum_{m=1,3,5,\ldots} (-1)^{\frac{m-1}{2}} \frac{1}{m^2} \sin\frac{m\pi x}{L} \tag{80}$$

Combining equations (78), (79), and (80) and adding $(M_o)_V$ to the right-hand side of equation (4), there is obtained, after some reduction, the equations of equilibrium (equations (18) modified):

$$B_m\left(\beta \sum_n n^2 B_n^2 - \beta \sum_n n^2 \lambda_n^2 + m^2 - S\right) = -\pi^2 K_m R + \lambda_m\left(m^2 - S\right) +$$

$$\sin \frac{m\pi}{2} \frac{\mu}{m^2} \sum_{n=1,3,5,\ldots} (-1)^{\frac{n-1}{2}} \left(\lambda_n - B_n\right) \tag{81}$$

where K_m is given by equation (17) and

$$\mu = \frac{2L^3}{\pi^4 EI} \alpha' \tag{82}$$

Since a simply supported beam with a unit concentrated load at its center has a deflection of $\frac{1}{48} \frac{L^3}{EI} \approx \frac{2}{\pi^4} \frac{L^3}{EI}$ under the load, μ is approximately the ratio of α' to the spring constant of a simply supported beam having the linear dimensions of the arch.

Consider a sinusoidal arch subject to sinusoidal loading. For simplicity let the initial thrust be zero and let the end hinges be rigid. Then if $m \neq 1$,

$$\beta = 1$$

$$S = 0$$

$$\lambda_m = 0$$

$$K_1 = \frac{1}{\pi^2}$$

$$K_m = 0$$

The governing equations are

$$B_m\left(\sum_n n^2 B_n{}^2 - \lambda_1{}^2 + m^2\right) = -\delta_{1m}R + \delta_{1m}\lambda_1 +$$

$$\begin{cases} (-1)^{\frac{m-1}{2}} \frac{1}{m^2}\,\mu\left[\lambda_1 - \sum_{n=1,3,\ldots} (-1)^{\frac{n-1}{2}} B_n\right] & \text{(if } m \text{ is odd)} \\ 0 & \text{(if } m \text{ is even)} \end{cases} \tag{83}$$

Let

$$\left.\begin{aligned} Q &= \lambda_1 - \sum_{n=1,3,\ldots} (-1)^{\frac{n-1}{2}} B_n \\ P &= \sum_{n=1,3,\ldots} n^2 B_n{}^2 \end{aligned}\right\} \tag{84}$$

then

$$B_1 = \frac{\lambda_1 - R + 2\mu Q}{P + 1 - \lambda_1{}^2}$$

$$B_m = (-1)^{\frac{m-1}{2}} \frac{2\mu Q}{m^2\left(P + m^2 - \lambda_1{}^2\right)} \qquad (m \text{ odd and } \geq 3)$$

With these values for B_m, there is obtained

$$Q = \lambda_1 + \frac{R - \lambda_1}{P + 1 - \lambda_1{}^2} - \sum_m \frac{2\mu Q}{m^2\left(P^2 + m^2 - \lambda_1{}^2\right)} \tag{85}$$

First calculate the critical load for unsymmetric buckling where $B_{2n} \neq 0$ for some n. Then according to equations (83),

$$P = \lambda_1^2 - 4n^2 \tag{86}$$

But P is also given by

$$P = \sum_m m^2 B_m^2$$

$$= 4\mu^2 Q^2 \sum_{m=1,3,\ldots} \frac{1}{m^2(m^2 - 4n^2)^2} + \frac{(\lambda_1 - R)(\lambda_1 - R + 4\mu Q)}{(1 - 4n^2)^2} + 4n^2 B_{2n}^2 \tag{87}$$

Neglect all except the $m = 1$ term of the series and substitute the value of P from equation (86):

$$\frac{(\lambda_1 - R + 2\mu Q)^2}{(1 - 4n^2)^2} = \lambda_1^2 - 4n^2 - 4n^2 B_{2n}^2 \tag{88}$$

The critical condition is again $B_{2n} = 0$. Solving equation (85) for Q and substituting together with $B_{2n} = 0$ into equation (88), one obtains

$$R_{cr} = \lambda_1 + (4n^2 - 1)\left[\sqrt{\lambda_1^2 - 4n^2} + 2\mu \frac{\lambda_1 - \sqrt{\lambda_1^2 - 4n^2}}{(4n^2 - 1)(1 + 2\mu\alpha) + 2\mu}\right]$$

where

$$\alpha = \sum_{m=1,3,\ldots} \frac{1}{m^2(m^2 - 4n^2)}$$

This expression is a minimum for $n = 1$, hence

$$\left.\begin{aligned} \alpha &\doteq -0.3087 \\ R_{cr} &= (R_{cr})_{sine} + \frac{2\mu}{3 + 0.147\mu}\left[4\lambda_1 - (R_{cr})_{sine}\right] \end{aligned}\right\} \tag{89}$$

These values are given in table VIII and plotted in figure 15 for $\mu = 0, 0.5, 1, 1.5, 2,$ and 3.

In this solution the effect of the higher modes ($m \geqq 3$) on the force exerted by the spring, which enters by the series $\sum_m \frac{1}{m^2(m^2 - 4)}$, is included, but the effect of the higher modes in lowering the buckling load, which enters by the faster converging series $\sum_m \frac{1}{m^2(m^2 - 4)^2}$, is neglected. In the analogous case of the arch with a concentrated central load this results in a maximum error of 3 percent for $\lambda_1 < 10$ and for this case it should be no more.

Consider next the case of symmetrical buckling which occurs for the smaller values of λ_1. As a first approximation neglect the effects of all the B_m's except B_1. Then from equations (83), there is obtained under the critical condition $\partial R/\partial B_1 = 0$ the critical load:

$$R_{cr} = \lambda_1(1 + 2\mu) + \sqrt{\frac{4}{27}}\left(\lambda_1^2 - 1 - 2\mu\right)^{3/2} \tag{90}$$

A procedure similar to that used in the section "Initial Shape of Arch Other Than Sinusoidal" can be applied to find further approximations. The results of such a calculation, with the effects of B_1 and B_3 included, are given in table VIII and are plotted in figure 15.

BUCKLING LOAD BASED ON KÁRMÁN AND TSIEN'S ENERGY CRITERION

It is well-known that the classical buckling criterion, on which the calculations of the preceding sections are based, leads to erroneous

results for cylindrical and spherical shells; while a fundamentally different criterion, first proposed by Kármán and Tsien, whose latest version is given in reference 7, gives much closer agreement with experiments. The criterion of Kármán and Tsien (henceforth referred to as energy criterion) is that the buckling load is reached when the total energy in a possible (buckled) equilibrium state is equal to the total energy in the unbuckled state. In other words, if the total potential energy is such that it is permissible for the structure to jump from the unbuckled state to a buckled state, then the structure will actually jump.

Both the classical and the energy criteria have been applied to curved beams and shells. In some cases the classical criterion gives closer agreement with experiments; in others, the energy criterion gives better results. The reason, as pointed out by Tsien, is that in some cases the energy "hump" between two equilibrium states (one buckled and one unbuckled) of the same energy level is large and in other cases it is small. If the hump is small, the ever present small disturbances will enable the structure to jump from the unbuckled state to the more stable buckled state. Otherwise, this jump will be hindered. The crucial decision of the proper criterion depends much on what one means by a "practical" experimental setup or a "practical" service condition of the structure.

The energy criterion has been applied to the low arch problem by Friedrichs (reference 5) who found a great reduction in R_{cr} based on the energy criterion from that based on the classical criterion. In order to decide which criterion actually applies to the buckling of low arches, the experimental setup to be described in the next section will be accepted as practical and the theoretical results will be compared with experiments.

In applying the energy criterion, one must distinguish a constant deflection loading (a rigid testing machine) from a constant force (dead-weight) load. In the former case the change in total energy in buckling is just equal to the change in the internal strain energy, while in the latter case it is equal to the change in the strain energy minus the force times the displacement. However, a laterally loaded arch cannot buckle if the point of loading is not allowed to jump; hence only the dead-weight loading case will be considered.

For dead-weight loading the total energy is

$$\phi = U - W \tag{91}$$

where U is the strain energy and W is the work done by the lateral loading. The energy ϕ can be expressed as a function of the

deflection δ. Then according to the energy criterion, buckling would occur under a dead weight F provided that

$$\left.\begin{aligned} \phi(\delta_1) &= \phi(\delta_2) \\ F(\delta_1) &= F(\delta_2) \end{aligned}\right\} \tag{92}$$

where δ_1 and δ_2 are two deflection configurations. Now the strain energy U, under the assumptions of the section "General Analysis," is given by

$$U = \frac{1}{2} EI \int_0^L \left(\frac{d^2y}{dx^2} - \frac{d^2y_o}{dx^2}\right)^2 dx + \frac{(H^2 - H_o^2)L}{2AE} \tag{93}$$

From equations (2), (3), and (9), equation (93) becomes

$$U = K \sum_m m^4 \left\{(\lambda_m - B_m)^2 \left[1 + \tfrac{1}{2}(\lambda_m + B_m)^2\right] + S\left(\lambda_m^2 - B_m^2\right)\right\} \tag{94}$$

where

$$K = \frac{\pi^4 EI^2}{AL^3}$$

The work done by the external load in the buckling process is

$$W = \int_0^L q(y_o - y)\, dx \tag{95}$$

For a sinusoidally distributed loading,

$$W = 2KR(\lambda_1 - B_1) \tag{96}$$

while for a concentrated load at the midspan

$$W = 4KR \sum_{m=1,3,5,\ldots} (-1)^{\frac{m-1}{2}} (\lambda_m - B_m) \tag{97}$$

The buckling load according to the energy criterion can then be obtained easily.

Sinusoidally Distributed Loading on a Sinusoidal Arch

It was shown in the section "Sinusoidal Arch under Sinusoidal Loading" that the only equilibrium position of a sinusoidal arch under sinusoidally distributed load is the one for which all the B_m's ($m = 2, 3, \ldots$) vanish. Hence if $S = 0$ (zero initial thrust),

$$\left.\begin{aligned} \frac{\phi}{K} &= (\lambda_1 - B_1)^2\left[1 + \frac{1}{2}(\lambda_1 + B_1)^2\right] - 2R(\lambda_1 - B_1) \\ R &= \lambda_1 + B_1(\lambda_1^2 - 1) - B_1^3 \end{aligned}\right\} \tag{98}$$

The buckling conditions that $\phi(B_1') = \phi(B_1'')$ and $R(B_1') = R(B_1'')$ are fulfilled when $R = \lambda_1$ at which

$$\frac{\phi}{K} = B_1^2 - \lambda_1^2 + \frac{1}{2}(\lambda_1^2 - B_1^2)^2 \tag{99}$$

and $\phi(B_1) = \phi(-B_1)$. A substitution of $R = \lambda_1$ into the second of equations (98) gives the arch rise at the critical condition:

$$(B_1)_{cr} = \sqrt{\lambda_1^2 - 1}$$

or

$$(B_1)_{cr} = 0$$

Hence

$$R_{cr} = \lambda_1 \tag{100}$$

Central Concentrated Load on a Sinusoidal Arch

Assuming no initial thrust (S = 0), from equations (94) and (97)

$$\frac{\phi}{K} = \left(\lambda_1 - B_1\right)^2\left[1 + \frac{1}{2}\left(\lambda_1 + B_1\right)^2\right] - 4R\left(\lambda_1 - B_1\right) + \sum_{m=3,5,\ldots}\left[m^4 B_m^2\left(1 + \frac{1}{2}B_m^2\right) + 4R(-1)^{\frac{m-1}{2}}B_m\right] \tag{101}$$

From equations (66)

$$2R = \lambda_1 - B_1\left(\sum_m m^2 B_m^2 - \lambda_1^2 + 1\right) \tag{102}$$

If all the B_m's except B_1 are neglected, the above equations become identical with those for the sinusoidal loading if R is replaced by 2R. Thus approximately, R_{cr} for the concentrated center load is one-half of that for the sinusoidal load. This is the same approximate ratio as for R_{cr} of the sinusoidal and the concentrated loadings based on the classical criterion.

The ratio of R_{cr} based on the energy criterion to that based on the classical criterion is plotted in figure 16 for sinusoidal loadings on a sinusoidal arch. This same ratio holds approximately for the central load on sinusoidal arches.

EXPERIMENTS

A series of pin-ended arches having rigid simple supports were loaded with a central concentrated load in the testing apparatus shown in figures 17 and 18. The ideal end conditions were approximated as closely as possible by supporting the arches on knife edges mounted in a heavy steel frame having a stiffness approximately 100 times that of the specimen. Allowing a 20-percent reduction in this stiffness due to the flexibility of the knife edges and fittings results in a value of β equal to 0.988. A reference to the section "Elastic Supports at Ends" and figure 14 shows that a maximum error of about 1 percent will result from considering the supports as perfectly rigid.

The knife-edge fittings were provided with sockets which alined the ends of the specimen with the knife edges. (See fig. 19.)

The most critical problem in setting up the specimens for testing was the spacing of the supports. A looseness or an initial compression results in a change in the initial arch shape and an appreciable error in the buckling load. In the tests the spacing adjustment was made by a wedge controlled by a screw which was rotated until the play between the specimen and the knife edges was just eliminated.

The specimens were cut from 24S-T3 and 75S-T6 sheets and milled to 1/2-inch width. The strips were then rolled to the desired curvature on a three-roll roller. To reduce the effect of roll eccentricity several passes were made at each setting of the rolls, the rolls being indexed to a new position at the start of each pass.

The curvature of each specimen was measured at 12 stations by a dial gage which could be read up to ten-thousandths of an inch, placed between knife edges 2 inches apart. These curvatures were numerically integrated to find the shape of the specimen for which a 12-term Fourier expansion (half-range sine series) was made. The first three coefficients are given in table IX. As a check on the accuracy of the method the central rise of the arch as predicted by the numerical integration was compared with the actual rise as measured with a vernier height gage. The difference was no more than 4 percent of the arch rise for each specimen measured. The central arch rise as predicted by the Fourier coefficients agreed with the numerical integration within 1 percent.

The Fourier coefficients λ_1, λ_2, and λ_3 were used in calculating the theoretical critical load. In such calculations use is made of the fact noted in the section "Central Concentrated Load on a Nonsinusoidal Arch" that, whereas for smaller λ_1 (say, $\lambda_1 < 2.4$) the joint effect of λ_2 and λ_3 on R_{cr} is not equal to the sum of the effects of λ_2 and λ_3 separately, for larger λ_1 (say, $\lambda_1 > 2.4$) the effects of λ_2 and λ_3 are superposable. Hence for $\lambda_1 < 2.4$ the more exact method of the aforementioned section was used, but for $\lambda_1 > 2.4$ the effects of λ_2 and λ_3 were calculated separately and added together algebraically. The effect of λ_3 is given by equation (72). That of λ_2, according to the previous argument, can be obtained, percentagewise, from figure 11(a) or table III.

Although no attempt was made to determine the arch shape during the loading process, visual observation showed that the test performance at least approximately agreed with the theoretical predictions. The gradual increase in the third mode with the load, resulting in a flattening of the arch and then a reversal of curvature for the higher values

of λ_1, was noted. For values of $\lambda_1 > 2.4$ the rapid increase in the unsymmetric second mode just before buckling was quite evident. The clearest indication of the onset of buckling, however, was obtained by noticing the vibration of the specimen as the individual weights were applied. Even a very careful application resulted in a slight vibration in the fundamental mode. When the load approached within a few pounds of the critical load there was a rapid decrease in the frequency of this vibration. Further load applications were made in extremely small increments.

The theoretical and experimental results are listed in table IX and plotted in figure 16. In figure 16, the ordinate is the ratio of R_{cr} determined by the test to that computed theoretically according to the classical criterion. In the same figure, the dashed line shows the ratio of R_{cr} given by the energy criterion to that given by the classical criterion. This curve is based on the simple sinusoidal arch $(\lambda_2 = \lambda_3 = 0)$. For arches used in the experiment λ_2 and λ_3 were so small that the variation of the ratio $(R_{cr})_{energy}/(R_{cr})_{class}$ does not vary much from the dashed curve of the figure.

It is seen that the test results agree quite well with results based on the classical criterion for higher values of λ_1 but drop appreciably below them for the lower values. All the test values, however, lie above the energy criterion curve. Although calculations for the series of arches representing the test specimens indicate that buckling would occur for $\lambda_1 \geqq 1.05$, no buckling was observed for $\lambda_1 \leqq 1.38$.

A calculation of the stresses in the specimens at buckling was made to determine if yielding occurred. With $H_o = 0$ and $\beta = 1$ the axial compressive force is given by equation (9). Using the nondimensional notation it becomes

$$\sigma_c = \frac{H}{A}$$

$$= \frac{\pi^2 EI}{AL^2} \sum_m m^2 \left(\lambda_m^2 - B_m^2\right) \tag{103}$$

For a sinusoidal arch with a sinusoidal load all the B_m's except B_1 are zero at the critical buckling load and $\left(B_1\right)_{cr}^2 = \frac{1}{3}\left(\lambda_1^2 - 1\right)$ for $1 \leqq \lambda_1^2 \leqq 5.5$ and $\left(B_1\right)_{cr}^2 = \lambda_1^2 - 4$ for $\lambda_1^2 \geqq 5.5$. Therefore

$$\frac{(\sigma_c)_{cr}}{\sigma_P} = \frac{H_{cr}}{P} = \begin{cases} \frac{1}{3}\left(1 + 2\lambda_1^2\right) & (\text{for } 1 \leq \lambda_1^2 \leq 5.5) \\ 4 & (\text{for } \lambda_1^2 \geq 5.5) \end{cases} \tag{104}$$

where $P = \pi^2 EI/L^2$ is the Euler buckling load of the beam and $\sigma_P = P/A$. Thus it can be seen that the critical compressive force is just equal to the Euler load if $\lambda_1 = 1$. As λ_1 increases the critical force increases until it reaches the Euler load for buckling in the second mode. At this point the arch buckles unsymmetrically and the critical compressive stress remains constant for all higher values of λ_1. This performance is also typical of symmetrical arches with a central concentrated load, but for arches with a slight asymmetry, as is the case for the specimens tested, the value $H_{cr}/P = 4$ is approached only as λ_1 becomes large. The values of H_{cr}/P for a series of arches are given in table VI.

The maximum bending stress at any point x is given by

$$\sigma_b = \frac{1}{2} Et\left(\frac{d^2y}{dx^2} - \frac{d^2y_o}{dx^2}\right) \tag{105}$$

where t is the thickness of the specimen. In terms of the nondimensional Fourier coefficients this becomes

$$\sigma_b = \frac{\pi^2 Et}{L^2}\sqrt{\frac{I}{A}} \sum_m m^2(\lambda_m - B_m) \sin\frac{m\pi x}{L} \tag{106}$$

The bending stresses at the midspan were calculated for the series of arches with $\lambda_2 = 0.005\lambda_1$ and $\lambda_3 = 0.040\lambda_1$ which are representative of the actual test specimens. The results are shown in table VI together with the total maximum stress for $t = 0.25$. The total stress for any other thickness is obtained by multiplying the last column of table VI by the factor $16t^2$.

All the specimens tested had maximum stresses well below the yield stress of the material at the buckling point. Yielding occurred in the post-buckling stage for all the specimens except those having the very lowest values of λ_1.

CONCLUSIONS

A Fourier analysis has been used to solve the problem of buckling of low arches under a lateral loading acting toward the center of curvature. The conclusions may be summarized as follows:

1. For a sinusoidal arch under a sinusoidal loading, the analysis gives a very simple exact solution for the nonlinear equation of equilibrium. The critical load can be expressed as a simple function of the beam dimension parameters. On the basis of the classical buckling criterion, it is shown that the buckling mode is symmetrical for arches having a nondimensional parameter λ_1 less than $\sqrt{5.5}$ and is unsymmetrical for λ_1 greater than $\sqrt{5.5}$. This dividing value is affected somewhat by the initial thrust in the arch and the elasticity of the support.

2. For arch shapes other than sinusoidal but under sinusoidal loading, it is shown that symmetrical deviations have only minor effects on the buckling load, while unsymmetrical modes of deviation cause serious reduction of the buckling load. The buckling mode is always unsymmetrical if the initial shape of the arch contains unsymmetrical modes. For sinusoidal loading the critical load is independent of the sign of $\lambda_m (m > 1)$; thus a pair of different arches can have the same critical load.

3. For a load distribution that deviates from sinusoidal, the unsymmetrical components again have serious effects. The critical load will be dependent upon the sign of $\lambda_m (m > 1)$. For symmetrical load distributions, the buckling loads are approximately proportional to the total loads (under the respective distributions) that are required to produce a unit deflection at the center of a straight simply supported beam without axial restraint.

4. Comparison with experiments shows that the classical criterion of buckling is applicable for larger values of λ_1, say, $\lambda_1 > 3$. But the classical criterion overestimates the buckling load for very flat arches. The experimental buckling load is always higher than that estimated according to the energy criterion of Kármán and Tsien but has a tendency to approach that criterion as λ_1 decreases. For $\lambda_1 \longrightarrow 1$ (with exact value depending on the initial thrust and support conditions), the arch deflects continuously and there is no buckling phenomenon.

California Institute of Technology
Pasadena, Calif., January 24, 1952

REFERENCES

1. Timoshenko, S.: Theory of Elastic Stability. First ed., McGraw-Hill Book Co., Inc., 1936.

2. Biezeno, C. B.: Das Durchschlagen eines schwach gekrümmten Stabes. Z.a.M.M., Bd. 18, Heft 1, Feb. 1938, pp. 21-30.

3. Marguerre, K.: Die Durchschlagskraft eines schwach gekrümmten Balkens. Sitzungsber. Berliner math. Gesell., Bd. 37, June 1938, pp. 22-40.

4. Marguerre, Karl: Über die Anwendung der energetischen Methode auf Stabilitätsprobleme. Jahrb. 1938, DVL, pp. 252-262. (Available in translation as NACA TM 1138.)

5. Friedrichs, K. O.: Lectures on Non-Linear Elasticity. Mimeo. notes by S. Schaaf. New York Univ., 1945.

6. Hoff, N. J., and Bruce, V. G.: Dynamic Analysis of the Buckling of Laterally Loaded Flat Arches. PIBAL Rep. 191, Contract Nonr-267 00, Office of Naval Res. and Polytechnic Inst. of Brooklyn, Oct. 1951.

7. Tsien, Hsue-Shen: A Theory for the Buckling of Thin Shells. Jour. Aero. Sci., vol. 9, no. 10, Aug. 1942, pp. 373-384.

TABLE I

VALUES OF R_{cr} AS A FUNCTION OF INITIAL THRUST AND ARCH RISE

S \ λ_1	$(1 - S)^{1/2}$	1.0	1.2	1.4	1.6	1.8	2.0
0	1.000000	1.000000	1.312338	1.762039	2.349955	3.090387	4.000000
.1	.853815	.912172	1.232735	1.680056	2.263209	2.997755	3.900829
.25	.649519	.798113	1.120608	1.562302	2.137273	2.862332	3.755138
.50	.353553	.636083	.950784	1.379012	1.938017	2.645717	3.520288
1.00	0	.384900	.665108	1.056166	1.576551	2.244738	3.079201

S \ λ_1	2.2	$(5.5 - S)^{1/2}$	2.4	2.6	3	3.5	4
0	5.096309	6.019436	6.379947	7.583975	9.708204	12.116843	14.392306
.1	4.990180	5.765646	6.251454	7.413459	9.474954	11.818911	14.035515
.25	4.833707	5.392701	6.053234	7.154805	9.123864	11.371428	13.500000
.50	4.580028	4.792269	5.709987	6.716641	8.535621	10.624117	12.606599
1.00	4.069398	3.674235	4.983975	5.817216	7.348470	9.124145	10.816653

TABLE II

VALUES OF $(B_m)_{cr}$, $(B_1)_{cr}$, AND R_{cr} COMPUTED FROM EQUATIONS (40) AND (41)

(a) m = 2

λ_1	λ_2	$(B_2)_{cr}$	$(B_2)_{cr}/\lambda_2$	$(B_1)_{cr}$	R_{cr}	λ_2	$(B_2)_{cr}$	$(B_2)_{cr}/\lambda_2$	$(B_1)_{cr}$	R_{cr}
	$\lambda_2/\lambda_1 = 0.01$					$\lambda_2/\lambda_1 = 0.05$				
1.0	0.010	0.01334	1.334	Imag.[1]	Imag.	0.05	0.06655	1.331	Imag.	Imag.
1.2	.012	.01773	1.478	0.3828	1.312	.06	.08824	1.471	0.3785	1.306
1.4	.014	.02372	1.694	.5656	1.761	.07	.1170	1.672	.5635	1.742
1.6	.016	.03259	2.037	.7214	2.348	.08	.1569	1.961	.7257	2.297
1.8	.018	.04744	2.636	.8660	3.084	.09	.2121	2.357	.8886	2.958
2.0	.020	.07663	3.832	1.0110	3.978	.10	.2817	2.817	1.0690	3.689
2.2	.022	.1339	6.088	1.1947	4.999	.11	.3568	3.243	1.2699	4.443
2.4	.024	.1990	8.294	1.4443	6.036	.12	.4302	3.585	1.4808	5.190
2.6	.026	.2534	9.748	1.7077	7.022	.13	.5002	3.847	1.6931	5.919
3.0	.030	.3428	11.43	2.2099	8.856	.15	.6307	4.204	2.110	7.322
3.5	.035	.4386	12.53	2.7936	10.99	.175	.7840	4.480	2.609	8.997
4.0	.040	.5267	13.17	3.3467	13.02	.20	.9271	4.636	3.096	10.616
	$\lambda_2/\lambda_1 = 0.1$					$\lambda_2/\lambda_1 = 0.2$				
1.0	0.10	0.1325	1.325	Imag.	Imag.	0.20	0.2606	1.303	Imag.	Imag.
1.2	.12	.1742	1.451	0.3640	1.289	.24	.3349	1.396	0.2964	1.240
1.4	.14	.2264	1.617	.5540	1.692	.28	.4187	1.495	.4976	1.562
1.6	.16	.2910	1.818	.7235	2.179	.32	.5094	1.592	.6668	1.925
1.8	.18	.3662	2.035	.8940	2.724	.36	.6039	1.677	.8272	2.309
2.0	.20	.4473	2.237	1.0715	3.298	.40	.6998	1.749	.9838	2.702
2.2	.22	.5296	2.407	1.2542	3.879	.44	.7955	1.808	1.1381	3.096
2.4	.24	.6108	2.545	1.4388	4.455	.48	.8906	1.855	1.2902	3.489
2.6	.26	.6900	2.654	1.6226	5.022	.52	.9848	1.894	1.4403	3.879
3.0	.30	.8432	2.811	1.9848	6.130	.60	1.170	1.951	1.7354	4.648
3.5	.35	1.027	2.934	2.426	7.470	.70	1.398	1.997	2.096	5.590
4.0	.40	1.205	3.013	2.816	8.709	.80	1.622	2.028	2.450	6.518
	$\lambda_2/\lambda_1 = 0.3$					$\lambda_2/\lambda_1 = 0.4$				
1.0	0.30	0.3829	1.276	Imag.	Imag.	0.40	0.5002	1.250	Imag.	Imag.
1.2	.36	.4824	1.340	0.1111	1.202	.48	.6212	1.294	Imag.	Imag.
1.4	.42	.5879	1.400	.3746	1.453	.56	.7456	1.332	Imag.	Imag.
1.6	.48	.6968	1.452	.5429	1.733	.64	.8716	1.362	0.3177	1.612
1.8	.54	.8071	1.495	.6907	2.024	.72	.9980	1.386	.4637	1.853
2.0	.60	.9208	1.535	.8093	2.319	.80	1.124	1.405	.5916	2.091
2.2	.66	1.028	1.557	.9620	2.615	.88	1.250	1.421	.7082	2.331
2.4	.72	1.137	1.580	1.0911	2.911	.96	1.376	1.433	.8181	2.571
2.6	.78	1.246	1.598	1.2174	3.205	1.04	1.500	1.443	.9236	2.810
3.0	.90	1.463	1.625	1.4640	3.789	1.20	1.749	1.458	1.1242	3.288
3.5	1.05	1.730	1.648	1.7640	4.510	1.40	2.058	1.470	1.3688	3.881
4.0	1.20	1.996	1.663	2.0581	5.224	1.60	2.365	1.478	1.6048	4.471

[1]Imaginary.

TABLE II

VALUES OF $(B_m)_{cr}$, $(B_1)_{cr}$, AND R_{cr} COMPUTED FROM EQUATIONS (40) AND (41) - Concluded

(b) m = 3

λ_1	λ_3	$(B_3)_{cr}$	$(B_3)_{cr}/\lambda_3$	$(B_1)_{cr}$	R_{cr}	λ_3	$(B_3)_{cr}$	$(B_3)_{cr}/\lambda_3$	$(B_1)_{cr}$	R_{cr}
	$\lambda_3/\lambda_1 = 0.01$					$\lambda_3/\lambda_1 = 0.05$				
1.0	0.010	0.01125	1.125	Imag.	Imag.	0.05	0.05623	1.125	Imag.	Imag.
1.2	.012	.01402	1.168	0.3779	1.312	.06	.07001	1.167	0.3762	1.308
1.4	.014	.01712	1.223	.5647	1.762	.07	.08540	1.220	.5617	1.750
1.6	.016	.02069	1.293	.7342	2.364	.08	.1030	1.287	.7183	2.323
1.8	.018	.02490	1.383	.8622	3.088	.09	.1236	1.374	.8530	3.035
2.0	.020	.02998	1.499	1.0000	3.996	.10	.1473	1.473	1.0025	3.894
2.2	.022	.03642	1.655	1.1265	5.083	.11	.1758	1.598	1.1425	4.903
2.4	.024	.04460	1.858	1.2611	6.381	.12	.2098	1.748	1.2817	6.054
3.0	-----	-------	-----	------	-----	----	-------	-----	------	-----
4.0	-----	-------	-----	------	-----	----	-------	-----	------	-----
	$\lambda_3/\lambda_1 = 0.1$					$\lambda_3/\lambda_1 = 0.2$				
1.0	0.10	0.1112	1.122	0.1463	0.9969	0.20	0.2234	1.117	Imag.	Imag.
1.2	.12	.1395	1.162	.3693	1.295	.24	.2760	1.150	0.3172	1.255
1.4	.14	.1696	1.211	.5538	1.716	.28	.3321	1.186	.5110	1.610
1.6	.16	.2032	1.270	.7109	2.249	.32	.3919	1.225	.6694	2.036
1.8	.18	.2408	1.338	.8587	2.893	.36	.4549	1.264	.8163	2.516
2.0	.20	.2828	1.414	1.0025	3.649	.40	.5203	1.301	.9601	3.038
2.2	.22	.3292	1.496	1.1466	4.476	.44	.5877	1.336	1.101	3.589
2.4	.24	.3794	1.581	1.2950	5.386	.48	.6562	1.367	1.2416	4.159
2.6	.26	.4324	1.663	1.4486	6.348	.52	.7254	1.395	1.3821	4.740
3.0	----	------	-----	------	-----	.60	.8644	1.441	1.6620	5.913
4.0	----	------	-----	------	-----	.80	1.209	1.512	2.3557	8.821
	$\lambda_3/\lambda_1 = 0.3$					$\lambda_3/\lambda_1 = 0.4$				
1.0	0.30	0.3327	1.109	Imag.	Imag.	0.40	0.4402	1.101	Imag.	Imag.
1.2	.36	.4082	1.134	0.2086	1.213	.48	.5370	1.119	Imag.	Imag.
1.4	.42	.4867	1.159	.4133	1.501	.56	.6358	1.135	0.2668	1.420
1.6	.48	.5677	1.183	.5854	1.828	.64	.7360	1.150	.4428	1.677
1.8	.54	.6503	1.204	.7293	2.184	.72	.8371	1.163	.5833	1.951
2.0	.60	.7341	1.224	.8636	2.556	.80	.9385	1.173	.7100	2.233
2.2	.66	.8185	1.240	.9942	2.938	.88	1.040	1.182	.8283	2.520
2.4	.72	.9032	1.254	1.1216	3.326	.96	1.142	1.189	.9422	2.808
2.6	.78	.9881	1.267	1.2464	3.716	1.04	1.243	1.196	1.0525	3.097
3.0	.90	1.158	1.286	1.4932	4.496	1.20	1.446	1.205	1.2508	3.666
3.5	1.05	1.369	1.303	1.7944	5.465	1.40	1.699	1.213	1.5276	4.391
4.0	1.20	1.579	1.315	2.092	6.423	1.60	1.951	1.219	1.7818	5.101

TABLE III

VALUES OF R_{cr} FOR A SINUSOIDALLY LOADED ARCH HAVING NONZERO λ_1 AND λ_m COMPUTED FROM EQUATION (44)

[Dashed lines indicate that there is no critical load]

(a) m = 3

λ_3/λ_1 \ λ_1	1.0	1.2	1.4	1.6	1.8	2.0	2.2	2.4	2.6	3.0	3.5	4.0
0.01	1.0000	1.3121	1.7615	2.3637	3.0881	3.9955	5.0877	6.3812	7.5720	9.6960	12.1039	14.3783
.05	------	1.3079	1.7499	2.3228	3.0349	3.8945	4.9029	6.0540	7.2662	9.3967	11.7881	14.0371
.1	------	1.2953	1.7161	2.2493	2.8926	3.6492	4.4765	5.3864	6.3485	8.3545	10.7127	12.8865
.2	------	1.2547	1.6105	2.0359	2.5164	3.0383	3.5892	4.1589	4.7396	5.9134	7.3769	8.8213
.3	------	1.2132	1.5011	1.8285	2.1840	2.5562	2.9384	3.3260	3.7159	4.4964	5.4650	6.4228
.4	------	------	1.4195	1.6772	1.9510	2.2332	2.5196	2.8081	3.0971	3.6657	4.3906	5.1012

(b) m = 2

λ_2/λ_1 \ λ_1	1.0	1.2	1.4	1.6	1.8	2.0	2.2	2.4	2.6	3.0	3.5	4.0
0.01	------	1.3121	1.7612	2.3476	3.0837	3.9775	4.9991	6.0364	7.0223	8.8561	10.9893	13.0235
.05	------	1.3060	1.7422	2.2970	2.9577	3.6889	4.4435	5.1904	5.9191	7.3218	8.9975	10.6163
.1	------	1.2887	1.6917	2.1790	2.7243	3.2982	3.8788	4.4548	5.0223	6.1296	7.4705	8.7094
.2	------	1.2397	1.5616	1.9248	2.3091	2.7019	3.0964	3.4892	3.8788	4.6475	5.5905	6.5179
.3	------	1.2017	1.4534	1.7328	2.0236	2.3185	2.6150	2.9106	3.2049	3.7888	4.5102	5.2240
.4	------	------	------	1.6120	1.8530	2.0910	2.3306	2.5705	2.8102	3.2878	3.8814	4.4714

TABLE IV

VALUES OF k FROM EQUATION (62)

λ_1	k
1.0	0.1929×10^{-3}
1.2	.3578
1.4	.7075
1.6	1.408
1.8	2.767
2.0	5.486
2.2	10.83
2.4	21.70

TABLE V

VALUES OF R_{cr} FOR A SINUSOIDAL ARCH WITH A CENTRAL CONCENTRATED LOAD

λ_1	R_{cr}
2.4	3.089
2.6	3.678
3.0	4.716
3.5	5.890
4.0	7.000
4.5	8.072
5.0	9.122
5.5	10.156
6.0	11.179
6.5	12.193
7.0	13.201
7.5	14.204
8.0	15.206
8.5	16.203
9.0	17.195

TABLE VI

CRITICAL CONDITIONS FOR CENTRALLY LOADED ARCHES WITH

$\lambda_2 = 0.005\lambda_1$ AND $\lambda_3 = 0.040\lambda_1$

λ_1	$(B_1)_{cr}$	$(B_2)_{cr}$	R_{cr}	$(B_3)_{cr}$	$\frac{(\sigma_c)_{cr}}{\sigma_p}$	$\frac{(\sigma_b)_{cr,max}}{\sigma_p}$	Max. critical stress (psi) (1)
1.2	0.3713	0.0088	0.651	0.075	1.28	3.85	8.4×10^3
1.5	.6310	.01351	.996	.108	1.84	4.50	10.4
2.0	.9895	.03263	1.878	.196	2.79	7.21	16.3
2.5	1.4003	.1157	3.048	.290	3.57	9.74	21.8
3.0	1.9770	.2175	4.193	.380	3.73	11.63	25.1
4.0	3.0494	.3605	6.236	.541	3.78	15.16	30.9
5.0	4.039	.4831	8.140	.693	3.79	18.7	36.8
6.0	4.990	.5991	9.986	.842	3.80	22.3	42.6
7.0	5.922	.7120	11.800	.990	3.80	25.9	48.5
8.0	6.841	.8231	13.596	1.136	3.81	29.5	54.5
9.0	7.752	.9332	15.380	1.282	3.81	33.1	60.3

(1) Highest outer fiber stress in arches representative of test specimens ($E = 10.3 \times 10^6$ psi, $L = 18$ in., and $t = 0.25$ in.).

TABLE VII

EFFECT OF FLEXIBILITY OF SUPPORT ON CRITICAL LOAD

(a) Values of R_{cr} as a function of β

β \ λ_1	1.0	1.2	1.4	1.6	1.8	2.0	2.2	2.4	2.6	3.0	3.5	4.0
1.0	1.000	1.312	1.762	2.350	3.080	4.000	5.096	6.380	7.584	9.708	12.12	14.39
.95	-----	1.288	1.716	2.277	2.983	3.850	4.895	6.135	7.391	9.564	12.01	14.30
.90	-----	1.265	1.671	2.204	2.876	3.701	4.694	5.873	7.166	9.402	11.88	14.20
.80	-----	1.226	1.584	2.062	2.664	3.404	4.295	5.349	6.584	9.000	11.58	13.95
.70	-----	1.200	1.504	1.924	2.457	3.155	3.897	4.829	5.917	8.439	11.17	13.62
.60	-----	-----	1.437	1.795	2.256	2.823	3.505	4.312	5.255	7.587	10.59	13.16
.50	-----	-----	-----	1.681	2.066	2.544	3.121	3.803	4.598	6.565	9.686	12.48

(b) Solution of equation (71)

β	$(\lambda_1)_o$
1.0	2.345
.95	2.406
.90	2.471
.80	2.622
.70	2.803
.60	3.028
.50	3.317

TABLE VIII

VALUES OF R_{cr} FOR A SINUSOIDAL ARCH WITH A CENTRAL ELASTIC SUPPORT AND $q = q_o \sin \frac{\pi x}{L}$

λ_1 \ μ	0.5	1.0	1.5	2.0	3.0
1.42	2.82	No solution in this region			
1.60	3.34				
1.74	3.87	5.10			
1.80	4.11	5.32			
2.00	5.06	6.25	7.61	9.28	12.46
2.20	6.21	7.40	8.54	9.62	11.66
2.40	7.43	8.43	9.38	10.29	12.00
3.00	10.45	11.17	11.84	12.49	13.70
3.50	17.73	13.32	13.87	14.40	16.40
4.00	14.92	15.42	15.89	16.34	17.20

TABLE IX

THEORETICAL AND EXPERIMENTAL DATA

Specimen (1)	Length (in.)	Width (in.)	Thickness (in.)	λ_1	λ_2	λ_3	Buckling load (lb)	$(R_{cr})_{exp}$	$\frac{(R_{cr})_{exp}}{(R_{cr})_{class}}$
1	18	0.500	0.249	3.78	0.0138	0.136	82.7	5.19	0.880
2	$17\frac{15}{16}$	.495	.1885	9.12	.0055	.344	85.7	16.37	1.004
3	18	.500	.249	4.25	.0097	.146	107.0	6.72	.955
4	18	.499	.249	3.32	.0055	.114	73.7	4.63	.915
5	$17\frac{31}{32}$	.501	.249	2.63	.0417	.097	33.9	2.11	.653
6	$18\frac{1}{32}$	.493	.249	1.83	.0146	.063	16.2	1.04	.671
7	18	.502	.250	4.71	.0842	.159	98.5	6.07	.884
8	18	.502	.251	4.07	.0496	.167	94.4	5.72	.976
9	18	.504	.251	3.67	.0666	.164	80.0	4.83	.988
10	18	.505	.250	3.30	.0178	.123	60.4	3.70	.781
11	18	.502	.250	3.90	.0264	.126	96.7	5.95	1.003
12	18	.505	.250	5.31	.0015	.185	139.8	8.55	.926
13	18	.503	.250	5.07	.0957	.131	115.8	6.98	.925
14	$17\frac{31}{32}$	.502	.374	1.86	.0076	.0582	83.3	1.02	.630
15	$17\frac{15}{16}$	.500	.375	1.67	.0170	.0610	73.0	.886	.703
16	$17\frac{31}{32}$	.501	.374	1.38	.0013	.0459	(2)	------	-----
17	$17\frac{15}{16}$	.501	.374	1.265	.0141	.0472	(2)	------	-----
18	$17\frac{31}{32}$	.502	.374	2.44	.0015	.0850	157.3	1.93	.666
19	$17\frac{31}{32}$	.499	.374	2.08	.0043	.0707	129.9	1.60	.773
20	$17\frac{15}{16}$	.503	.374	1.34	.0244	.0500	(2)	------	-----
21	$17\frac{31}{32}$	.502	.374	2.43	.0112	.0883	176.9	2.16	.745
22	18	.501	.186	6.08	.0058	.237	48.2	9.70	.930
23	18	.499	.185	6.43	.0031	.236	53.6	10.96	.978
24	18	.500	.185	7.23	.0225	.257	62.5	12.89	1.031
25	18	.500	.186	9.15	.0007	.311	73.0	14.73	1.016

[1]Material: Specimens 1 to 13 and 22 to 25, 24S-T3; specimens 14 to 21, 75S-T6.
$E = 10.3 \times 10^7$ psi.

[2]Specimen did not buckle.

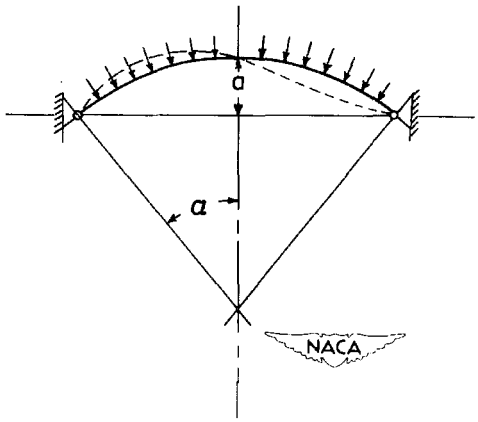

Figure 1.- Buckling mode for a high arch.

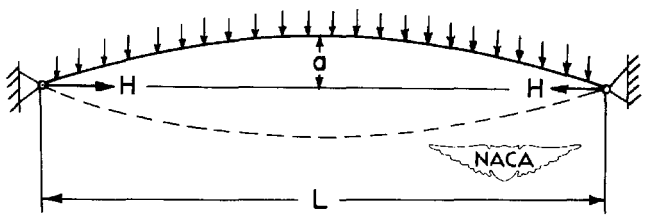

Figure 2.- Possible buckling mode for a low arch.

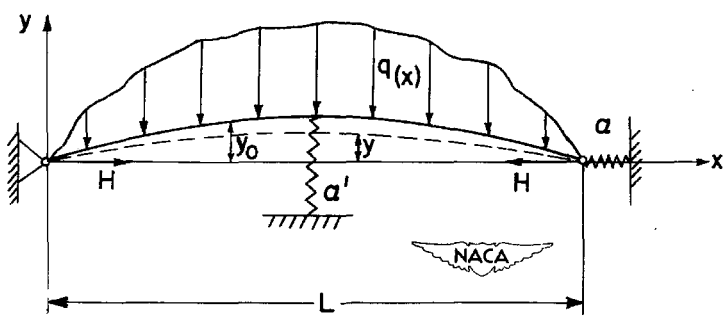

Figure 3.- Coordinate system.

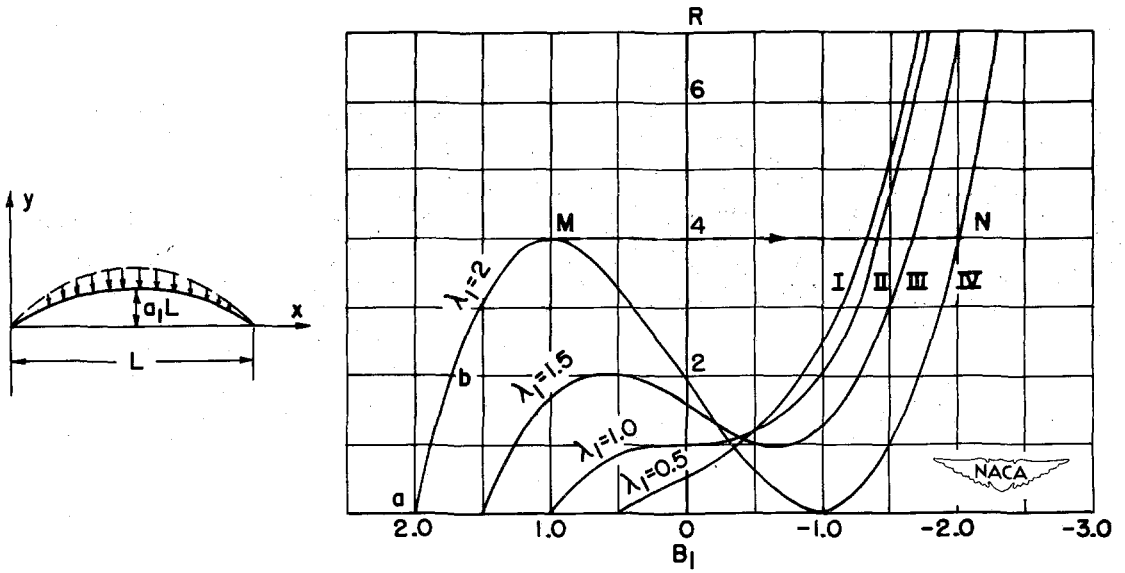

Figure 4.- Relation between B_1 and R for symmetrical buckling of a sinusoidal arch under a sinusoidal load.

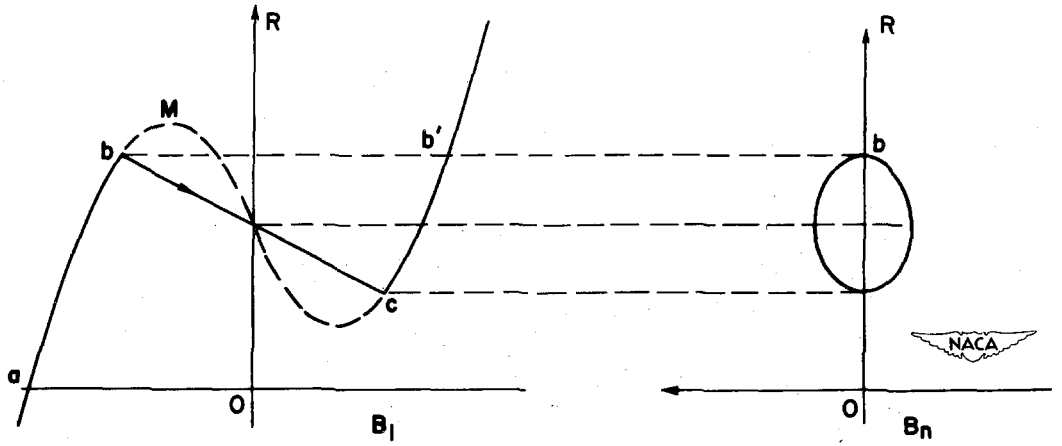

Figure 5.- Relations between B_1, B_n, and R for a sinusoidal arch which buckles in the -nth mode.

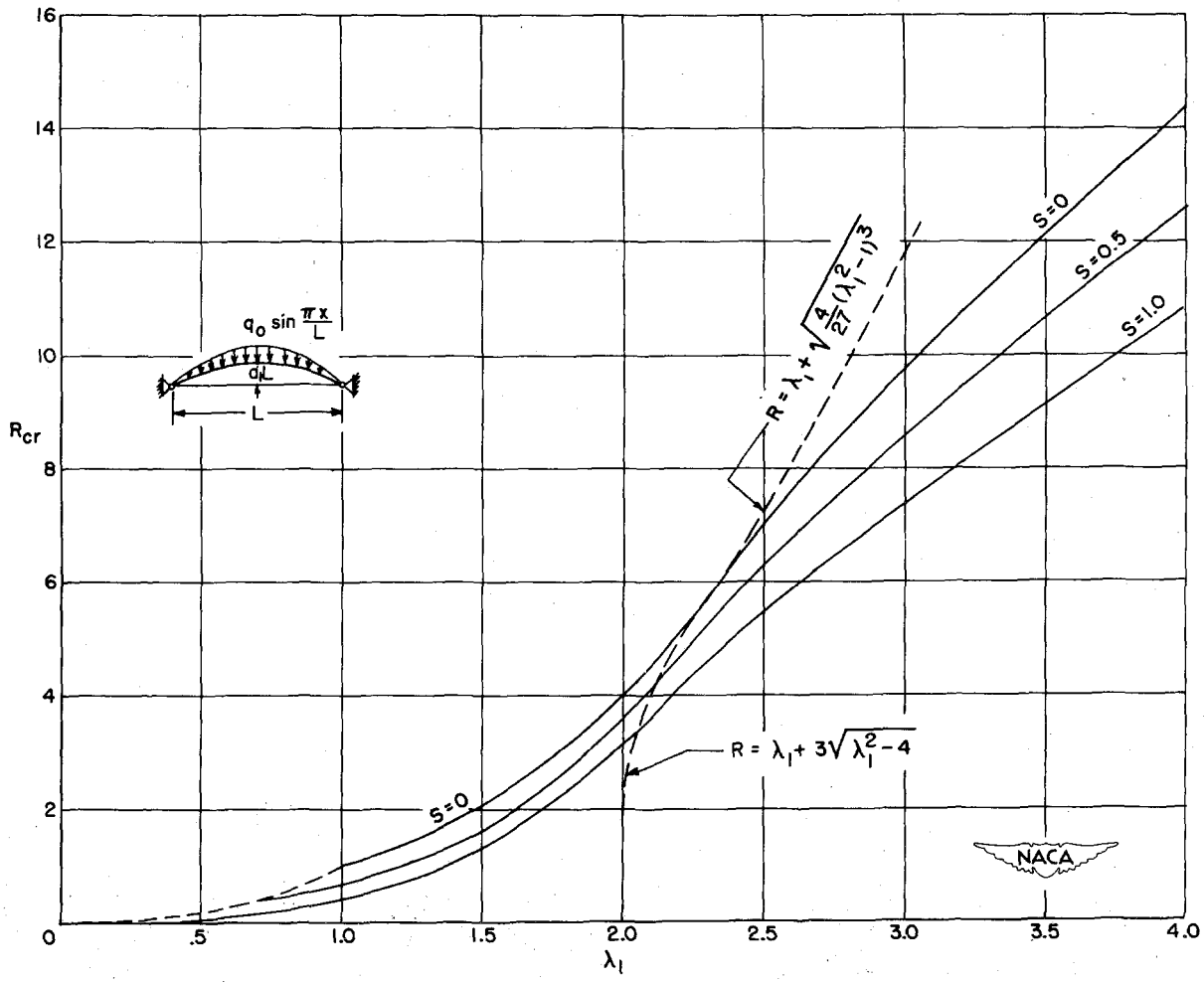

Figure 6.- Critical load on a sinusoidal arch as a function of arch rise.

$$\lambda_1 = \frac{a_1 L}{2}\sqrt{\frac{A}{I}};\quad R = \frac{q_o L^4}{2\pi^4 EI}\sqrt{\frac{A}{I}}.$$

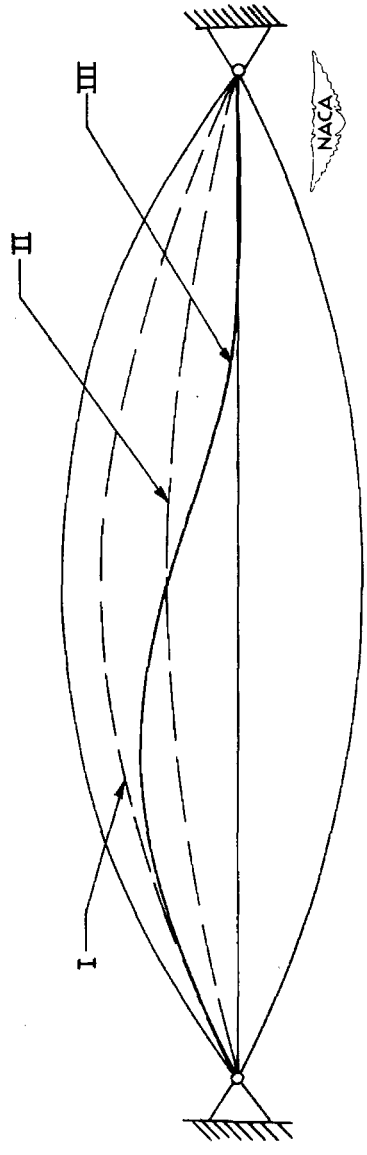

Figure 7.- Deformation history of a sinusoidal arch.

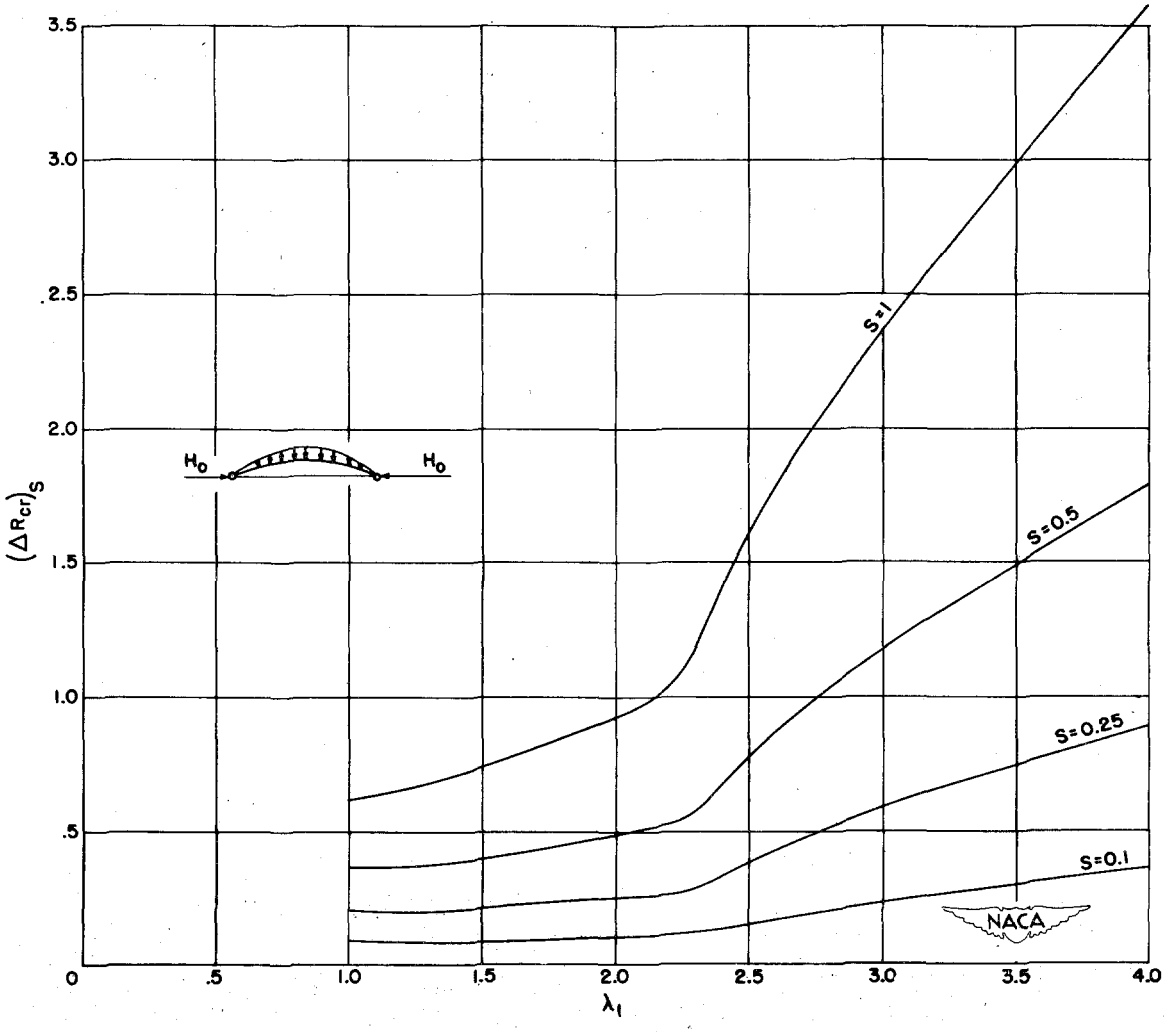

Figure 8.- Change of critical load due to initial thrust H_o.
$(\Delta R_{cr})_S = (R_{cr})_{S=0} - (R_{cr})_{S=S}$; $S = H_o L^2/\pi^2 EI$.

(a) m = 2; $a_2/a_1 = -1/3$.

(b) m = 3; $a_3/a_1 = -1/3$.

(c) m = 3; $a_3/a_1 = 1/3$.

Figure 9.- Examples of low arches having nonsinusoidal center lines.

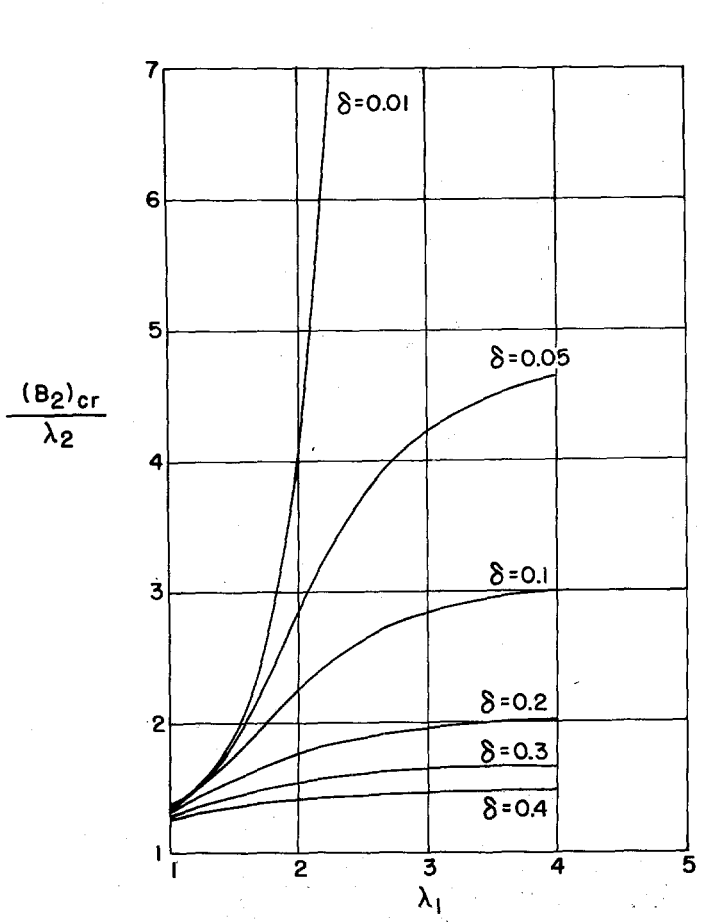

(a) Ratio of $(B_2)_{cr}/\lambda_2 = (b_2)_{cr}/a_2$.

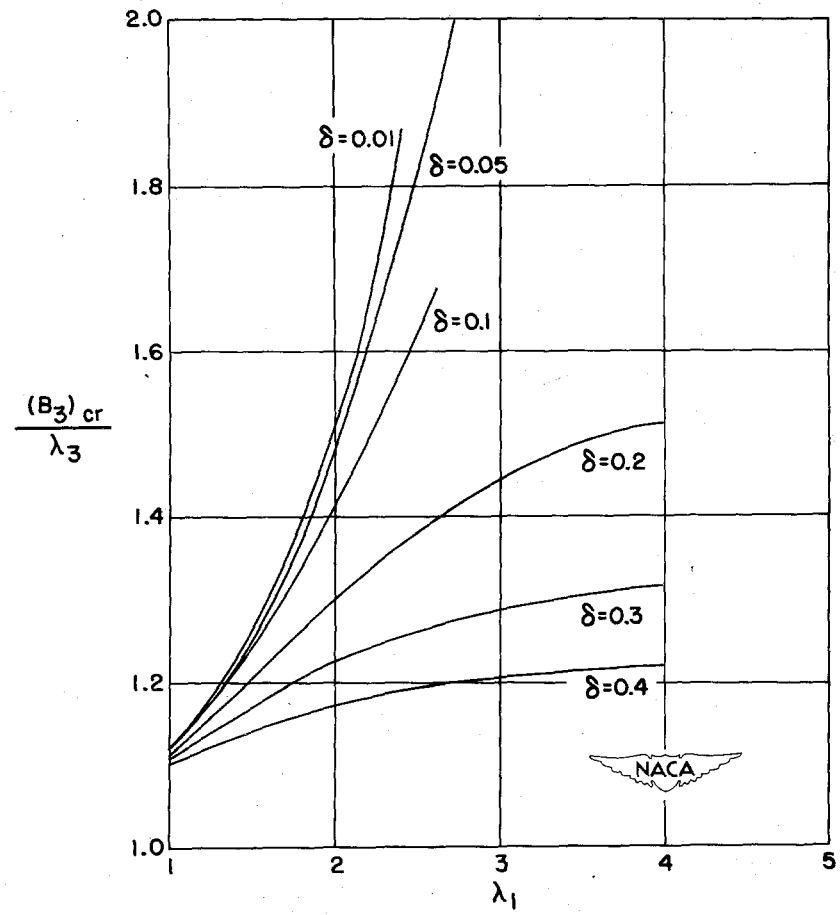

(b) Ratio of $(B_3)_{cr}/\lambda_3 = (b_3)_{cr}/a_3$.

Figure 10.- Solution of equation (40) for m = 2 and m = 3.

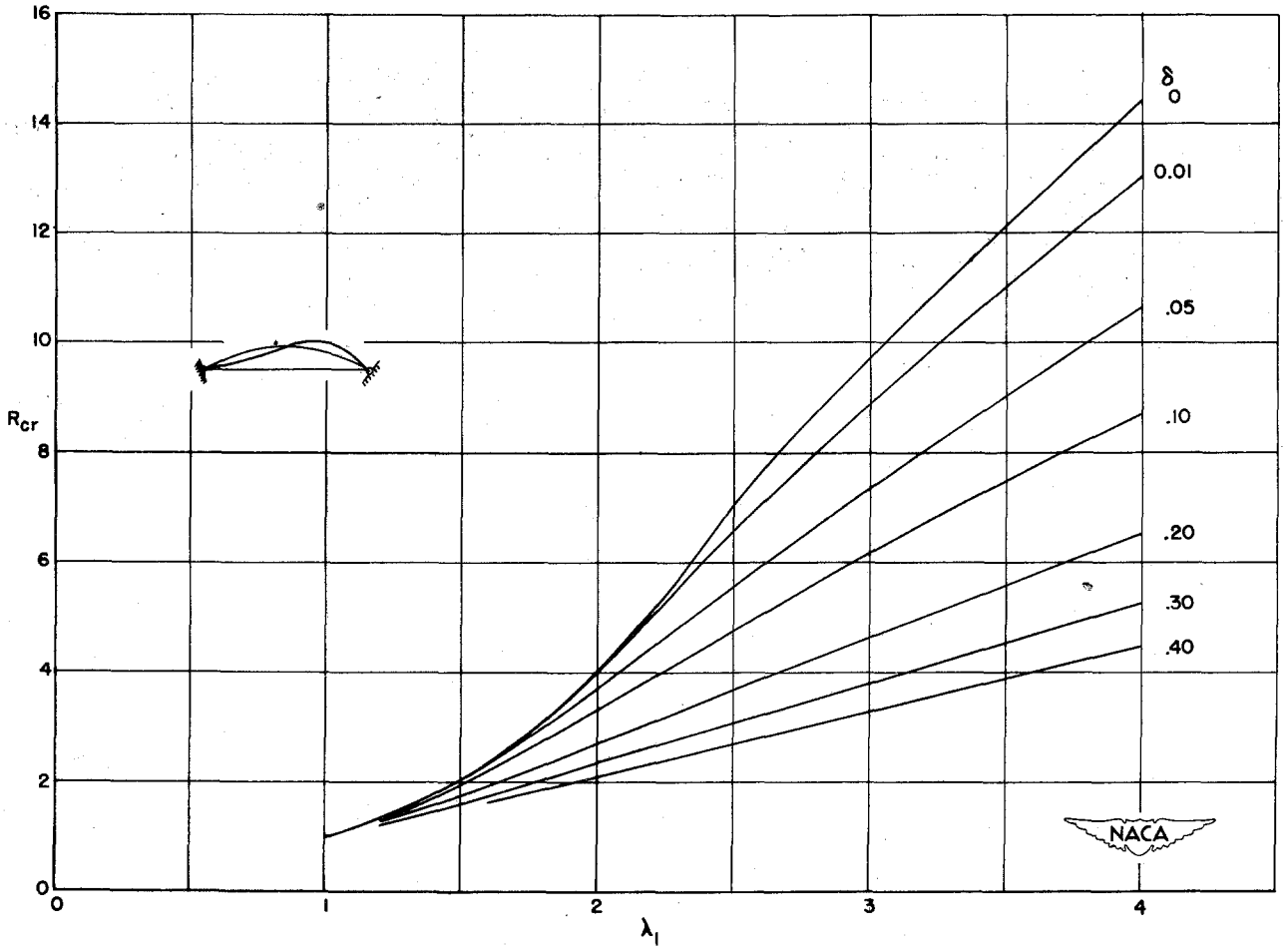

(a) $m = 2$; $\delta = \left|\frac{a_2}{a_1}\right|$.

Figure 11.- R_{cr} (sinusoidal) for arch forms $\frac{y_o}{L} = a_1 \sin\frac{\pi x}{L} + a_m \sin\frac{m\pi x}{L}$ with $m = 2$ and 3.

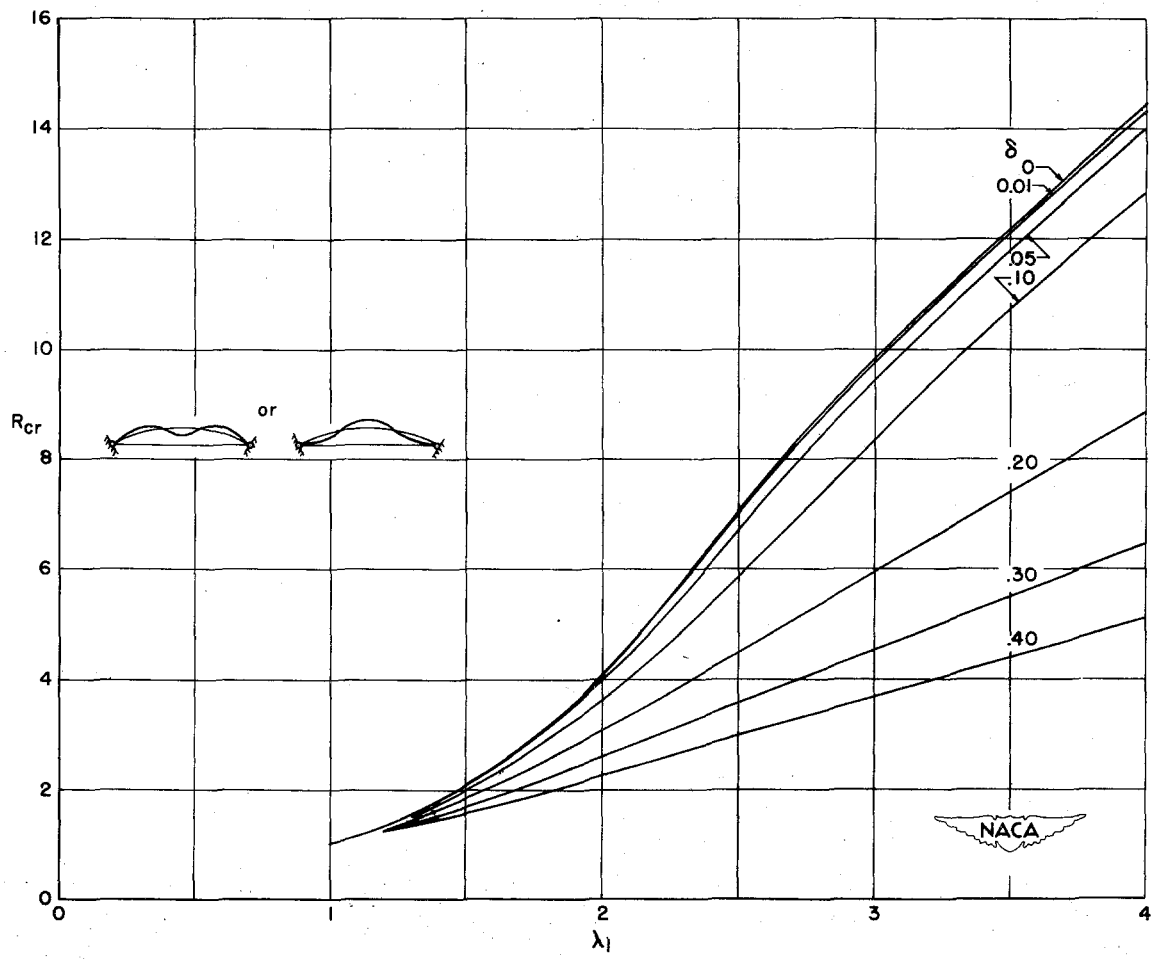

(b) $m = 3$; $\delta = \left|\frac{a_3}{a_1}\right|$.

Figure 11.- Concluded.

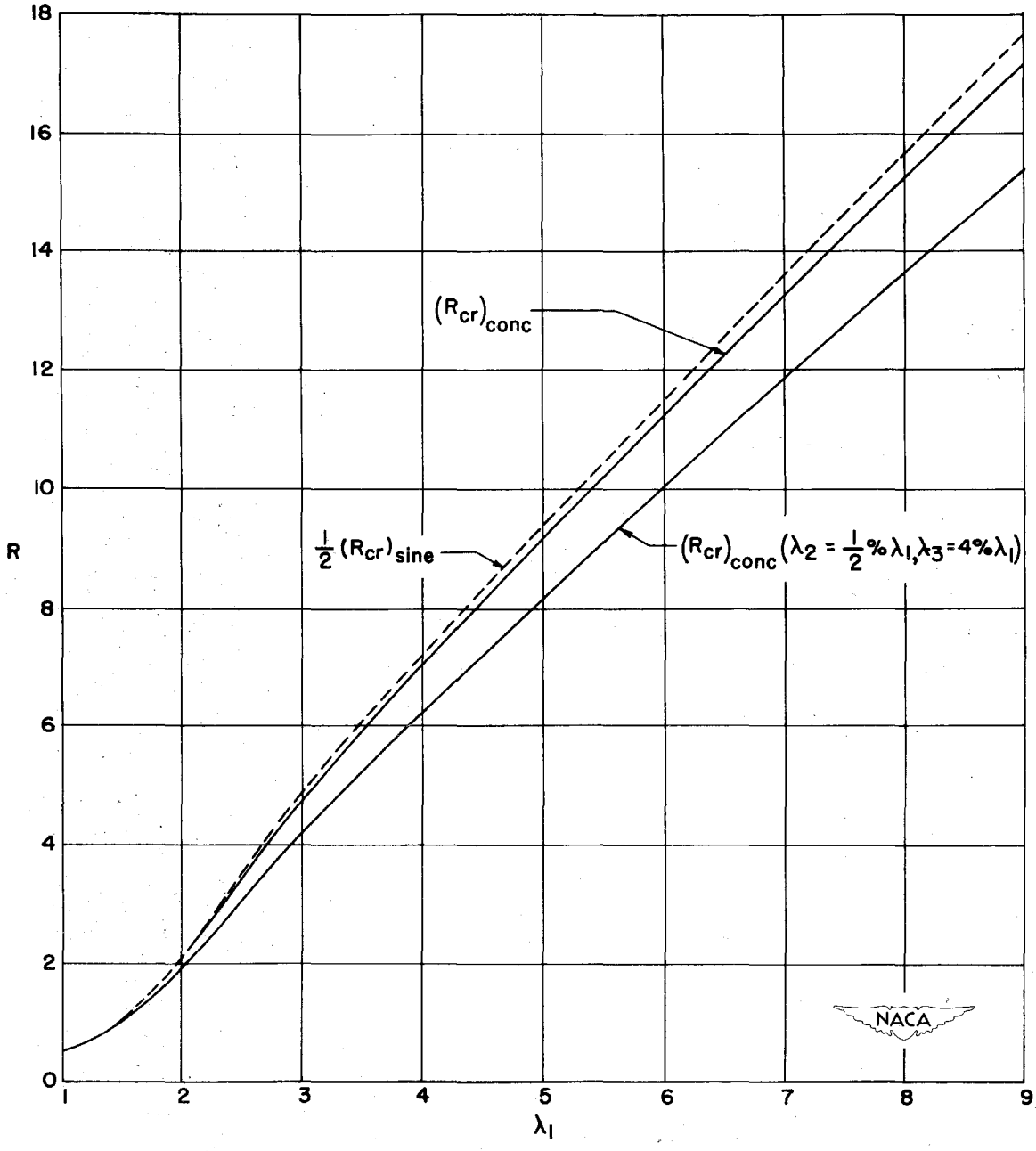

Figure 12.- R_{cr} for arches under a concentrated central load.

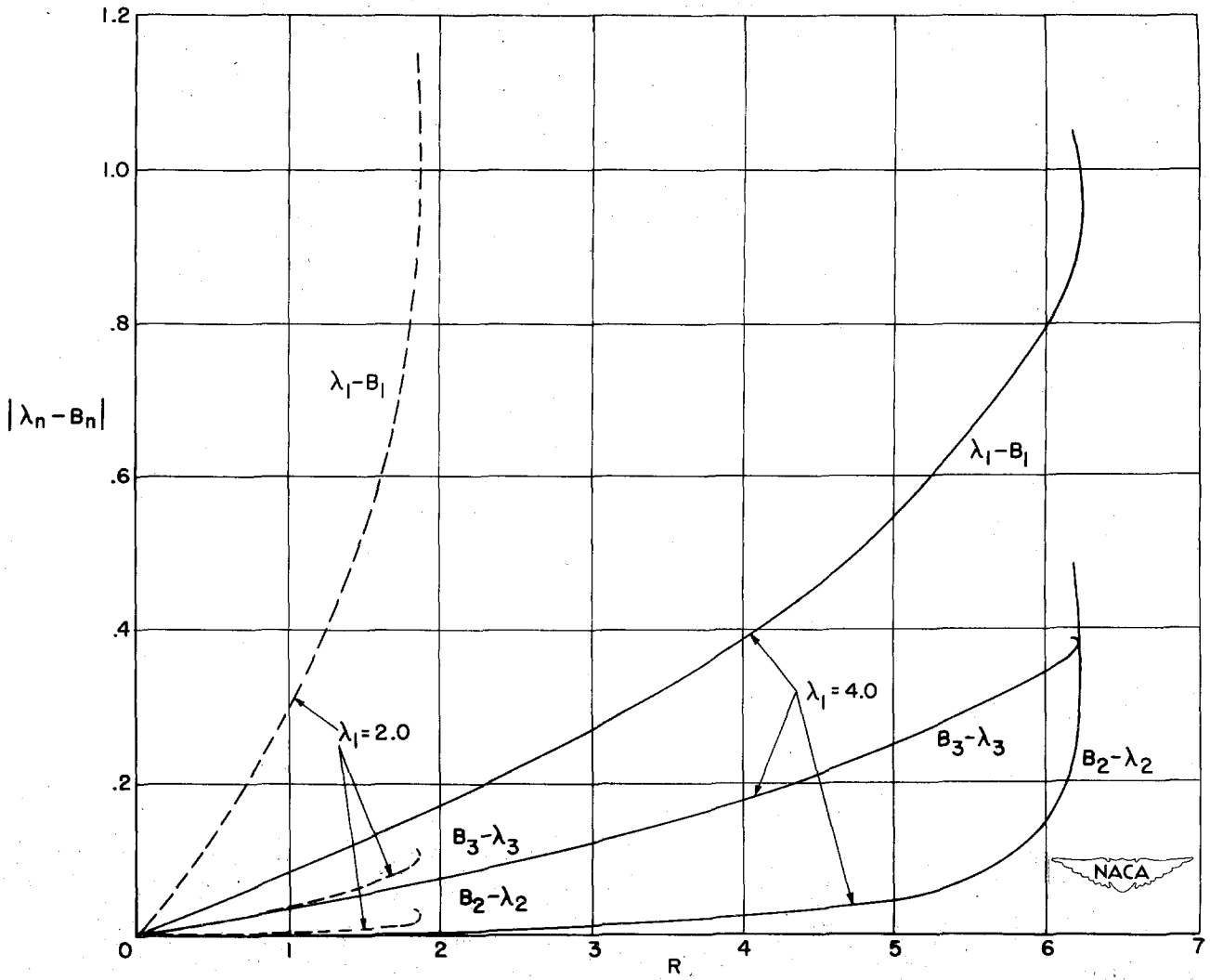

Figure 13.- Variation with load of first three modes of two centrally loaded arches having $\lambda_2/\lambda_1 = 0.005$ and $\lambda_3/\lambda_1 = 0.040$.

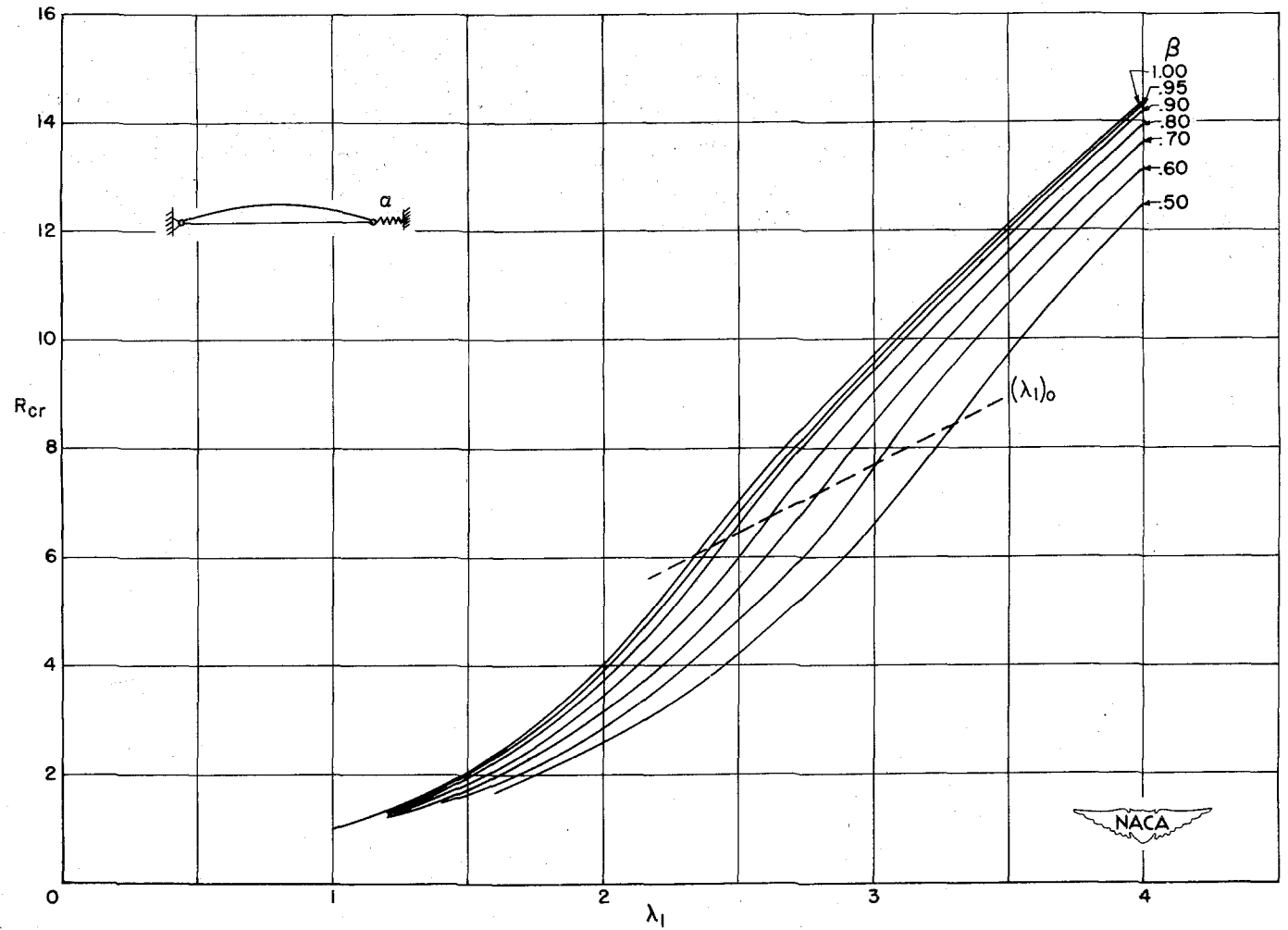

Figure 14.- Effect of support flexibility on critical load. $\beta = \dfrac{\alpha}{\alpha + \frac{EA}{L}}$.

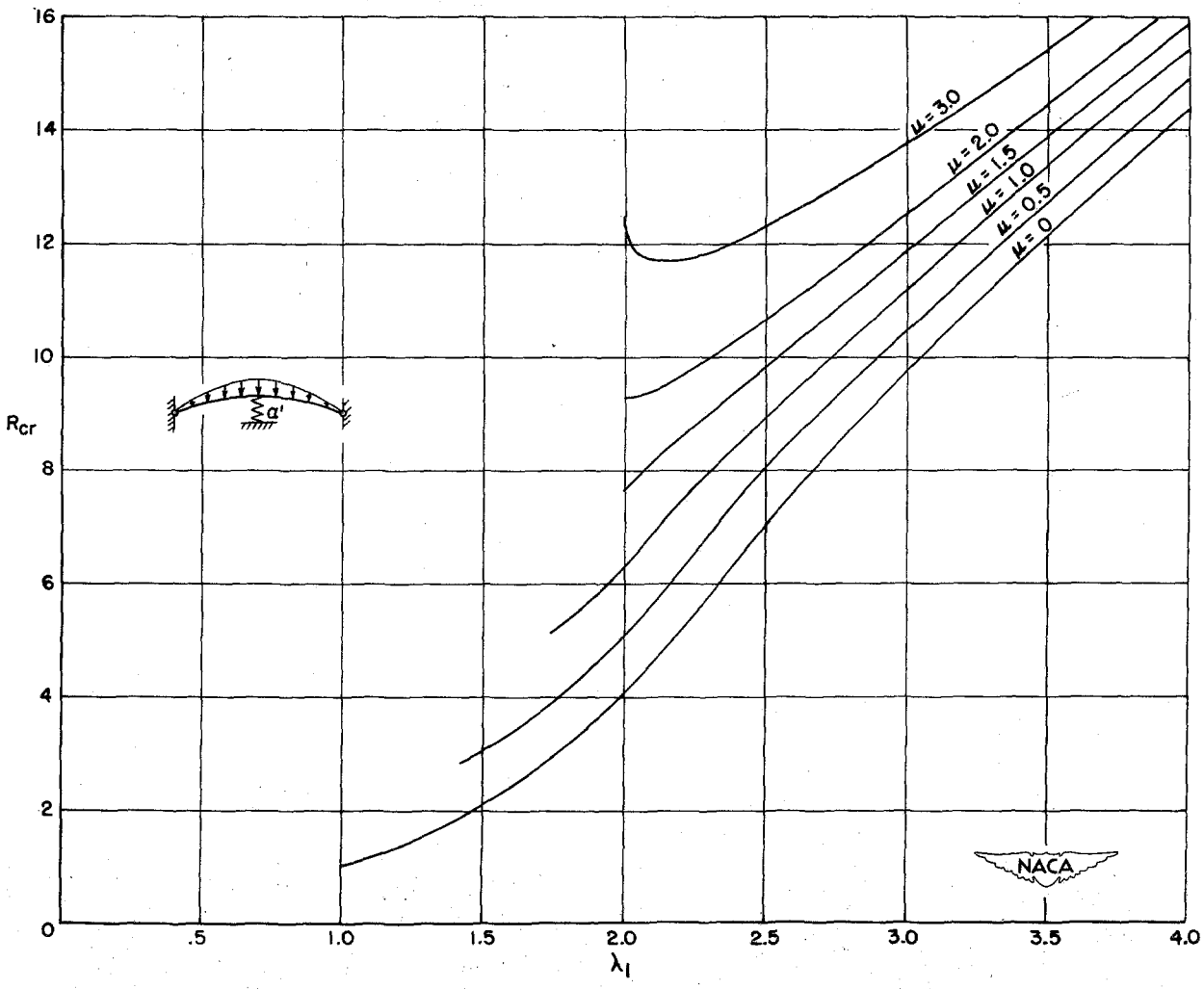

Figure 15.- Critical load of a sinusoidal arch having a central elastic support. $\mu = 2L^3\alpha'/\pi^4 EI$.

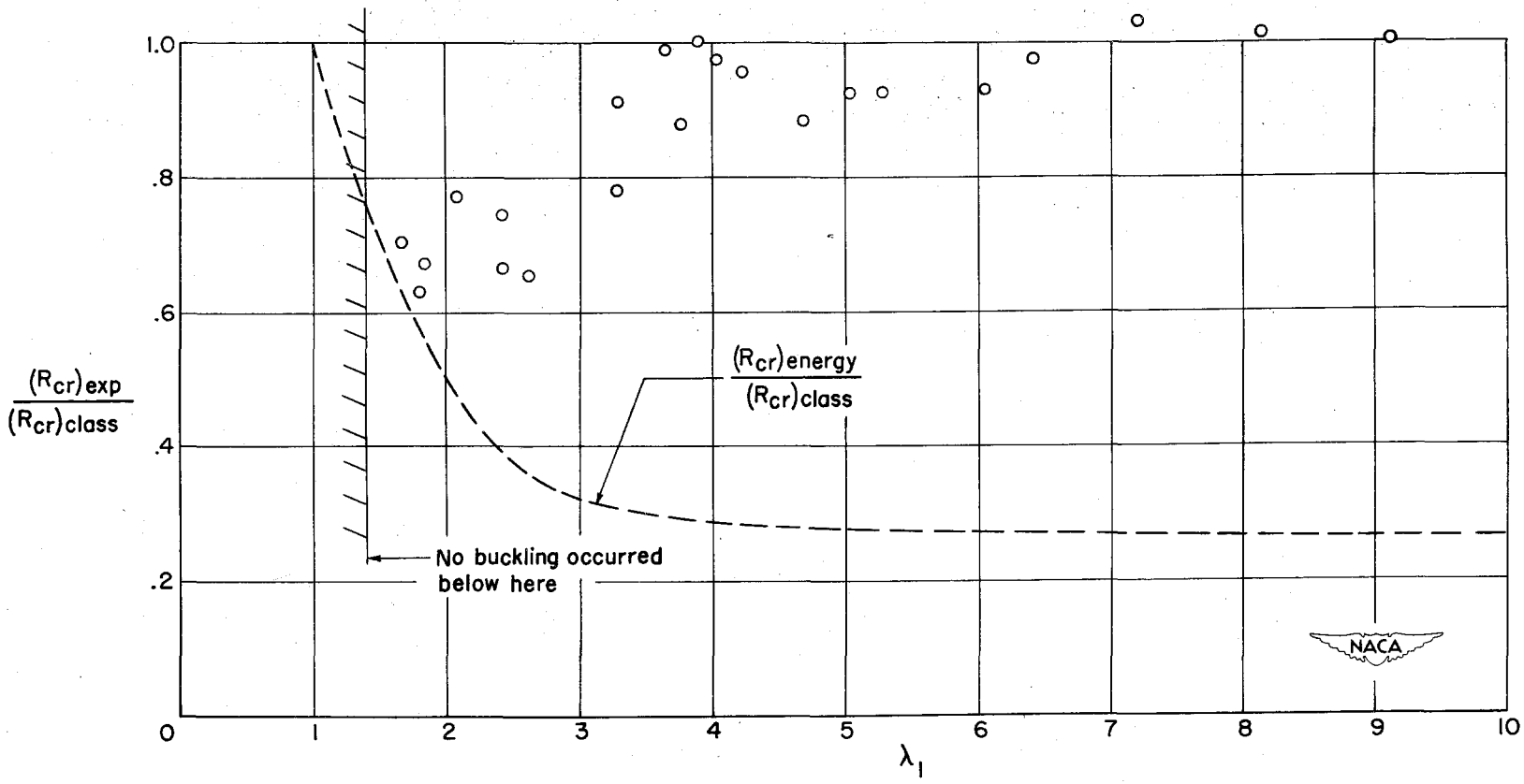

Figure 16.- Theoretical and experimental results.

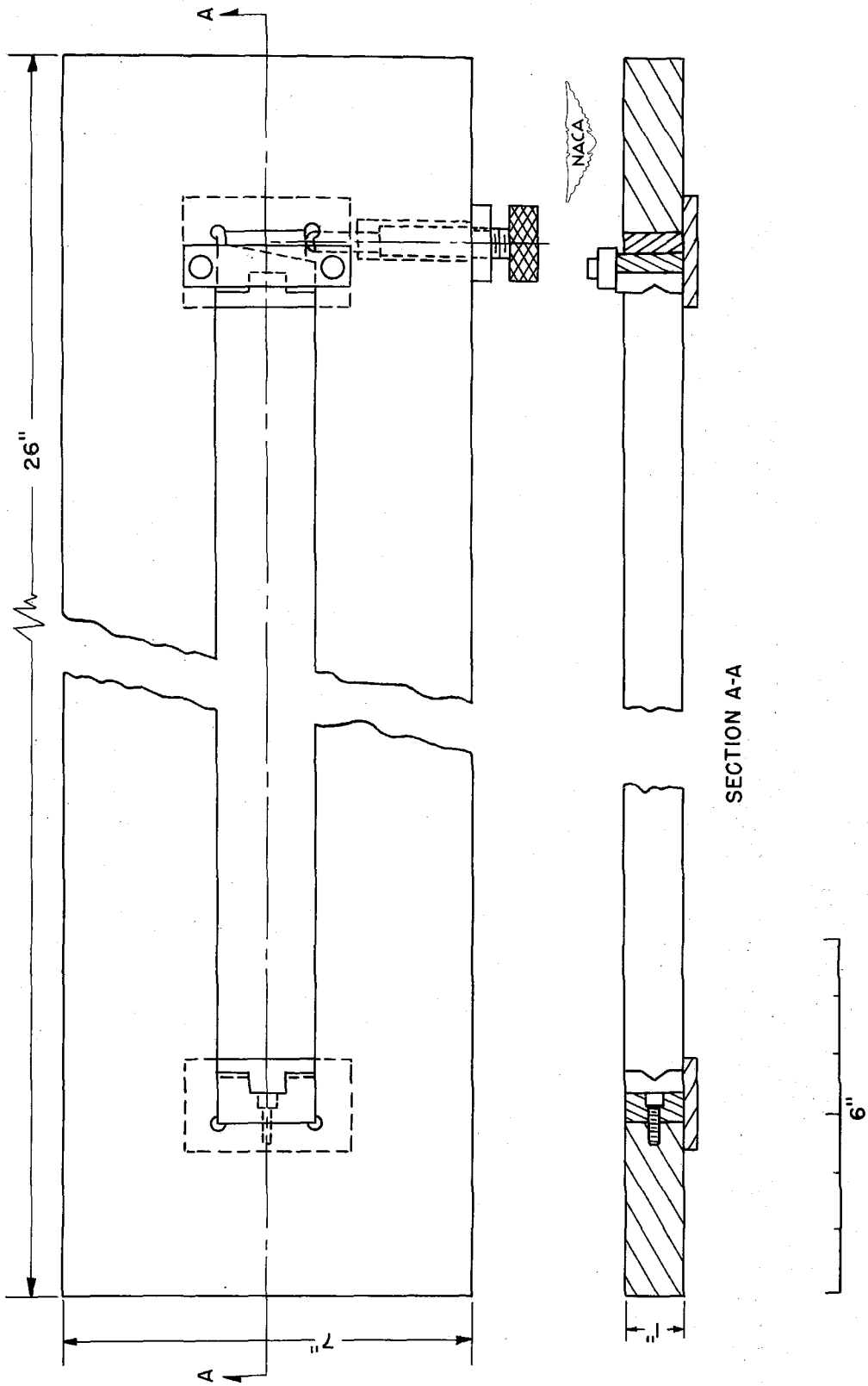

Figure 17.- Testing jig.

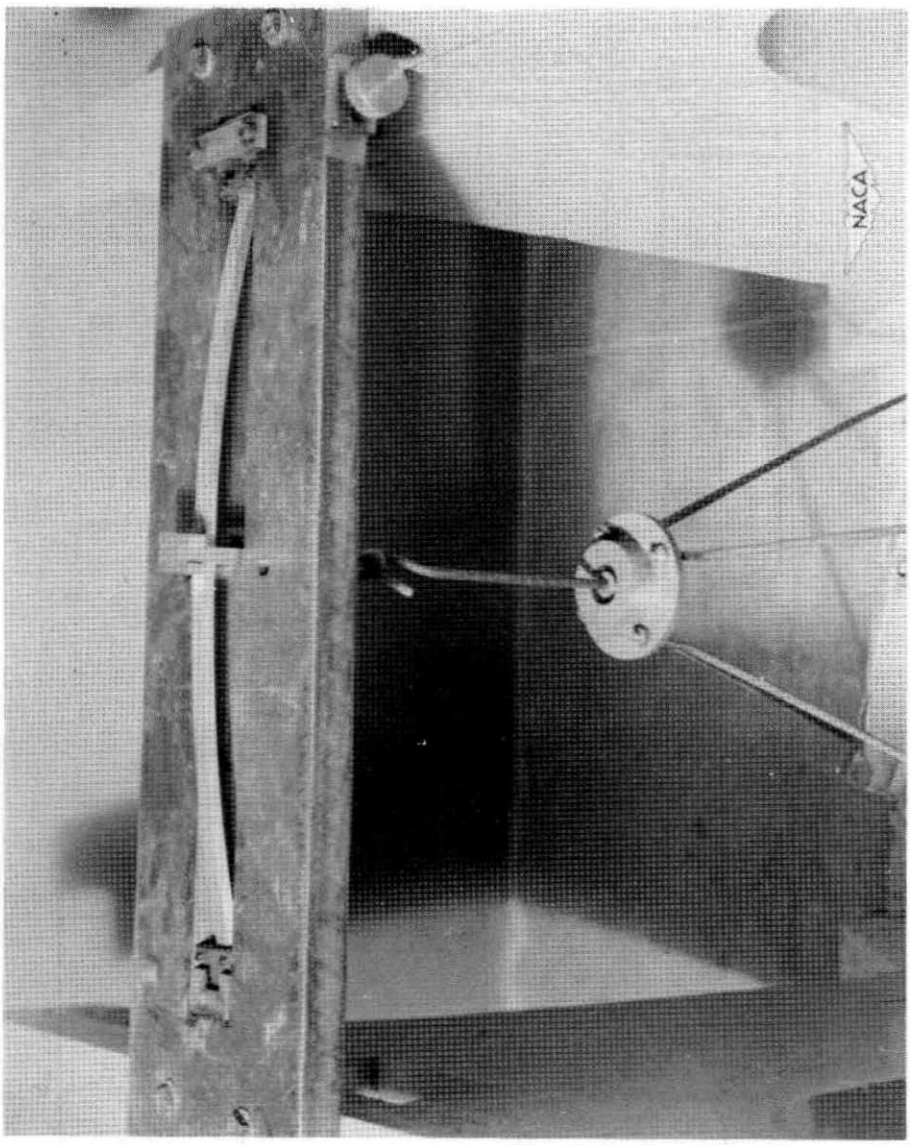

Figure 18.- Testing apparatus with specimen in place.

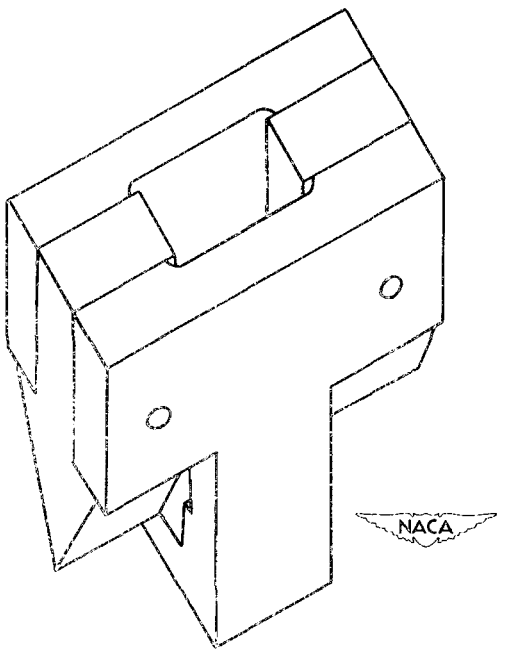

Figure 19.- Knife-edge fitting.

NACA TN 2840
National Advisory Committee for Aeronautics.
BUCKLING OF LOW ARCHES OR CURVED BEAMS OF SMALL CURVATURE. Y. C. Fung and A. Kaplan, California Institute of Technology. November 1952. 75p. diagrs., photo., 9 tabs. (NACA TN 2840)

A general solution, based on the classical buckling criterion, is given for the problem of buckling of low arches under a lateral loading acting toward the center of curvature. For a sinusoidal arch under sinusoidal loading, the critical load can be expressed exactly as a simple function of the beam dimension parameters. For other arch shapes and load distributions, approximate values of the critical load can be obtained by summing a few terms of a rapidly converging Fourier series. The effects of initial end thrust and axial and lateral elastic support are discussed. The buckling load based on the

Copies obtainable from NACA, Washington (over)

1. Columns, Beam (4.3.1.2)
2. Plates, Curved - Unstiffened (4.3.3.2.1)
3. Loads and Stresses, Structural - Normal Pressures (4.3.7.8)

I. Fung, Yuan-Cheng
II. Kaplan, A.
III. NACA TN 2840
IV. Guggenheim Aeronautical Lab., Calif. Inst. of Tech.

NACA TN 2840
National Advisory Committee for Aeronautics.
BUCKLING OF LOW ARCHES OR CURVED BEAMS OF SMALL CURVATURE. Y. C. Fung and A. Kaplan, California Institute of Technology. November 1952. 75p. diagrs., photo., 9 tabs. (NACA TN 2840)

A general solution, based on the classical buckling criterion, is given for the problem of buckling of low arches under a lateral loading acting toward the center of curvature. For a sinusoidal arch under sinusoidal loading, the critical load can be expressed exactly as a simple function of the beam dimension parameters. For other arch shapes and load distributions, approximate values of the critical load can be obtained by summing a few terms of a rapidly converging Fourier series. The effects of initial end thrust and axial and lateral elastic support are discussed. The buckling load based on the

Copies obtainable from NACA, Washington (over)

1. Columns, Beam (4.3.1.2)
2. Plates, Curved - Unstiffened (4.3.3.2.1)
3. Loads and Stresses, Structural - Normal Pressures (4.3.7.8)

I. Fung, Yuan-Cheng
II. Kaplan, A.
III. NACA TN 2840
IV. Guggenheim Aeronautical Lab., Calif. Inst. of Tech.

NACA TN 2840
National Advisory Committee for Aeronautics.
BUCKLING OF LOW ARCHES OR CURVED BEAMS OF SMALL CURVATURE. Y. C. Fung and A. Kaplan, California Institute of Technology. November 1952. 75p. diagrs., photo., 9 tabs. (NACA TN 2840)

A general solution, based on the classical buckling criterion, is given for the problem of buckling of low arches under a lateral loading acting toward the center of curvature. For a sinusoidal arch under sinusoidal loading, the critical load can be expressed exactly as a simple function of the beam dimension parameters. For other arch shapes and load distributions, approximate values of the critical load can be obtained by summing a few terms of a rapidly converging Fourier series. The effects of initial end thrust and axial and lateral elastic support are discussed. The buckling load based on the

Copies obtainable from NACA, Washington (over)

1. Columns, Beam (4.3.1.2)
2. Plates, Curved - Unstiffened (4.3.3.2.1)
3. Loads and Stresses, Structural - Normal Pressures (4.3.7.8)

I. Fung, Yuan-Cheng
II. Kaplan, A.
III. NACA TN 2840
IV. Guggenheim Aeronautical Lab., Calif. Inst. of Tech.

NACA TN 2840
National Advisory Committee for Aeronautics.
BUCKLING OF LOW ARCHES OR CURVED BEAMS OF SMALL CURVATURE. Y. C. Fung and A. Kaplan, California Institute of Technology. November 1952. 75p. diagrs., photo., 9 tabs. (NACA TN 2840)

A general solution, based on the classical buckling criterion, is given for the problem of buckling of low arches under a lateral loading acting toward the center of curvature. For a sinusoidal arch under sinusoidal loading, the critical load can be expressed exactly as a simple function of the beam dimension parameters. For other arch shapes and load distributions, approximate values of the critical load can be obtained by summing a few terms of a rapidly converging Fourier series. The effects of initial end thrust and axial and lateral elastic support are discussed. The buckling load based on the

Copies obtainable from NACA, Washington (over)

1. Columns, Beam (4.3.1.2)
2. Plates, Curved - Unstiffened (4.3.3.2.1)
3. Loads and Stresses, Structural - Normal Pressures (4.3.7.8)

I. Fung, Yuan-Cheng
II. Kaplan, A.
III. NACA TN 2840
IV. Guggenheim Aeronautical Lab., Calif. Inst. of Tech.

NACA TN 2840

energy criterion of Kármán and Tsien is also calculated. Results for both the classical and the energy criteria are compared with experimental results.

Copies obtainable from NACA, Washington

NACA TN 2840

energy criterion of Kármán and Tsien is also calculated. Results for both the classical and the energy criteria are compared with experimental results.

Copies obtainable from NACA, Washington

NACA TN 2840

energy criterion of Kármán and Tsien is also calculated. Results for both the classical and the energy criteria are compared with experimental results.

Copies obtainable from NACA, Washington

NACA TN 2840

energy criterion of Kármán and Tsien is also calculated. Results for both the classical and the energy criteria are compared with experimental results.

Copies obtainable from NACA, Washington

PART II

A NONLINEAR THEORY OF BENDING AND BUCKLING OF THIN ELASTIC SHALLOW SPHERICAL SHELLS

ABSTRACT

The shallow spherical dome subjected to lateral pressure is a structure for which the deformation departs appreciably from the linear theory at very small values of the deflection amplitude. It is also one for which the buckling process is characterized by a rapid decrease in the equilibrium load once the buckling load has been surpassed. For structures having this type of buckling characteristic, the question arises as to whether the proper buckling criterion to apply is the classical criterion, which considers equilibrium with respect to infinitesimal displacements or the finite displacement "energy criterion" proposed by Tsien.

In this paper the problem of the finite displacement and buckling of a shallow spherical dome is investigated both theoretically and experimentally. In the theoretical approach the nonlinear equations are converted into a sequence of linear equations by expanding all of the variables in powers of the center deflection and then equating the coefficients of equal powers. The basic parameter for the shallow dome is proportional to the ratio of the central height of the dome, h, to its thickness, t. For small values of this ratio the expansions converge rapidly and enough terms are computed to determine the buckling load. For higher values of h/t, convergence deteriorates rapidly and the buckling load is not computed. However, even for these higher values of h/t the deflection shapes are determined for deflection amplitudes below the amplitude at which buckling occurs. These deflection shapes are characterized by their rapid change as h/t increases and by the fact that, over most of the range of h/t studied, the maximum deflection does not occur at the

center of the dome.

The experimental program was carried out on a series of clamped-edge, eight inch base diameter shells, subjected to uniform pressure. The deflection shapes and the buckling loads agreed quite well with the values computed theoretically. It was also found that there was no significant difference between the buckling loads observed using air pressure and those observed using oil pressure. Thus it is concluded that for the shallow domes studied the classical buckling criterion holds rather than the "energy criterion" proposed by Tsien.

SYMBOLS

A_n, B_n, C_n, D_n, E_n integration constants

a base radius of shell

a_n, b_n, c_n coefficients in power series expansion of F_2 in terms of λx ; see Eq. (A-5)

$D = \frac{Et^3}{12(1-\mu^2)}$

d_n, g_n, h_n coefficients in power series expansion of F_2 in terms of λx ; see Eq. (A-7)

E Young's modulus

F_n functions of f_n and ω_n; see Eq. (28)

f_n coefficients of expansion for S_r in powers of W_o

h central height of shell above base plane

$K = \sqrt{12(1-\mu^2)}$

M_r radial bending moment per unit length

M_t circumferential bending moment per unit length

N_r radial membrane force per unit length

N_t circumferential membrane force per unit length

$P = \frac{1-\mu^2}{E}\left(\frac{a}{t}\right)^4 q$

P_n coefficient of expansion for $\mathbf{P}$ in powers of W_o

Q shear force per unit length perpendicular to middle surface of shell

q pressure on surface of shell; positive when directed downward

R initial radius of curvature of shell

r horizontal distance from axis of symmetry of shell

$S_r = \frac{a^2}{Et^3} N_r$

$S_t = \frac{a^2}{Et^3} N_t$

t thickness of shell

u radial displacement of middle surface of shell measured tangential to initial surface and positive in the outward direction

w vertical displacement of middle surface of shell measured perpendicular to initial surface and positive in the downward direction

$w_o = w(r = 0)$

$W = w/t$

$W_o = w_o/t$

w_n coefficient of expansion for W in powers of W_o

$x = r/a$

Z_o initial distance of point on middle surface of shell above the base plane

α segment angle of a possible deflected surface

$\alpha_n, \beta_n, \gamma_n$ functions of θ_n and ϕ_n, see Eq. (35)

β semi-included angle of shell

δ finite difference interval

ϵ_r radial strain

ϵ_t circumferential strain

$\eta = x^2$

θ $\sin^{-1}(r/R)$

θ_n particular integral of Eq. (26) for f_n

$\lambda^2 = \frac{ka^2}{Rt} \approx 4\sqrt{3(1-\mu^2)}\, h/t$

μ Poisson's ratio

ρ = bei λ ber' λ + (1 - ber λ) ber' λ

φ circumferential position angle

φ_n integrals of W_n; see Eq. (29)

I. INTRODUCTION

The development of the theory of bending of thin-walled spherical shells has a long record. A survey of the problem can be found in Refs. 1 and 2. The fundamental equations are developed by Hans Reissner (1912) who shows that for a thin-walled spherical dome that is not shallow, the membrane stresses in the shell maintain equilibrium with the external pressure, while the bending of the shell has relatively little effect except near the edge of the shell where the shell adjusts itself quickly to the prescribed boundary conditions. Bending in the shell is therefore essentially an "edge effect" or "boundary layer" phenomenon. Asymptotic solutions of the bending problem have been obtained by Blumenthal (1912), Havers (1935), Jacobsen (1937) and others on the basis that the parameter $(R/t)^2$ is very large, where R is the radius of the spherical shell and t its wall thickness. Both symmetrical and nonsymmetrical loading and edge conditions are discussed, including the case of a dome supported on columns.

The asymptotic solutions are, however, not valid for shallow spherical shells,* for which the effect of edge conditions is no longer limited to a thin layer near the edge and the interaction of bending and membrane stresses is strong. In 1946 Eric Reissner (Ref. 3) developed the governing equations for shallow spherical shells on the explicit assumption that the ratio h/a is so small that $(h/a)^2$ is negligible in comparison to h/a, h being the height of the dome and a its base radius.

---

* By shallow is meant a spherical segment for which the ratio of the height to the base radius is small, say, less than 1/8.

(See Fig. 1.) A few special cases are solved in Ref. 3.

Eric Reissner's solutions are based on linearized equations. Since the effect of bending on the membrane stresses is strong in the case of a shallow dome, one naturally asks the question: to what extent is the process of linearization valid? Expressed in terms of the ratio of the vertical deflection at the center of the dome to the wall thickness, w_o/t, the question is: how soon does the solution deviate from linearity as w_o/t increases?

To answer this question the nonlinear problem is treated, using a perturbation method, in the present paper. The particular problem of a shallow spherical shell with a clamped edge carrying a uniform pressure is chosen so that a convenient experimental comparison can be made. It is shown that the behavior of the shell depends fundamentally upon a parameter λ which is defined as

$$\lambda^2 = \sqrt{12(1-\mu^2)} \quad \frac{a^2}{tR} \tag{1}$$

where μ is the Poisson's ratio, and t, a, and R are as previously defined (see Fig. 1). The range of w_o/t in which the linear solution is valid is small indeed. For example at $\lambda = 4$, the equilibrium pressure given by the linear solution is respectively 9, 23, and 50 percent too high when w_o/t is 0.1, 0.25, and 0.5.

Consider now the problem of buckling of thin-walled spherical shells. For a complete sphere under uniform pressure, the classical solution, on the basis of linearized equations, is obtained by Zoelly (1915), Schwerin (1922), and Van der Neut (1932). (See Ref. 2, p. 491.) The buckling stress σ_{cl} is given by

$$\sigma_{cr} = \frac{Et}{R\sqrt{3(1-\mu^2)}}, \quad \left(\sigma_{cr} = \frac{R}{2t} q_{cr}\right) \tag{2}$$

where q is in the intensity of external pressure. This stress has the same magnitude as the critical stress for an axially compressed cylindrical shell of radius R and of thickness t. It is relatively high in comparison with experimental results. The corresponding buckling mode predicted by the theory is also at variance with laboratory experience. To reconcile the differences between theory and experiment von Karman and Tsien in 1939 (Ref. 6) introduced a new concept into the theory of elasticity: the "lower buckling load". They discovered that for values of pressure q considerably below that given by Eq. (2), quite different stable states of equilibrium exist, which could be revealed only by abandoning the classical linearization of the problem. The minimum of such values of q is the "lower buckling load" q_K. If q exceeds q_K, the chances are great that buckling will occur. In Ref. 4 the lower buckling load is computed (subject to a number of simplifying assumptions) with respect to a special class of buckling modes. Friedrichs in Ref. 5 avoids some of the arbitrary assumptions by applying asymptotic integration in the manner of a boundary layer theory. Application of Friedrich's equations, however, yields no minimum buckling load, and it is pointed out (Ref. 6) that the minimum obtained in Ref. 4 is due to the special form of displacements assumed in that investigation.

The final "energy criterion" of buckling is formulated by Tsien in Ref. 6. It is stated that under average laboratory and actual service conditions the most probable equilibrium state is the state with the

lowest possible energy level. In other words it is assumed that there are disturbances of sufficient magnitude so that the transitions from higher energy levels to lower energy levels are always possible. Two conditions must be satisfied in defining the "possible energy levels": (1) the corresponding external forces and internal stresses must be in equilibrium; (2) the geometric restraint and loading conditions, if any, must be satisfied. Tsien points out that these necessary conditions for possible energy levels are not checked in Refs. 4 and 5. When the check is applied, a lower buckling load is obtained for spherical shells on the basis of Friedrichs' equations (Ref. 6). The agreement with experiments is good.

It appears that these arguments apply equally well to spherical domes as to the complete sphere. Therefore, the first theoretical question to be settled is whether the "classical criterion" of buckling or the "energy criterion" should be used in calculating the critical buckling load. The classical buckling criterion is based on the assumption that a given state of equilibrium of a shell becomes unstable when there are equilibrium positions infinitesimally near to that state of equilibrium under the same external load. Thus in applying the classical criterion an equilibrium state is compared with its neighboring equilibrium states and the incipient buckling is revealed by a negative slope of the load-deflection curve, i. e. when an increase of deflection corresponds to a decrease in the corresponding applied load. The important contrast between the classical criterion and the energy criterion is that in the former only continuous load deflection process is considered, while in the latter a jump to the state of lower

energy level is permitted even though the intervening states involve higher energy levels. The linearization of the governing equations, ordinarily made purely for mathematical simplicity, should not be regarded as a part of the classical criterion.

Although the energy criterion seems plausible, nevertheless it can only be verified by comparison with experiments. The energy criterion necessarily yields a buckling load which is never greater than that given by the classical criterion. If there is a wide difference between the two buckling loads the problem becomes simply to choose the criterion that gives closer agreement with the experiments.

For shallow spherical domes the buckling load calculated on the basis of the classical criterion, but without linearizing the governing equations, is known only in very few cases. In the comparison with experiments presented in Fig. 20 of Ref. 6, the curve labeled "classical theory" is really the one given by Eq. (2), which is applicable to a complete sphere and is calculated from linearized equations. When the nonlinear equations applicable to shallow spherical dome are used the buckling load is lower than that given by Eq. (2). For example when $\lambda = 4$ the calculation of the present report gives a buckling load which is about one-half that given by Eq. (2). Thus the wide difference between the classical theory and experiments exhibited in the figure cited above may be entirely caused by an improper mathematical process.

To clarify the argument further, let us consider the case of a flat arch, as a two-dimensional analog of the spherical dome. For such an arch two buckling modes are possible. If the arch rise is high, it

buckles in the mode shown in Fig. 2: the centerline of the arch remains essentially "inextensional". If the arch rise is small, it may buckle downward with a sudden reversal of curvature, as shown in Fig. 3: a phenomenon sometimes described as "oil-canning" or "durchschlag". The axial compressive strain plays a dominant role in the latter case and linearization of the governing equations is not permissible. A detailed study made in Ref. 7 shows that in practice the classical criterion agrees better with experiments, except for very low arches (arches whose rise is of the order of the wall thickness) for which the energy hump tends to vanish and the gap between the two criteria tends to be closed.

For shallow spherical domes the prevailing buckling mode is of the oil-canning type, in which the membrane stress plays an important part, and is basically a nonlinear phenomenon.

There exists only one paper on the oil-canning of shallow spherical domes based on the classical criterion. This is Biezeno's work (Ref. 8) which treats a shallow dome whose edge is free to expand so that the membrane stress in the radial direction vanishes on the edge; and the dome is subjected to a concentrated load acting at the center. The following equations (which are equivalent to those of the present paper) are obtained:

$$r^2\frac{d^2N_0}{dr^2}+r\frac{dN_0}{dr}-N_0+r^2\left(\frac{r}{R}+\psi\right)+(2-\mu)\frac{r^2}{R}\psi + \frac{1-\mu}{2}r\psi^2=-\frac{Pr}{2\pi}\frac{(1-\mu^2)}{Et}\left\{\frac{1}{R}+\frac{d\psi}{dr}\right\} \tag{3}$$

$$r^2 \frac{d^2\psi}{dr^2} + r \frac{d\psi}{dr} - \psi = \frac{r}{D}\left\{\frac{P}{2\pi} + r N_r \left(\frac{r}{R} + \psi\right)\right\} \qquad (4)$$

$$N_r = \frac{Et}{1-\mu^2}\left\{\frac{dv_o}{dr} + \mu \frac{v_o}{r} + \left(\frac{r}{R} + \frac{1}{2}\psi\right)\psi\right\} \qquad (5)$$

where **P** is the central load, $\psi = \frac{dw}{dr}$ is the slope of the deflection surface in a meridianal section, w is the radial displacement normal to the original spherical shell, and v_o is the component of displacement normal to the axis of symmetry, i.e.

$$v_o = u \cos\theta - w \sin\theta \ . \qquad (6)$$

(See Fig. 1.) Other symbols are defined in the table of notations of the present paper. Biezeno makes the following simplifying assumptions to obtain a solution: (1) that the term on the right hand side of Eq. (3) may be neglected; (2) that in Eqs. (3), (5), and on the right hand side of Eq. (4), the slope of the radial displacements ψ can be written as

$$\psi = \psi_1 = C_1 \frac{r}{R} + C_2 \frac{r}{R} \log \frac{a}{r} \qquad (7)$$

where C_1 and C_2 are two undetermined constants. Eq. (4) is then solved with proper boundary conditions. Let the solution be denoted by ψ_2, which, of course, is different in form than (7). Biezeno then determines the constants C_1 and C_2 by requiring that ψ_1 and ψ_2 yield the same values of vertical displacement at the edge of the plate ($r = a$) and at the center ($r = 0$). The load - deflection curve can then be calculated from (7) and the buckling load determined.

The influence of Biezeno's simplifying assumptions on the buckling load is not easy to assess; and there exist no experimental results to compare with the theory.

The case considered in the present paper is that of a shell clamped at the edge and subjected to uniform lateral pressure. The equations of equilibrium (equivalent to Eqs. (3), (4), (5)) are solved as perturbation series expressed in powers of the parameter ω_o /t, i. e. the ratio of the deflection on the axis of symmetry and the wall thickness of the shell. The load-deflection curve so determined is used to obtain the buckling load.

Relatively few assumptions are made in the present calculation. Unfortunately the perturbation series seems to deteriorate rapidly for large λ , so the result is satisfactory only for λ of order 5 or smaller. In this range of λ the buckling loads computed on the basis of the classical criterion agree quite well with experiments.

On the other hand, the calculation of the buckling load on the basis of Tsien's energy criterion also offers considerable difficulty. If the formulas of Ref. 6 are extended to cover the shallow shells studied in the present paper it is found that the so-called "lower buckling load" has an equal or higher value than that given by Eq. (2) when $\lambda \leqslant 10$. This unreasonable result is obtained because the energy expressions and the mode shape assumed are not sufficiently accurate. It is not clear how to improve the results. Theoretical deflection curves derived from the bending theory do not permit a very simple representation. In any case, the refinement of Tsien's calculation would have been a major endeavor. For the same reason the

calculation of the buckling load on the basis of classical criterion using the Rayleigh-Ritz method is not pursued. Therefore the most convenient theoretical determination of the critical buckling load remains an open question. The author believes, however, that the shallow spherical shell behaves in a manner similar to the low arch; that for shells not too flat the energy "barrier" for jumping into the state of the lowest energy level is so high that the classical criterion gives the correct buckling load corresponding to the average laboratory and actual service conditions; and that for a very flat shell the energy barrier becomes lower and the two criteria tend to yield the same buckling load.

One more point should be mentioned before the presentation of the main analysis. In Ref. 5, Friedrichs suggests that it may be possible that a boundary layer occurs at the edge of a certain segment, the width of which in its turn shrinks to zero with the thickness of the shell. This suggestion seems plausible because as the shell becomes thinner and thinner the bending of the shell becomes less and less important. In the limit $t \longrightarrow 0$ the deflected surface must be "applicable" to the original surface.* In the upper part of Fig. 4 the shell represented by the dotted line is applicable to that represented by the solid line; in other words, a deformation of the solid line into the dotted line involves no strain energy due to the membrane stresses. To account for the small but finite bending energy of the shell the deflection surface may take the form represented by the lower figure of Fig. 4. A

---

* Two surfaces are called "applicable" to each other in differential geometry if one can deform into the other by continuous bending without stretching or tearing the surface.

boundary layer may be developed at the segment angle α . This conjecture, however, turns out to be wrong for a shell subjected to uniform external pressure; since it can be shown that the segment angle α tends to zero at a higher order in t (the shell thickness) than does the boundary layer thickness. Therefore the boundary layer can be developed only at a pole $\alpha = 0$ which is the case presented in Ref. 5.

II. THEORETICAL ANALYSIS

Derivation of Equations

Consider the spherical shell segment of radius R, base diameter 2a, height h, and constant thickness t, shown in Fig. 1. The initial position of a point in the central surface is given by the cylindrical coordinates r, ψ , z_o, where r is the radial distance from the center, measured parallel to the base, ψ is the circumferential angle, and z_o is the vertical distance, measured upward, from the base plane. It is assumed that h/a is small enough that

$$z_o = h + \sqrt{R^2 - r^2} - R \approx h - \frac{1}{2}\frac{r^2}{R}$$
$$\frac{dz_o}{dr} \approx -\frac{r}{R} \tag{8}$$

The deformation of the middle surface is assumed to be radially symmetric and is therefore specified by u , measured tangential to the middle surface in the outward radial direction, and w , measured perpendicular to the middle surface in the downward direction. The deflections are considered to be finite, but small enough so that $\left(\frac{dw}{dr}\right)^2$ can be neglected with respect to unity.

Since under these conditions, the magnitudes of vectors tangential to the middle plane are equal to their components parallel to the base plane, the equations for forces and moments in the middle plane are identical with those for a flat plate. That is

$$\frac{d}{dr}\left(r M_r\right) - M_t - r Q = 0 \tag{9}$$

$$\frac{d}{dr}\left(r N_r\right) - N_t = 0 \tag{10}$$

where N_r and N_t are respectively the radial and circumferential membrane stresses, M_r and M_t the corresponding bending moments, and Q the shear stress in the direction perpendicular to the deformed middle surface. Vertical equilibrium of a central cylindrical section of radius r , Fig. 5, requires that

$$Q = -\frac{1}{r}\int_0^r r q\, dr + N_r\left(\frac{dz_0}{dr} - \frac{dw}{dr}\right) \tag{11}$$

where q is the applied pressure. Substituting Eq. (11) into Eq. (9) and using the approximation Eq. (8) results in

$$\frac{d}{dr}(r M_r) - M_t + \int_0^r r q\, dr + r N_r\left(\frac{r}{R} + \frac{dw}{dr}\right) = 0 \tag{12}$$

The bending moments are expressed in terms of the deflections using the strain deflection relations

$$\epsilon_r = \frac{du}{dr} + \frac{1}{2}\left(\frac{dw}{dr}\right)^2 - \frac{w}{R}$$
$$\epsilon_t = \frac{u}{r} - \frac{w}{R} \tag{13}$$

where ϵ_r and ϵ_t are the longitudinal strains of the middle surface in the radial and circumferential directions respectively. Then

$$N_r = \frac{Et}{1-\mu^2}\left\{\frac{du}{dr} - \frac{w}{R} + \frac{1}{2}\left(\frac{dw}{dr}\right)^2 + \mu\left(\frac{u}{r} - \frac{w}{R}\right)\right\}$$

$$N_t = \frac{Et}{1-\mu^2}\left\{\frac{u}{r} - \frac{w}{R} + \mu\left\{\frac{du}{dr} - \frac{w}{R} + \frac{1}{2}\left(\frac{dw}{dr}\right)^2\right\}\right\} \tag{14}$$

$$M_r = -D\left(\frac{d^2w}{dr^2} + \frac{\mu}{r}\frac{dw}{dr}\right) \qquad M_t = -D\left(\frac{1}{r}\frac{dw}{dr} + \mu\frac{d^2w}{dr^2}\right)$$

where $D = \frac{Et^3}{12(1-\mu^2)}$

Using these expressions for M_r and M_t, Eq. (12) becomes

$$D_r \frac{d}{dr}\left\{\frac{1}{r}\frac{d}{dr}\left(r\frac{dw}{dr}\right)\right\} = r\,N_r\left(\frac{r}{R}+\frac{dw}{dr}\right)+\int_0^r q\,r\,dr \qquad (15)$$

This is the first basic equation. Now from Eq. (13)

$$\frac{u}{r} = \epsilon_t + \frac{w}{R} = \frac{1}{Et}(N_t - \mu N_r) + \frac{w}{R}$$

so that

$$\frac{du}{dr} = \frac{1}{Et}\frac{d}{dr}\left\{r N_t - \mu r N_r + Et\,\frac{wr}{R}\right\} \qquad (16)$$

These values are substituted in the first of Eqs. (14) to obtain a second relation between N_t and N_r

$$N_r = \frac{Et}{1-\mu^2}\left[\frac{1}{Et}\frac{d}{dr}\left\{r N_t - \mu r N_r + Et\,\frac{wr}{R}\right\} - \frac{w}{R} + \frac{1}{2}\left(\frac{dw}{dr}\right)^2 + \frac{\mu}{Et}(N_t - \mu N_r)\right] \qquad (17)$$

Combining this equation with Eq. (10), the second basic equation is obtained

$$r\frac{d}{dr}\,\frac{1}{r}\,\frac{d}{dr}\left(r^2 N_r\right) + \frac{1}{2}Et\left(\frac{dw}{dr}\right)^2 + Et\,\frac{r}{R}\frac{dw}{dr} = 0 \qquad (18)$$

Knowing w and N_r, N_t can be obtained from Eq. (10). In the problem to be studied q is a constant so that Eq. (15) becomes

$$D\frac{d}{dr}\left\{\frac{1}{r}\frac{d}{dr}\left(r\frac{dw}{dr}\right)\right\} = N_r\left(\frac{r}{R}+\frac{dw}{dr}\right) + \frac{1}{2}\,q\,r \qquad (19)$$

These equations are transformed into non-dimensional form by the use of the following variables

$$x = \frac{r}{a} \qquad W = \frac{w}{t} \qquad K^2 = 12(1-\mu^2)$$

$$S_r = \frac{a^2}{Et^3} N_r \qquad S_t = \frac{a^2}{Et^3} N_t \tag{20}$$

$$P = \frac{1-\mu^2}{E}\left(\frac{a}{t}\right)^4 q \qquad \lambda^2 = \frac{Ka^2}{Rt}$$

The parameter λ^2 can also be expressed as (see Fig. 1)

$$\lambda^2 = K\frac{R}{t}\sin^2\beta \approx K\frac{R\beta^2}{t} \quad \text{or}$$

$$\lambda^2 = K\frac{h}{t}\frac{\sin^2\beta}{1-\cos\beta} = K\frac{h}{a}(1+\cos\beta) \approx 2K\frac{h}{t} \tag{21}$$

Thus for the assumed range of β , λ^2 is proportional to the ratio of the central height of the dome to its thickness and can therefore be interpreted as representing the ratio of the compression stiffness to the bending stiffness.

On substituting these new variables, Eqs. (18), (19), and (10) become

$$\frac{d}{dx}\left\{\frac{1}{x}\frac{d}{dx}(x^2 S_r)\right\} + \frac{1}{2x}\left(\frac{dW}{dx}\right)^2 + \frac{\lambda^2}{K}\frac{dW}{dx} = 0 \tag{22}$$

$$\frac{1}{x}\frac{d}{dx}\left\{\frac{1}{x}\frac{d}{dx}\left(x\frac{dW}{dx}\right)\right\} - K\left(\lambda^2 + \frac{K}{x}\frac{dW}{dx}\right)S_r = 6P \tag{23}$$

$$S_t = \frac{d}{dx}(x S_r) \tag{24}$$

With $\lambda = 0$ ($R = \infty$) these are Karman's equations for the finite deflection of a flat plate, expressed in polar coordinates. Their derivation is exactly analagous to Chien's (Ref. 9) derivation of the equations for the finite deflection of a flat circular plate.

Expansion in Terms of $W_o (= \omega_o / t)$

As in Chien's paper the procedure used for solving these equations is to consider the center deflection ratio $W(0) = W_o$ as a parameter and to expand all of the variables in powers of W_o. Thus

$$P = p_1 W_o + p_2 W_o^2 + p_3 W_o^3 + \cdots$$

$$W = \omega_1(x) W_o + \omega_2(x) W_o^2 + \omega_3(x) W_o^3 + \cdots \qquad (25)$$

$$S_R = f_1(x) W_o + f_2(x) W_o^2 + f_3(x) W_o^3 + \cdots$$

These expansions are valid for small enough values of the deflection ratio W_o, but their exact range of convergence is unknown. For the case of the flat circular plate Chien obtained good convergence for values of W_o as high as 4.

Substitution of these series in Eqs. (22) and (23) and the equating of equal powers of W_o results in a sequence of pairs of simultaneous equations of f_n and w_n. Each of these pairs of equations can then be combined to obtain an equation for f_n alone

$$\frac{1}{x^3}\frac{d}{dx}\left[\frac{1}{x}\frac{d}{dx}\left\{x^5\frac{d}{dx}\left(\frac{1}{x}\frac{df_n}{dx}\right)\right\}\right] + \lambda^4 f_n = -\frac{6}{K}\lambda^2 p_n - F_n \qquad (26a)$$

or

$$\frac{d^4 f_n}{dx^4} + \frac{6}{x}\frac{d^3 f_n}{dx^3} + \frac{3}{x^2}\frac{d^2 f_n}{dx^2} - \frac{3}{x^3}\frac{df_n}{dx} + \lambda^4 f_n = -\frac{6}{K} p_n \lambda^2 - F_n \qquad (26b)$$

plus an equation for w_n in terms of f_n

$$w_n = \frac{K}{\lambda^2 x}\frac{d}{dx}(x^2 f_n) - \frac{K^3}{\lambda^2}\varphi_n + E_n \qquad (27)$$

where E_n is a constant, and F_n and φ_n are the following functions

$$F_1 = 0$$

$$F_2 = K\lambda^2 \frac{1}{x} f_1 \frac{dw_1}{dx} + \frac{1}{x}\frac{d}{dx}\left\{\frac{1}{x}\frac{d}{dx}\frac{1}{2}\left(\frac{dw_1}{dx}\right)^2\right\}$$

$$F_3 = K\lambda^2 \frac{1}{x}\left\{f_2 \frac{dw_1}{dx} + f_1 \frac{dw_2}{dx}\right\} + \frac{1}{x}\frac{d}{dx}\left\{\frac{1}{x}\frac{d}{dx}\left(\frac{dw_1}{dx}\frac{dw_2}{dx}\right)\right\} \quad (28)$$

$$F_4 = K\lambda^2 \frac{1}{x}\left\{f_1 \frac{dw_3}{dx} + f_2 \frac{dw_2}{dx} + f_3 \frac{dw_1}{dx}\right\}$$
$$+ \frac{1}{x}\frac{d}{dx}\left[\frac{1}{x}\frac{d}{dx}\left\{\frac{dw_1}{dx}\frac{dw_3}{dx} + \frac{1}{2}\left(\frac{dw_2}{dx}\right)^2\right\}\right]$$

$$\varphi_1 = 0 \qquad \varphi_2 = \int_0^x \frac{1}{2}\left(\frac{dw_1}{dx}\right)^2 \frac{dx}{x}$$

$$\varphi_3 = \int_0^x \frac{dw_1}{dx}\frac{dw_2}{dx}\frac{dx}{x} \qquad \varphi_4 = \int_0^x \left\{\frac{1}{2}\left(\frac{dw_2}{dx}\right)^2 + \frac{dw_1}{dx}\frac{dw_3}{dx}\right\}\frac{dx}{x} \quad (29)$$

On making the substitution

$$\eta = x^2$$

Eq. (26) becomes

$$\frac{d^2}{d\eta^2}\left(\eta^3 \frac{d^2 f_n}{d\eta^2}\right) + \lambda^2 \eta f_n = -\frac{3}{8K}\lambda^2 \rho_n - \frac{1}{16} F_n \quad (30)$$

which can be recognized as the equation for the lateral deflection of a linearly tapered beam on an elastic support whose spring constant is a linear function of position along the span. This interpretation is useful in the numerical work which follows.

The solution of the homogeneous part of Eq. (19), i.e. the complementary function is

$$f_n = \frac{1}{x}\left\{A_n \mathrm{ber}'\lambda x + B_n \mathrm{bei}'\lambda x + C_n \mathrm{ker}'\lambda x + D_n \mathrm{kei}'\lambda x\right\}$$

where

$$\text{ber}'z = \frac{d}{dz}\ \text{ber}\ z$$

and the ber and bei functions are defined in terms of J_o, the zero order Bessel function of the first kind, by

$$J_o\left(zi^{3/2}\right) = \text{ber}\ z + i\,\text{bei}\ z$$

with an analogous relation between ker z and kei z and $K_o(zi^{3/2})$.

Boundary Conditions

The boundary conditions for a clamped edge shell subjected to a radially symmetric distributed load are

$$\begin{aligned} &at\ x=0\ \ \frac{dw}{dx}=0 \qquad\qquad S_r \text{ is finite;} \\ &at\ x=1,\quad w=\frac{dw}{dx}=u=0 \end{aligned} \tag{31}$$

To satisfy the first two conditions it is necessary that

$$C_n = D_n = 0$$

In terms of the expansion coefficients, Eq. (25), the remaining boundary conditions become

$$\left.\begin{aligned} &w_n=0,\ \ \frac{dw_n}{dx}=0 \\ &(1-\mu)f_n + x\frac{df_n}{dx}=0 \end{aligned}\right\} x=1 \tag{32a}$$

Because of the nature of the expansion there is the additional condition that

$$w_n(0) = \begin{cases} 1, & n=1 \\ 0, & n\geq 2 \end{cases} \tag{32b}$$

The constant E_n can be eliminated by combining (32a) and (32b)

so that the boundary condition on w_n becomes

$$w_n(0) - w_n(1) = \begin{cases} 1, & n=1 \\ 0, & n \geq 2 \end{cases} \tag{32c}$$

Let θ_n be the particular solution corresponding to F_n on the right hand side of (19), then the complete solution for f_n becomes

$$f_n = \frac{1}{x}\left\{A_n \, ber'\lambda x + B_n \, bei'\lambda x\right\} + \theta_n - \frac{6}{K}\frac{\rho_n}{\lambda^2} \tag{33}$$

while

$$w_n = \frac{K}{\lambda}\left\{A_n \, bei\,\lambda x - B_n \, ber\lambda x\right\} - \frac{K}{\lambda^2 x}\frac{d}{dx}(x^2\theta_n) - \frac{K}{\lambda^2}\varphi_n + E_n$$

Substitution of these values into the boundary conditions (32) and their solution for A_n, B_n, and ρ_n results in

$$A_n = \frac{1}{\rho}\left\{\alpha_n \, ber'\lambda + \beta_n (1 - ber\lambda)\right\} \tag{34a}$$

$$B_n = \frac{1}{\rho}\left\{\alpha_n \, bei'\lambda - \beta_n \, bei\,\lambda\right\} \tag{34b}$$

$$\rho_n = -\frac{K\lambda^2}{6(1-\mu)\rho}\left[\left\{(1+\mu)(ber'^2\lambda + b^2ei'\lambda) + \lambda(ber'\lambda \, bei\lambda - bei'\lambda \, ber\lambda)\alpha_n\right\}\right.$$

$$\left. + \left\{(1+\mu)\left((1-ber\lambda)ber'\lambda - bei\lambda \, bei'\lambda\right) + \lambda \, bei\lambda\right\}\beta_n\right] + \gamma_n \tag{34c}$$

where

$$\rho = bei\lambda \, ber'\lambda + (1 - ber\lambda)ber'\lambda \tag{35a}$$

$$\alpha_n = \frac{1}{\lambda}\left|\frac{1}{x}\frac{d}{dx}(x^2\theta_n)\right|_{x=0}^{x=1} + \frac{K^2}{2\lambda}\varphi_n(1) \tag{35b}$$

$$\beta_n = \frac{1}{\lambda^2}\left\{\frac{d}{dx}\left(\frac{1}{x}\frac{d}{dx}(x^2\theta_n)\right)\right\}_{x=1} \tag{35c}$$

$$\gamma_n = \frac{K\lambda^2}{6}\left\{\theta_n + \frac{1}{1-\mu}\frac{d\theta_n}{dx}\right\}_{x=1} \qquad (35d)$$

First Order Solution

The particular solution, θ_1, of the first order equation is zero and the equations for A_1, B_1, and p_1 reduce to

$$A_1 = \frac{\lambda\, ber'\lambda}{K\rho} \qquad B_1 = \frac{\lambda\, bei'\lambda}{K\rho} \qquad (36)$$

$$p_1 = \frac{\lambda^2}{6(1-\mu)\rho}\left\{(1+\mu)(ber'^2\lambda + bei'^2\lambda) + \lambda(ber'\lambda\, bei\lambda - bei'\lambda\, ber\lambda)\right\}$$

The values of A_1, B_1, and p_1 are given in Table 1, while the values of w_1 and f_1 are given in Tables 2 and 3, and are plotted in Figs. 7 and 8 respectively. This first order solution is identical with the linear solution previously found by E. Reissner (Ref. 3).

For the higher order equations no solution was found in terms of known functions and so it was necessary to resort to power series expansion and numerical methods.

Power Series Solutions

Judging from the work of Chien it was felt that calculation of the first two terms, p_1 and p_2, of the expansion for the pressure P would permit at least an approximate determination of the buckling load. Therefore a power series solution for θ_2 was obtained even though it was realized that the succeeding solutions could not be obtained by this method because of the involved form of the functions F_n. The procedure and formulas used are shown in the Appendix. Since the expansions are

all in terms of λx it was necessary to restrict the calculations to values of $\lambda \leq 8$. The values of p_2 obtained are shown in Table 4 and plotted in Fig. 6. These values are negative for small values of λ, but become positive at $\lambda = 6.5$ and are rapidly increasing at $\lambda = 8$. Since buckling can only occur when some of the p_n's are negative it was clearly necessary to obtain the higher order terms of p_n. These additional values of p_n were obtained numerically.

Numerical Solutions

The differential equation (26) contains the unknown parameter p_n and also has the unwieldy boundary condition that S_r is finite, at $x = 0$. As a result a complete numerical solution would be very difficult. Therefore only the particular solution is determined numerically, using arbitrary boundary conditions. The required boundary conditions are then satisfied using the known solution of the homogeneous equation.

In terms of the finite difference approximations

$$
\begin{aligned}
f'(x) &= \frac{1}{2\delta}\{f(x+\delta) - f(x-\delta)\} \\
f''(x) &= \frac{1}{\delta^2}\{f(x+\delta) - 2f(x) + f(x-\delta)\} \\
f'''(x) &= \frac{1}{2\delta^3}\{f(x+2\delta) - 2f(x+\delta) + 2f(x-\delta) - f(x-2\delta)\} \\
f^{IV}(x) &= \frac{1}{\delta^4}\{f(x+2\delta) - 4f(x+\delta) + 6f(x) - 4f(x-\delta) + f(x-2\delta)\}
\end{aligned}
\tag{37}
$$

where δ is the difference interval, Eq. (26) (with the constant term, $-3/8 \frac{\rho_n \lambda^2}{K}$, omitted) becomes

$$\left(\frac{6}{\delta^4} - \frac{6}{\delta^2 x^2} + \lambda^4\right)\theta_n(x) - \left(\frac{4}{\delta^4} + \frac{6}{\delta^3 x} - \frac{3}{\delta^2 x^2} + \frac{3}{2\delta x^3}\right)\theta_n(x+\delta)$$
$$+\left(-\frac{4}{\delta^4} + \frac{6}{\delta^3 x} + \frac{3}{\delta^2 x^2} + \frac{3}{2\delta x^3}\right)\theta_n(x-\delta) + \left(\frac{1}{\delta^4} + \frac{3}{\delta^3 x}\right)\theta_n(x+2\delta) \quad (38)$$
$$+\left(\frac{1}{\delta^4} - \frac{3}{\delta^3 x}\right)\theta_n(x-2\delta) = 16 F_n(x)$$

The desirable boundary conditions for θ_n are the ones which give a smooth solution. For the tapered beam analogy of Eq. (30) the obvious boundary conditions meeting these requirements are those representing unsupported ends. When these boundary conditions are transformed in terms of the variable x they become

$$\text{at } x = 0, \quad \frac{d\theta_n}{dx} = \frac{d^3\theta_n}{dx^3} = 0 \quad (39)$$
$$\text{at } x = 1, \quad \frac{d^2\theta_n}{dx^2} = \frac{d^3\theta_n}{dx^3} = 0$$

A first attempt to solve the finite difference equation (39) by relaxation was unsuccessful due to slow and erratic convergence. Instead, Crout's method of solving simultaneous equations (Ref. 10) was used to determine the values of θ_n at 11 points ($\delta = 0.10$) at once. This could be done rapidly, but unfortunately 11 points were not enough to accurately determine the end values and derivatives which were required. Instead of decreasing the spacing to 0.05 throughout, it was decided to add two end sections from 0 to 0.3 and from 0.7 to 0.1 with 0.05 spacing. The solutions in these end sections were joined with the original solution at the 0.30 and 0.70 stations where the function and its first derivative were matched. Since the higher derivatives were small at the junction points (especially for λ = 4 and 7) this method was adequate, but did cause some trouble

when higher derivatives were required for the succeeding calculations.

Calculations of θ_2 were made for $\lambda = 4, 7, 10$ and 13, while for $\lambda = 4$ and 7 the calculations were continued to determine θ_3 and θ_4. As λ increases convergence of the series for P deteriorates rapidly and the function θ_n has increasing large oscillations. It was decided therefore not to continue the calculations for $\lambda = 10$ and 13. The values of p_n obtained are shown in Table 4, while the values of w_n and f_n are shown in Tables 2 and 3, and plotted in Figs. 9 and 10.

For $\lambda = 4$ the convergence of the series for p_n was very satisfactory, the contribution of the fourth order term still being small at the critical buckling load. In Fig. 15 is shown a plot of load P versus the center deflection ratio W_o and in Fig. 11 are shown the deflection modes for several values of the center deflection ratio W_o. These deflection modes have their maximum at the center, and as W_o grows they become increasingly peaked toward the center.

For $\lambda = 7$, however, the convergence is poor and the coefficients p_n all being positive, no buckling can be determined using just four terms. The convergence is good enough to determine the deflection shapes W for small values of W_o and these are plotted in Fig. 11. These deflection shapes give an explanation of why p_2 is positive (which implies increasing stiffness with respect to the center deflection as the load increases) since they show that the maximum deflection is no longer at the center and that with increasing load the center deflection becomes a progressively small portion of the maximum deflection. This characteristic is corroborated by the experimental measurements.

The deflection modes for $\lambda = 10$, which are also shown in Fig. 11, exhibit the same characteristic, but with the position of the

maximum deflection moved outward toward the edge. However, since these curves are calculated using only two terms of the expansion for W, these curves should not be taken as indicating accurately what happens at the larger values of W_o.

The rapid change which must occur at buckling from a shape in which the maximum deflection occurs near the edge to one in which the maximum deflection occurs at the center is probably also an explanation for the poor convergence. Since the experimental results show that at $\lambda = 10$ the maximum deflection is again at the center it may be that for these higher values of λ the convergence is actually improved. However, to obtain accurate values of θ_n for these higher values of λ it would be necessary to start with a smaller finite difference interval than was used here.

Since the influence of the p_3 and p_4 terms at the buckling load for $\lambda = 4$ was small, it was felt that for $\lambda < 5$ an adequate approximation to the buckling load could be obtained using just the first two terms p_1 and p_2. The critical conditions occur when $\frac{dP}{dW_o} = 0$ so that for

$$P = p_1 Wo + p_2 Wo^2$$

the critical conditions are

$$W_{o_{cr}} = \frac{-p_1}{2p_2} \qquad P_{cr} = \frac{-p_1^2}{4p_2}$$

This value of P_{cr} is plotted in Fig. 18 where it is compared with the experimental results. The minimum value of λ for which P_{cr} exists is that for which the critical deflection equals the initial height of the dome, that is for $W_{o_{cr}} = h/t$.

III. EXPERIMENTAL PROGRAM

Equipment

An experimental program was carried out on a series of shallow domes having a base diameter of eight inches, nominal radii of curvature of 20 and 30 inches, and thicknesses varying from 0.032 to 0.102 inches. The edges of the specimens were held between two rings which were bolted to a circular plate, Figs. 12 and 13, thus providing a rigid built-in edge support and a closed pressure chamber. A separate set of clamping rings were used for each of the two radii of curvature. The specimens were subjected to a uniform normal load using both oil and air pressure; the oil provided an approximation to a constant volume characteristic during buckling while the air provided a constant pressure characteristic.

The specimens were made by spinning from flat sheet. After unsuccessful attempts to heat-treat aluminum spinnings, magnesium alloy QQ-M-44 was selected because of its favorable ratio of yield stress to Young's modulus compared to other nonheat-treated metals. Magnesium also has the advantage that since it is spun while hot most of the residual stresses are eliminated. This is evidenced by the small separation when a radial cut is made in a magnesium spinning. Because of the difficulty of spinning such shallow shells the preliminary specimens were very disappointing, but by a combination of spinning on concave and convex molds the quality was greatly improved. Unfortunately it is still not as good as would be desired.

Pressure measurements were made using a Bourdon tube for pressure over 20 psi and a mercury manometer for pressures under

20 psi. Exceptions were two of the early specimens having low buckling loads which were tested using the Bourdon gage. This gage of course gives a closer approximation to a constant volume characteristic than does the manometer.

Deflection measurements were taken with a 1/1000 inch scale dial gage riding on a channel beam fastened at its ends to a circular ring which rotated in a groove cut in the upper clamping ring. Readings were made to the nearest 1/2 thousandth of an inch. Traverses were made on two or more diameters to determine the initial shape of the shell and were repeated at intervals during the loading. Intermediate measurements were also made of the center deflection. Because of the variations of the specimens from a true spherical form the question arose as to what should be taken as the radius R from which the parameter λ was calculated. It was decided to assume that the central rise h would determine the radius since λ can be simply expressed in terms of h (Eq. (21)) and because experience with the buckling of shallow arches showed that for arches having the same central height small symmetrical variations in shape have only a small effect on the buckling load. In Fig. 14 the variations from the assumed radii are shown for typical examples of each of the six combinations of the two nominal radii, 20 and 30 inches, and each initial sheet thickness 0.033, 0.054, and 0.102. It is seen that the variations increased markedly with the thinness of the sheet and the flatness of the dome.

Oil Tests

The oil pressure tests were made first, and two or more tests of

each combination of thickness and radius were made. The early preliminary tests made on aluminum samples all showed a very distinct unsymmetrical buckling mode. This is believed due to the high residual stresses resulting from the spinning operation since the majority of the magnesium specimens buckled symmetrically. In the cases in which unsymmetrical buckle did occur in the magnesium specimens the mode was not of the overall unsymmetrical form such as the unsymmetrical mode of vibration of a flat circular plate. Rather it appeared that the buckles themselves were inherently symmetrical but were displaced from a central position on the shell, probably due to initial asymmetries of the shell.

The unsymmetrical buckling only occurred in the range of λ between 6.0 and 8.6 and was associated with a prebuckling deflection mode in which the displacement at about half the radius from the center was greater than that at the center.

In Fig. (14) are shown the deflection curves of the specimens. There is a distinct change in the deflection modes as λ increases. For λ near 4 the deflection is peaked at the center and decreases steadily towards the edge. As λ increases, the peak gradually flattens out, until at $\lambda = 5.45$ the maximum deflection no longer occurs at the center. Instead at large deflections there are two peaks symmetrically placed at about a half radius from the center. With a further increase in λ the peaks move outward until finally when $\lambda = 8.8$ a third peak appears in the center. This gradually becomes the predominant peak. These trends agree very well with the theoretical deflection curves for $\lambda = 4$, 7, and 10 shown in Fig. 8.

In Figs. 15 and 16 are plotted the pressure vs. center deflection curves of the specimens. For low values of λ , ($\lambda < 5$), the specimens buckled in a continuous manner. As more oil was pumped into the chamber the pressure increased more slowly, reached a maximum and then decreased. But for $\lambda > 5$, the process was discontinuous. Usually there would be a slight movement of the shell without the addition of oil followed by a sudden jump to a lower pressure and a greater displacement. There was no regular trend in the ratio of the pressure after buckling $(P_{cr})_2$ to the buckling pressure P_{cr} as λ increased and also surprisingly no significant difference in this ratio between the tests made using the Bourdon tube and those using the manometer.

Air Pressure Tests

For the air pressure tests an accumulator tank was connected to the air line close to the testing fixture so that the buckling process was practically a constant pressure process. Buckling occurred very suddenly and with a sharp report. The final buckled shapes were symmetrical with deflections very much larger than those of the oil tests. Deflection traverses were made during loading but it was inadvisable to make them at loads approaching the expected buckling load. Two examples of these deflection traverses are shown in Fig. 14d.

The specimens remained in their buckled position after the pressure was released. An approximate determination of the pressure required to unbuckle them was made by unbolting the clamping rings, inverting the rings with the specimens still placed between them and

then bolting the inverted assembly to the base plate. The pressures required to unbuckle the specimens were considerable and are included in Table 3.

Summary of Experimental Results

The physical parameters and buckling loads of all the specimens are shown in Table 5. In Fig. 17 are plotted the buckling loads as a function of λ . The oil pressure tests are shown with black dots, while the air tests are shown with open circles. For the oil tests the points at the lower ends of the dashed lines indicate the value to which the pressure jumped during the buckling process, while a wing on the left of a lower circle indicates an unsymmetrical buckling mode. When plotted on log-log paper the results tended to follow two intersecting lines. In Fig. 17 the corresponding power-law curves are shown.

In Fig. 18 the experimental buckling loads are compared with the theoretical loads calculated using two terms of the series for $\lambda < 5$, and the one point calculated using four terms for $\lambda = 4$. In Fig. 15 the corresponding load-center deflection curves are also compared. Although the experimental results are low compared with the theory, the difference (approximately 15 percent at $\lambda = 4$) is not great considering the variations of the initial shapes from a true spherical surface. Part of the difference can be attributed to yielding which occurred at the higher loads, especially for the specimens having values of λ near 5. It is felt that the results are close enough to corroborate the theory proposed and establish the applicability of the classical criterion for buckling for the low range of λ .

From Fig. 17 it is clear that the type of loading, air or oil has little if any effect on the buckling load. This is in direct contrast with the behavior predicted by Tsien's "energy criterion", for in that theory when the buckled and unbuckled energy levels are compared the loss in potential energy of the load during buckling must be included. Thus in the buckling process the strain energy can increase an amount equal to the loss in potential of the load. Since the loss in potential energy is a maximum when the pressure remains constant, the allowable increase in strain energy is greatest and therefore buckling in a constant pressure system should occur at a lower load than for any system in which the pressure decreases during buckling.

As this is not found to be the case, the energy criterion does not appear to hold for the shallow shells which were tested. In terms of the theory the intermediate energy "hump" is too high to be overcome.

IV. CONCLUSIONS

In this paper an attack upon the problem of the finite deflection of a shallow spherical shell has been made. The theoretical approach has been to transform the nonlinear equations into a sequence of linear equations by expanding all the unknown functions in powers of the nondimensional center deflection W_o and equating coefficients of equal powers of W_o. The initial equation can be solved exactly in terms of the ber and bei functions, but the succeeding equations have had to be solved either by power series or numerically. For small values of the parameter, λ, the resulting expansion for the pressure converges rapidly enough that a determination of the buckling load can be made using only four terms of the expansion. For higher values of λ the convergence deteriorates rapidly, so that for λ greater than 5, no determination of the buckling load can be made. However, for deflections smaller than the critical buckling deflection, the deflection modes can be determined for a much wider range of λ. These deflection modes change rapidly with λ and for values of λ near 7 have the surprising characteristic that the maximum deflection occurs approximately halfway between the center and the edge of the shell.

The results of the experimental program agreed substantially with those of the theoretical analysis. The buckling load near $\lambda = 4$ was only about 15 percent below the theoretical value while the trend of the buckling loads as λ increased was approximately the same as predicted by the theory. The deflection modes also showed the

same characteristics as predicted by the theory. The experimental buckling mode was inherently symmetrical as assumed in the theory; the few exceptions can be attributed to large initial asymmetries in the specimens.

Tests were made with both air and oil pressure, which approached the extremes of constant pressure and constant volume buckling characteristics, respectively. The buckling loads obtained by the two methods showed no significant difference. This is in conflict with predictions based on Tsien's "energy criteria" for buckling. Since the experimental results agree with classical criteria for the small values of λ , it is concluded that the "energy criteria" are not applicable to the buckling of shallow spherical shells subjected to lateral loading.

APPENDIX

Infinite Series Expansion

After substituting the expressions for f_n and ω_n, Eq. (33), into Eq. (28) for F_2, it becomes

$$F_2 = \frac{3}{8}\frac{\rho_1 K}{x}\left(A_1 bei'\lambda x - B_1 ber'\lambda x\right) - \frac{K^2\lambda^2}{16x^2}\left\{A_1B_1\left(b^2 ei'\lambda x - b^2 er'\lambda x\right)+\left(A_1^2-B_1^2\right)ber'\lambda x\, bei'\lambda x\right\} - \frac{K^2}{32x^2}\left(\frac{d^2}{dx^2}-\frac{1}{x}\frac{d}{dx}\right)\left(A_1 bei'\lambda x - B_1 ber'\lambda x\right)^2 \quad \text{(A-1)}$$

The particular integral of Eq. (26) corresponding to the first term of Eq. (A-1) is

$$\theta_2' = -\frac{3}{2}\frac{\rho_1 K}{\lambda^3}\left(A_1 bei'\lambda x - B_1 ber'\lambda x\right) \quad \text{(A-2)}$$

The particular integral for the remaining terms of F_2 (all quadratic in ber' and bei') is obtained by expanding in series. The series expansions for ber' λx and bei' λx are

$$ber'\lambda x = \sum_{n=1}^{\infty}(-)^n\frac{\left(\frac{1}{2}\lambda x\right)^{4n-1}}{(2n-1)!(2n)!} \quad \text{(A-3)}$$

$$bei'\lambda x = \sum_{n=0}^{\infty}(-)^n\frac{\left(\frac{1}{2}\lambda x\right)^{4n+1}}{(2n)!(2n+1)!}$$

In terms of the above series the expansion of the quadratic terms of F_2 becomes

$$F_2'' = -\frac{K^2\lambda^2}{64}\left[A_1B_1\left\{a_n + b_n + 2(n+1)(2n+1)\,c_{n+1}\right\}\left(\frac{\lambda x}{2}\right)^{4n} + \left\{\left(A_1^2 - B_1^2\right)c_n + n(2n+1)\left(A_1^2 a_n - B_1^2 b_n\right)\right\}\left(\frac{\lambda x}{2}\right)^{4n-2}\right] \tag{A-4}$$

where

$$a_n = (-)^n \sum_{m=0} \frac{1}{(2n-2m)!\,(2n-2m+1)!\,(2m)!\,(2m+1)!}$$

$$b_n = (-)^n \sum_{m=1} \frac{1}{(2n-2m+1)!\,(2n-2m+2)!\,(2m-1)!\,(2m)!} \tag{A-5}$$

$$c_n = (-)^n \sum_{m=1} \frac{1}{(2n-2m)!\,(2n-m+1)!\,(m-1)!\,m!}$$

The corresponding particular integral of Eq. (26) is

$$\theta_2'' = \frac{1}{4}K^2 \sum_{n=0}\left\{A_1B_1 d_n\left(\frac{\lambda x}{2}\right)^{4n} + \left(A_1^2 q_n + B_1^2 h_n\right)\left(\frac{\lambda x}{2}\right)^{4n-2}\right. \tag{A-6}$$

Where

$$d_n = \frac{1}{4n^2(4n^2-1)}\left\{2n(2n-1)\,c_n - a_{n-1} - b_{n-1} - d_{n-1}\right\} \quad n \geq 1$$

$$q_n = \frac{-1}{(2n-1)^2\left\{(2n-1)^2-1\right\}}\left\{(n-1)(2n-1)\,a_{n-1} + c_{n-1} + q_{n-1}\right\} \quad n \geq 2 \tag{A-7}$$

$$h_n = \frac{1}{(2n-1)^2\left\{(2n-1)^2-1\right\}}\left\{(n-1)(2n-1)\,b_{n-1} + c_{n-1} - h_{n-1}\right\} \quad n \geq 2$$

$$q_0 = h_0 = 0$$

The values of d_o, g_1 and h_1 are arbitrary with respect to the recursion formula of the differential equation, but when Eq. (A-6) is combined with Eq. (A-2) it is required that

$$d_o = \frac{1}{2} , \qquad h_1 = \frac{1}{2} \tag{A-8}$$

in order that $\theta_2 = \theta_2' + \theta_2''$ have the proper limiting value as $\lambda \rightarrow 0$.

The coefficient q_1 is completely arbitrary and for convenience was taken as equaling unity.

The infinite series expansion for φ_2 is

$$\varphi_2 = \sum_{n=0} \left\{ \frac{A_1^2 a_n - B_1^2 b_n}{4n+2} \left(\frac{\lambda x}{2}\right)^{4n+2} - A_1 B_1 \frac{c_n}{2n} \left(\frac{\lambda x}{2}\right)^{4n} \right\} \tag{A-9}$$

θ_2 and its derivatives, and φ_2 are substituted in Eqs. (35) to determine α_n and β which are in turn substituted into the boundary conditions Eqs. (34) to obtain A_2, B_2, and p_2.

REFERENCES

1. Timoshenko, S.: Theory of Plates and Shells. McGraw-Hill (1940).

2. Timoshenko, S.: Theory of Elastic Stability. McGraw-Hill (1936).

3. Reissner, E.: Stresses and Small Displacements of Shallow Spherical Shells, (I). J. Math. Phys. 25, 80-85 (1946). (II) J. Math. Phys. 25, 279-300 (1947).

4. von Karman, Th., and Tsien, H. S.: The Buckling of Spherical Shells by External Pressure. Jour. Aero. Sciences, 7, 2, 43-50 (1939).

5. Friedrichs, K. O.: On the Minimum Buckling Load for Spherical Shells. Applied Mechanics, Theodore von Karman Anniversary Volume (California Institute of Technology) (1941).

6. Tsien, H. S.: A Theory for the Buckling of Thin Shells. Jour. Aero. Sciences, 9, 10, 373-384 (1942).

7. Fung, Y. C., and Kaplan,A.: Buckling of Low Arches or Curved Beams of Small Curvature. NACA TN 2840 (1952).

8. Biezeno, C. B.: Uber die Bestimmung der "Durchschlagkraft" einer schwachgekrummten, Kreisformigen Platte. Zeit. f. angew. Math. u. Mech. 15, 10-22 (1935). This is reproduced in the book Technische Dynamik, by Biezeno and Grammel, Berlin, Julius Springer (1939).

9. Chien, W. Z.: Large Deflection of a Circular Clamped Plate Under Uniform Pressure. Chinese Journal of Physics, Vol. VII, No. 2 (Dec. 1947).

10. Milne, W. E.: Numerical Calculus, Princeton University Press, Chapter 1 (1949).

TABLE 1

Values of A_1, B_1, and p_1

λ	A_1	B_1	p_1
0.5	-4.875	155.9	5.333
0.7	-3.481	56.78	5.361
1.0	-2.434	19.39	5.441
1.5	-1.614	5.614	5.877
2.0	-1.194	2.200	7.061
3.0	-0.7298	0.4093	14.35
4.0	-0.4275	-0.06698	35.97
5.0	-0.1835	-0.2078	89.55
6.0	-0.005114	-0.1892	206.2
7.0	0.07882	-0.09905	426.1
8.0	0.07857	-0.01571	784.7
9.0	0.4214	-0.02332	1311
10.0	0.009895	0.02615	2043
11.0	-0.005344	0.01498	3031
12.0	-0.007743	0.004468	4343
13.0	-0.004895	-0.0009003	6048
14.0	-0.001736	-0.002132	8219
15.0	-0.00003355	-0.001506	10932

TABLE 2

Values of w_n for $\lambda = 4, 7, 10, 13$

	$\lambda = 4$				$\lambda = 7$				$\lambda = 10$		$\lambda = 13$
x	w_1	w_2	w_3	w_4	w_1	w_2	w_3	w_4	w_1	w_2	w_1
0.00	1.0000	0	0	0	1.000	0	0	0	1.000	0	1.0000
0.05	0.9965	-0.0021	-0.0018	- .0008	1.0011	0.0080	0.020	0.052	1.0002	-0.0014	0.9999
0.10	0.9859	-0.0082	-0.0072	- .0032	1.0044	0.032	0.079	0.206	1.0010	-0.0053	0.9995
0.15	0.9683	-0.0181	-0.016	- .0068	1.0093	0.070	0.173	0.453	1.0025	-0.0091	0.9988
0.20	0.9436	-0.0312	-0.027	-0.011	1.0152	0.121	0.300	0.782	1.0053	-0.011	0.9979
0.25	0.9116	-0.0470	-0.039	-0.015	1.0211	0.182	0.449	1.173	1.0099	-0.018	0.9970
0.30	0.8724	-0.065	-0.051	-0.019	1.0254	0.250	0.614	1.604	1.0168	0.017	0.9964
0.40	0.7725	-0.101	-0.073	-0.023	1.0214	0.386	0.938	2.435	1.0381	0.112	0.9993
0.50	0.6453	-0.130	-0.081	-0.019	0.9825	0.477	1.141	2.952	1.0625	0.300	1.0148
0.60	0.4958	-0.141	-0.074	-0.0092	0.8832	0.480	1.129	2.903	1.0608	0.517	1.0438
0.70	0.3338	-0.126	-0.053	0.0006	0.7016	0.366	0.863	2.187	0.9708	0.614	1.0437
0.75	0.2533	-0.110	-0.039	0.0034	0.5787	0.289	0.684	1.777	0.8672	0.581	0.9955
0.80	0.1769	-0.087	-0.025	0.0037	0.4391	0.191	0.473	1.242	0.7149	0.463	0.8851
0.85	0.1085	-0.059	-0.013	0.0031	0.2920	0.106	0.280	0.740	0.5169	0.306	0.6945
0.90	0.0525	-0.032	-0.0048	0.0018	0.1528	0.040	0.127	0.348	0.2938	0.139	0.4290
0.95	0.0143	-0.0087	-0.0011	0.0052	0.0448	0.0087	0.032	0.089	0.0931	0.034	0.2960
1.00	0	0	0	0	0	0	0	0	0	0	0

TABLE 3

Values of f_n for λ = 4, 7, 10, and 13

	λ = 4				λ = 7				λ = 10	λ = 13
x	f_1	f_2	f_3	f_4	f_1	f_2	f_3	f_4	f_1	f_1
0.00	-4.244	1.353	0.180	0.0788	-16.246	-2.038	-7.04	-17.56	-37.21	-65.43
0.05	-4.240	1.354	0.180	0.0781	-16.250	-2.069	-7.11	-17.77	-37.21	-65.43
0.10	-4.227	1.358	0.183	0.0760	-16.262	-2.159	-7.34	-18.38	-37.22	-65.42
0.15	-4.206	1.364	0.186	0.0724	-16.282	-2.305	-7.71	-19.38	-37.23	-65.41
0.20	-4.176	1.372	0.191	0.0675	-16.306	-2.504	-8.21	-20.72	-37.25	-65.40
0.25	-4.137	1.381	0.196	0.0612	-16.334	-2.749	-8.82	-22.36	-37.27	-65.39
0.30	-4.089	1.391	0.200	0.0538	-16.360	-3.030	-9.52	-24.23	-37.32	-65.37
0.40	-3.968	1.409	0.207	0.0361	-16.392	-3.670	- 11.08	-28.39	-37.45	-65.37
0.50	-3.811	1.418	0.207	0.0169	-16.353	-4.293	- 12.54	-32.25	-37.64	-65.44
0.60	-3.623	1.410	0.198	-0.0002	-16.178	-4.760	-13 .58	-34.92	-37.82	-65.67
0.70	-3.409	1.377	0.184	-0.0127	-15.795	-4.952	- 13.92	-35.80	-37.76	-65.95
0.75	-3.294	1.350	0.176	-0.0163	-15.507	-4.929	- 13.83	-35.57	-37.54	-65.96
0.80	-3.177	1.317	0.167	-0.0179	-15.153	-4.837	- 13.58	-34.94	-37.12	-65.73
0.85	-3.060	1.278	0.159	-0.0182	-14.737	-4.697	- 13.22	-34.02	-36.46	-65.09
0.90	-2.945	1.236	0.152	-0.0180	-14.271	-4.530	-12.79	-32.91	-35.56	-63.92
0.95	-2.837	1.193	0.146	-0.0175	-13.780	-4.360	- 12.33	-31.75	-37.46	-62.18
1.00	-2.737	1.153	0.141	-0.0170	-13.304	-4.206	- 11.90	-30.65	-33.30	-60.12

TABLE 4

Values of $p_n (n \geqslant 2)$ Calculated

λ	p_2		p_3	p_4
	Power Series	Numerical		
1.0	-1.120			
1.5	-2.726			
2.0	-4.919			
3.0	-12.39			
4.0	-26.47	-26.5	3.77	1.08
5.0	-45.2			
6.0	-38.1			
7.0	-53.7	56.6	314	801
8.0	219			
10.0		392		
13.0		537		

TABLE 5

Experimental Data

$\mu = 0.32$, $E = 6.5 \times 10^6$ psi

Hydraulic Pressure Tests

Spec	t inches	h inches	λ	q_{cr} psi	P_{cr}	Method of pressure measurements*	$(P_{cr})_2$
1	0.101	0.251	4.04	36.2	12.3	B	--
2	0.099	0.253	4.08	32.5	11.8	B	--
3	0.101	0.256	4.16	35.8	12.1	B	--
4	0.100	0.365	4.80	60.5	21.0	B	--
5	0.101	0.376	4.94	72.5	24.8	B	--
6	0.053	0.240	5.45	15.9	61.3	M	25.3
7	0.053	0.251	5.57	12.1	54.3	M	25.3
8	0.052	0.297	6.08	15.2	71.3	B	48.3
9	0.055	0.380	6.75	31.0	122.4	B	60.0
10	0.051	0.410	7.22	27.5	147	B	85.1
11	0.051	0.422	7.40	25.2	136	B	60.9
12	0.031	0.303	8.04	4.2	165	B	106
13	0.032	0.361	8.59	6.02	201	M	124
14	0.031	0.353	8.69	6.52	185	M	137
15	0.033	0.394	8.82	7.33	213	M	111
16	0.033	0.410	8.98	8.96	255	M	179
17	0.029	0.444	10.1	7.5	354	B	201

Air Pressure Tests

Spec	t inches	h inches	λ	q_{cr} psi	P_{cr}	Pressure required to unbuckle specimen psi
18	0.101	0.382	4.98	73.5	24.9	16.5
19	0.101	0.426	5.26	99.5	33.8	35
20	0.055	0.265	5.62	16.85	65.2	
21	0.054	0.413	7.10	33.6	143	12.6
22	0.032	0.347	8.45	5.67	190	1.8
23	0.033	0.399	8.91	11.70	310	3.3

* B = Bourdon Gage, M = Manometer

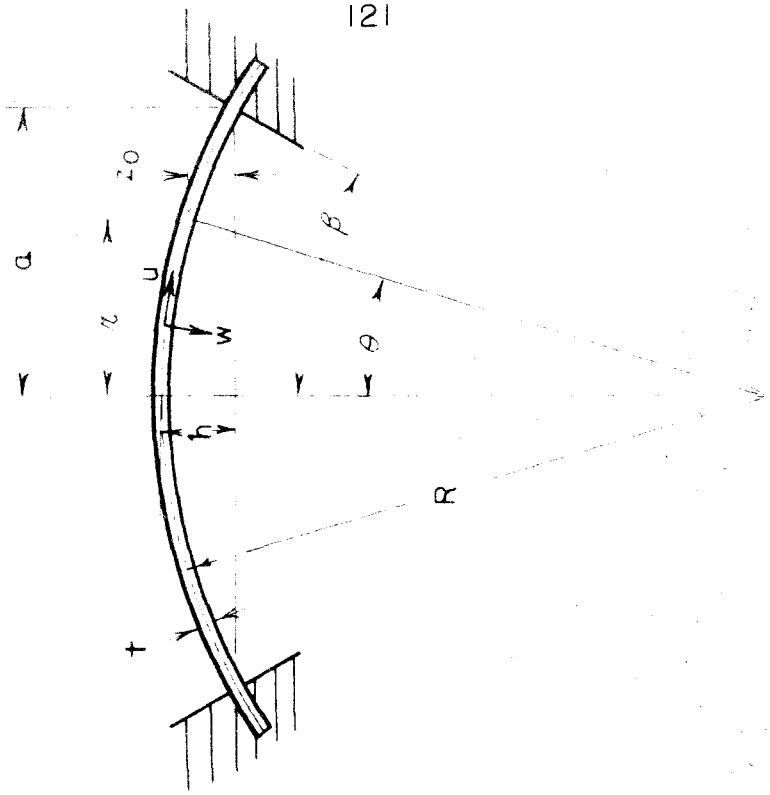

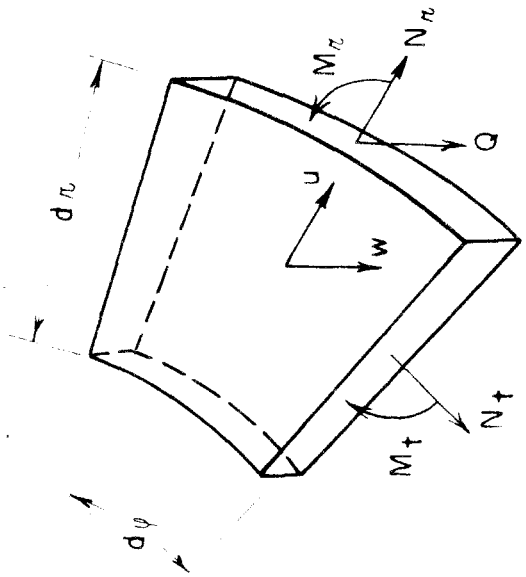

FIG. 1 — NOTATION

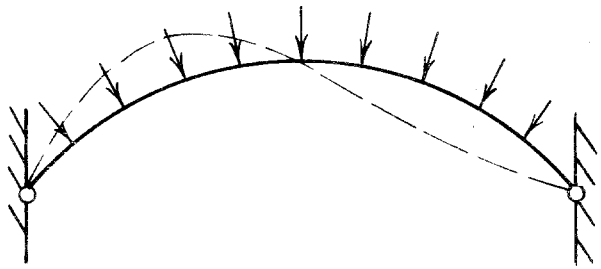

FIG. 2 – BUCKLING MODE FOR A HIGH ARCH

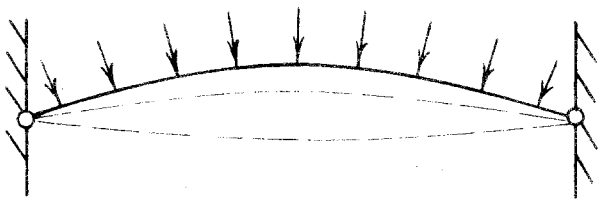

FIG. 3 – POSSIBLE BUCKLING MODE OF LOW ARCH

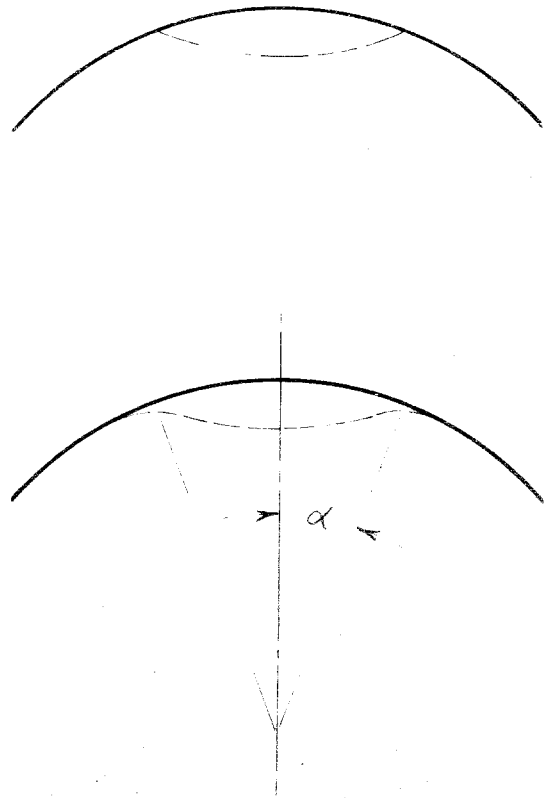

FIG. 4 – "APPLICABLE" AND APPROXIMATELY "APPLICABLE" SURFACES

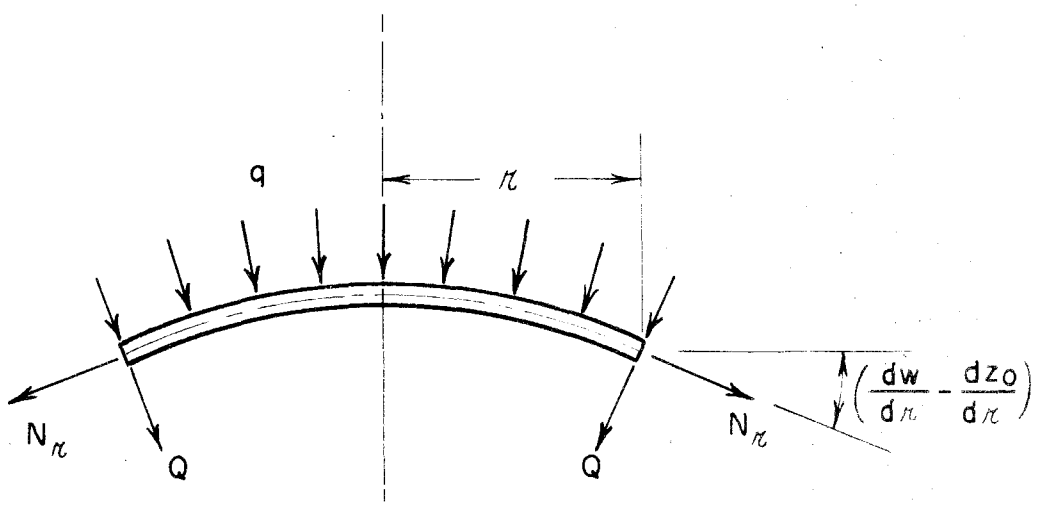

FIG. 5 – EQUILIBRIUM OF A CENTRAL CYLINDRICAL SECTION

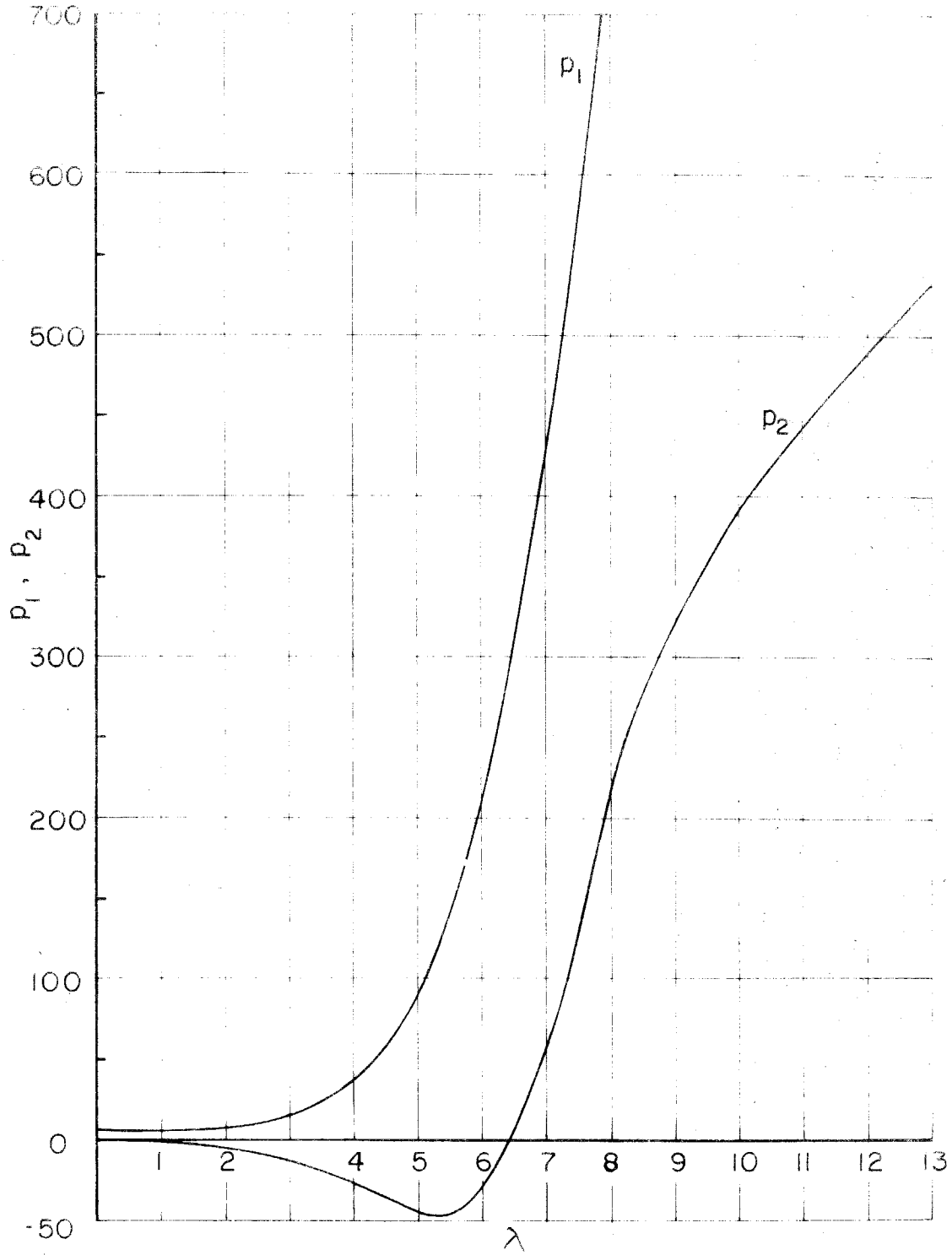

FIG. 6 – VARIATION OF p_1 AND p_2 WITH λ

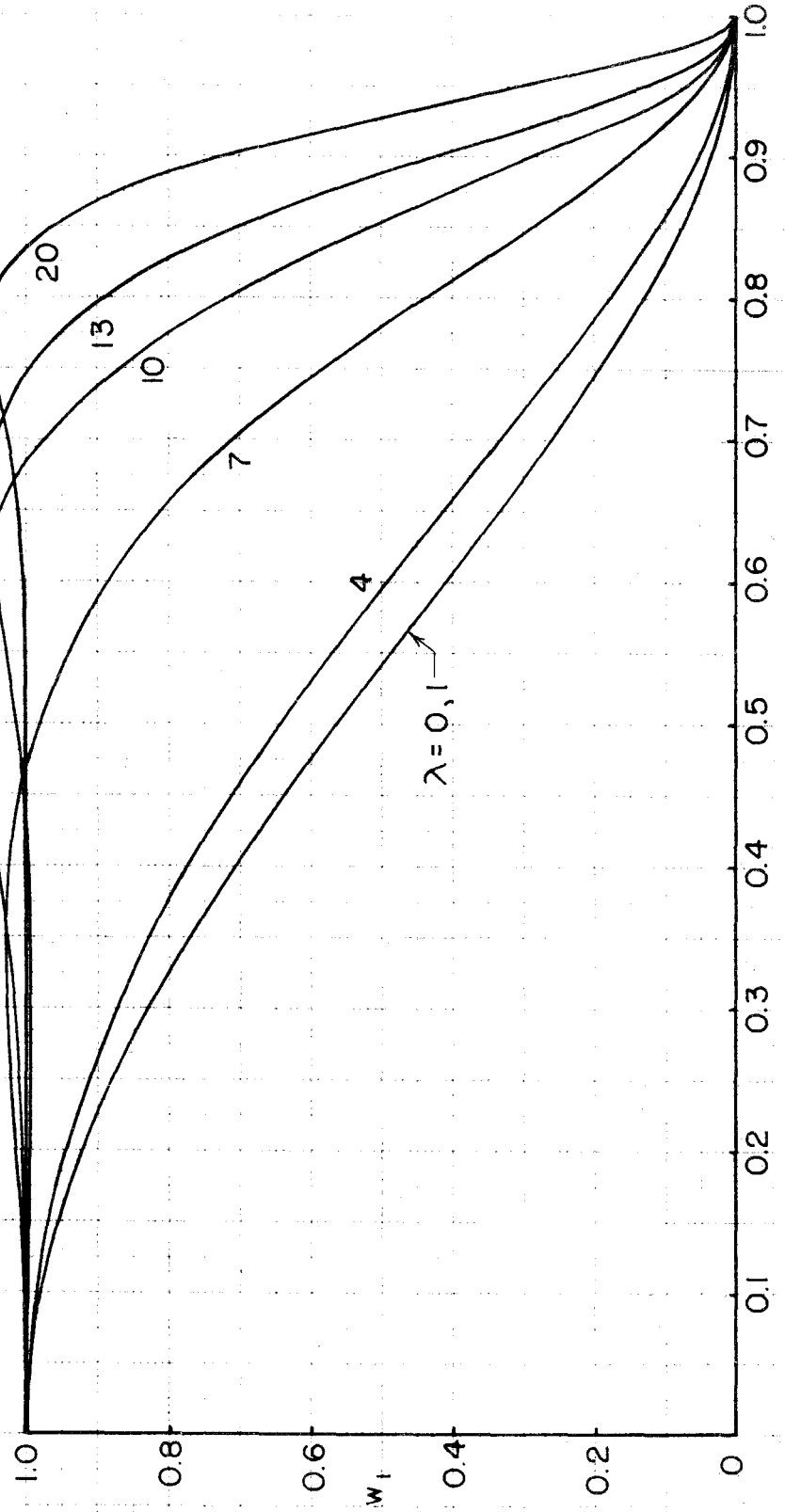

FIG. 7– VARIATION OF THE LINEAR DEFLECTION MODE, w_1, WITH λ

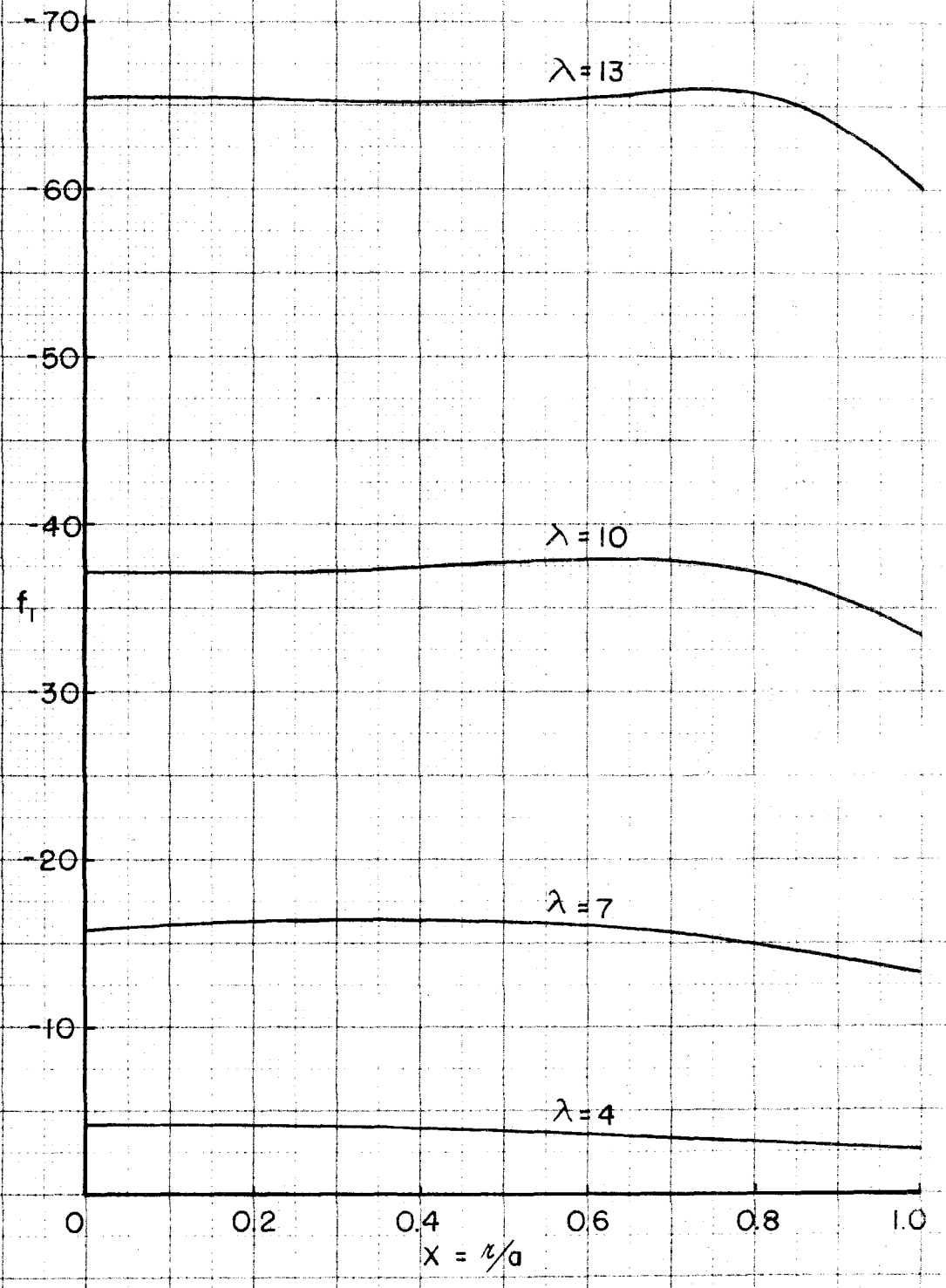

FIG. 8 – VARIATION OF THE LINEAR MEMBRANE STRESS, f_1, WITH λ

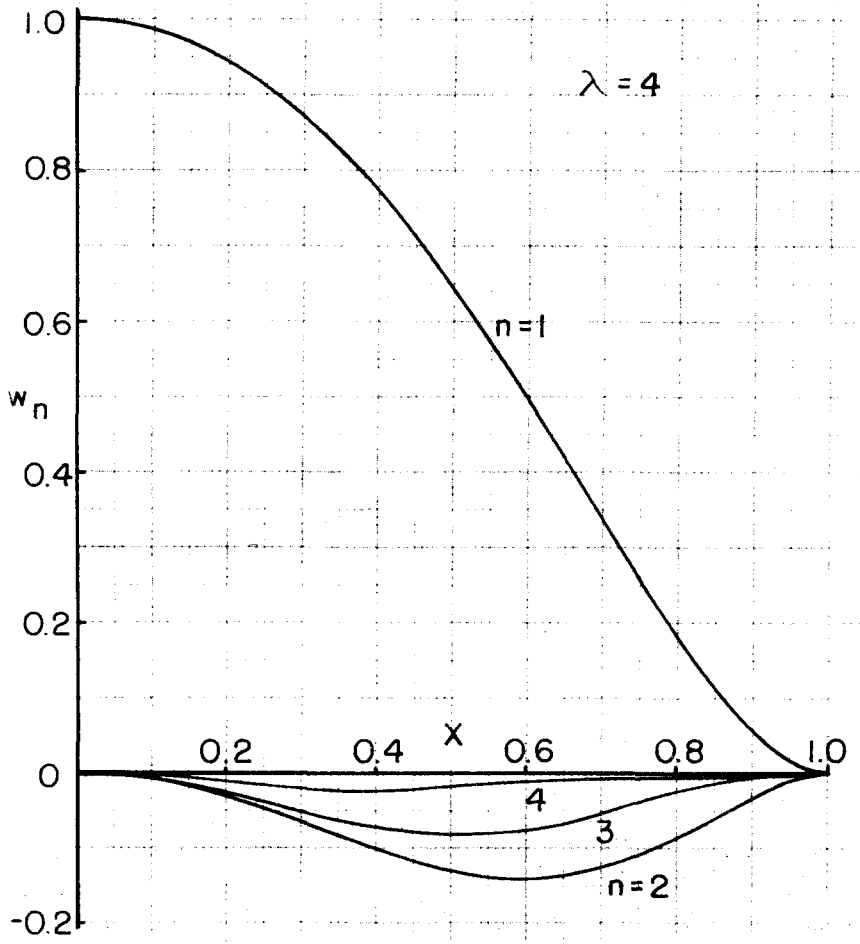

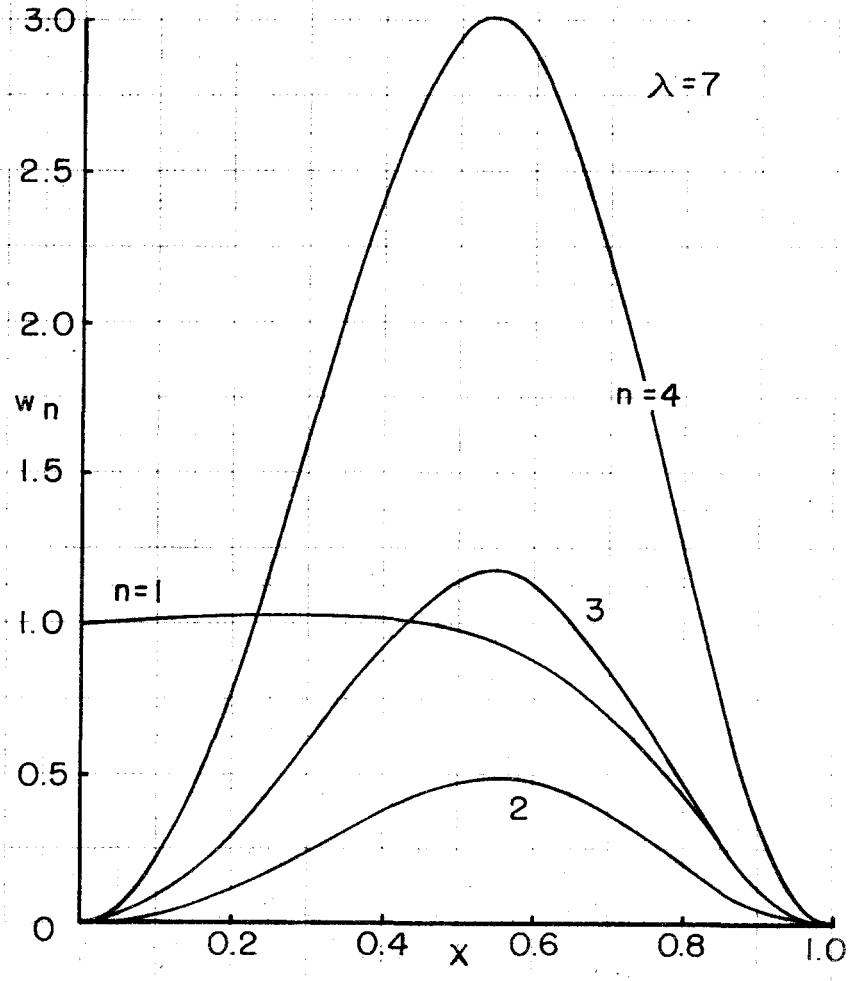

FIG. 9 – FIRST FOUR TERMS OF w_n FOR $\lambda = 4$ AND 7

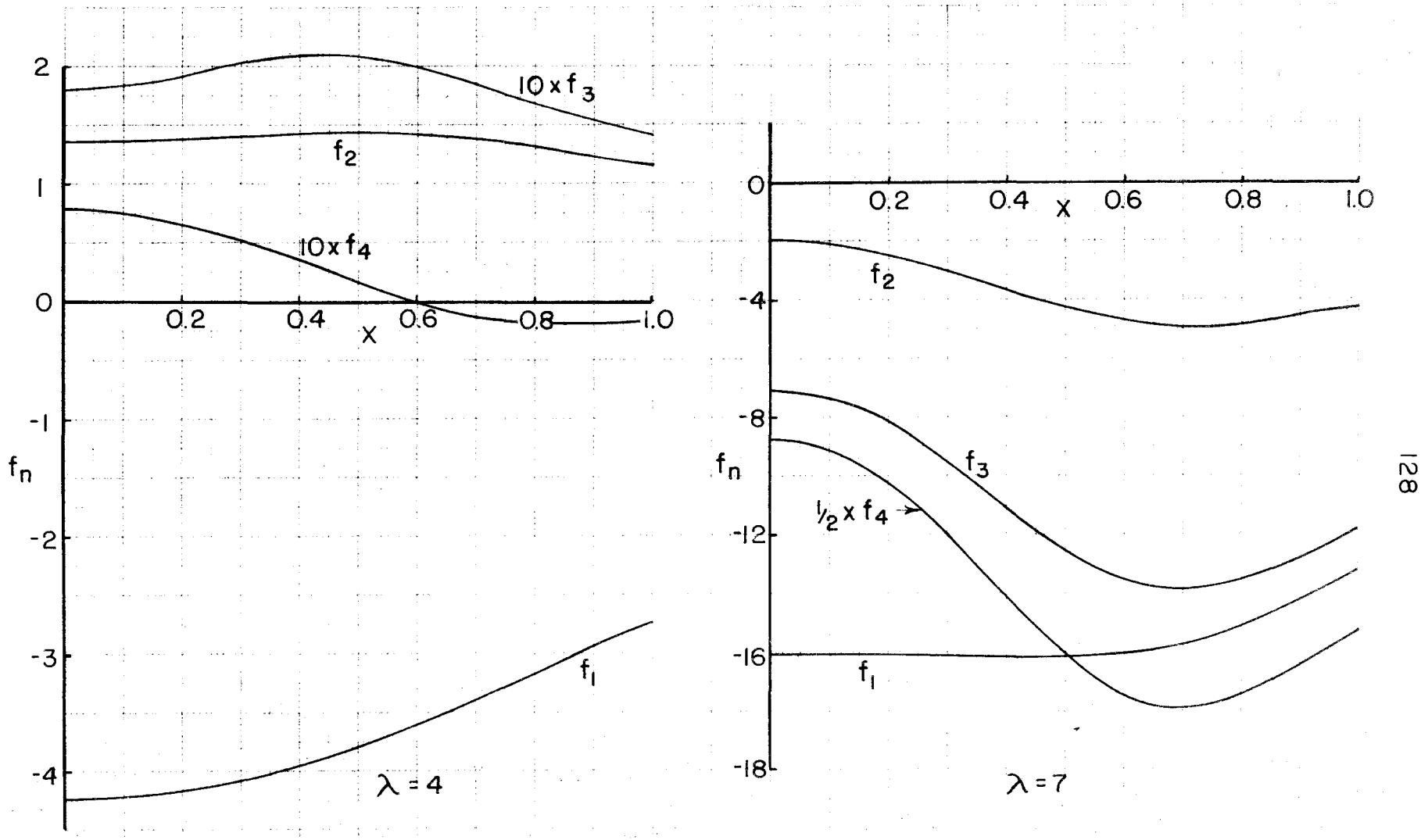

FIG. 10 – FIRST FOUR TERMS OF f_n FOR $\lambda = 4$ AND 7

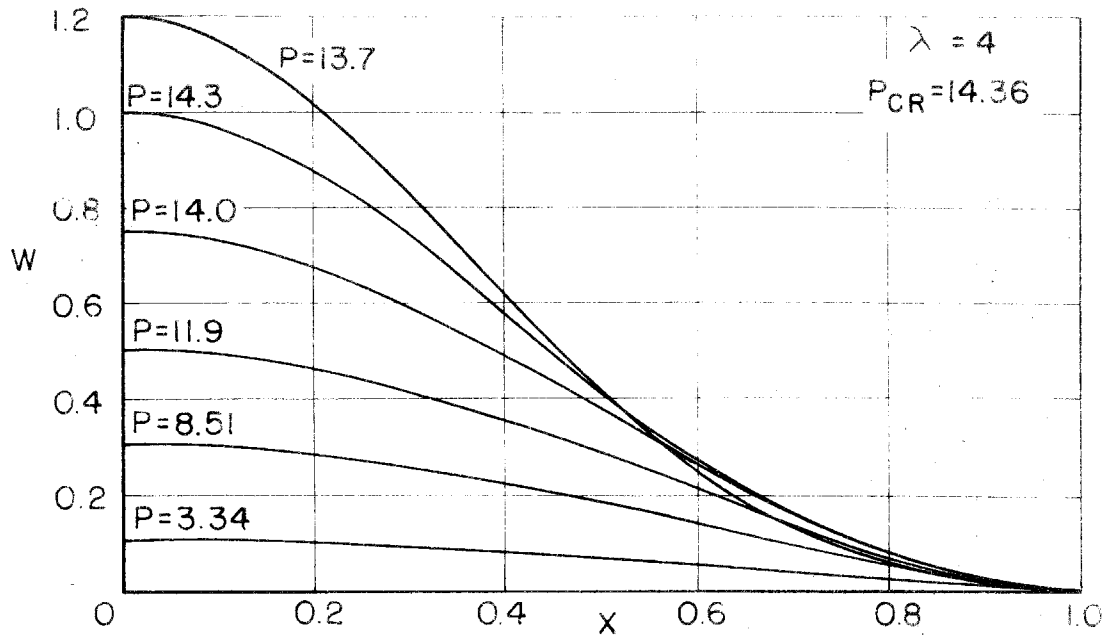

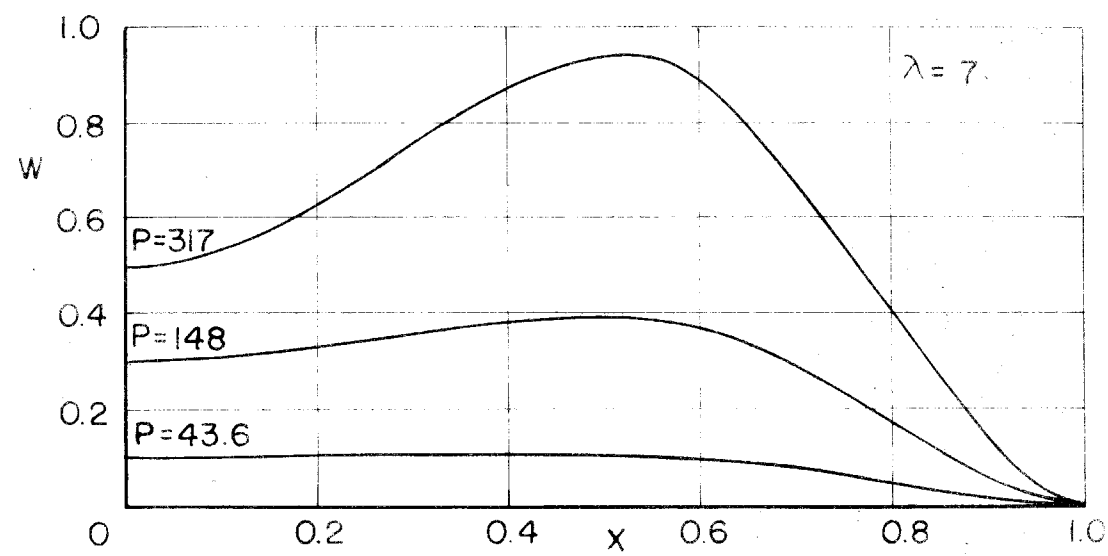

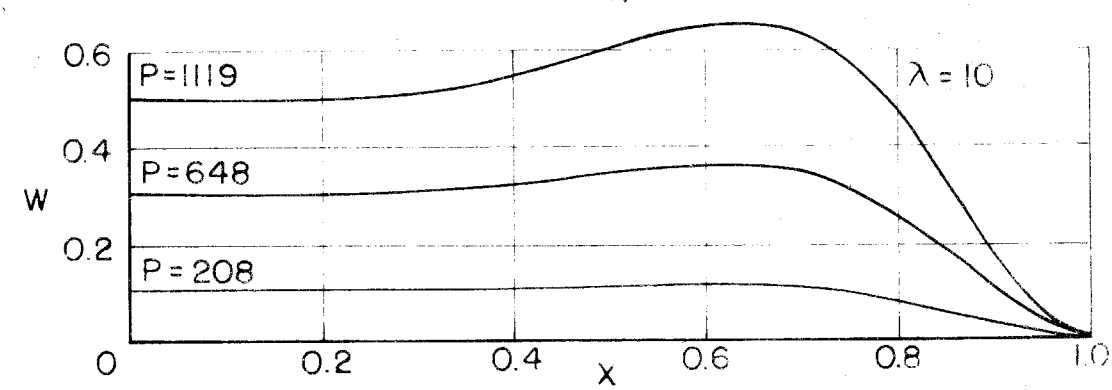

FOR $\lambda = 4, 7$, $W = \sum_{n=1}^{4} \omega_n W_o^n$ FOR $\lambda = 10$, $W = \sum_{n=1}^{2} \omega_n W_o^n$

FIG. 11 – DEFLECTION MODES FOR $\lambda = 4, 7,$ AND 10

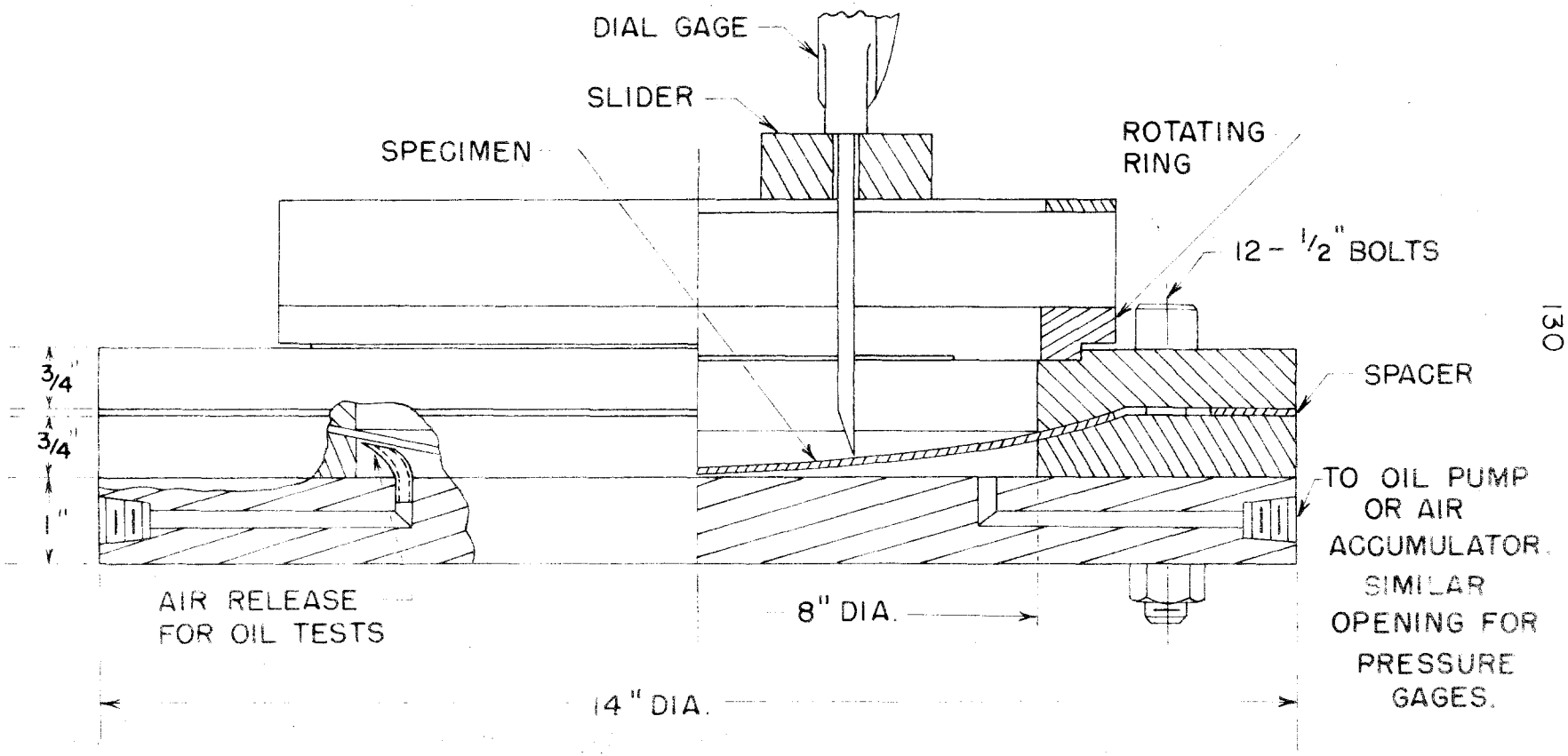

FIG. 12 - TESTING JIG

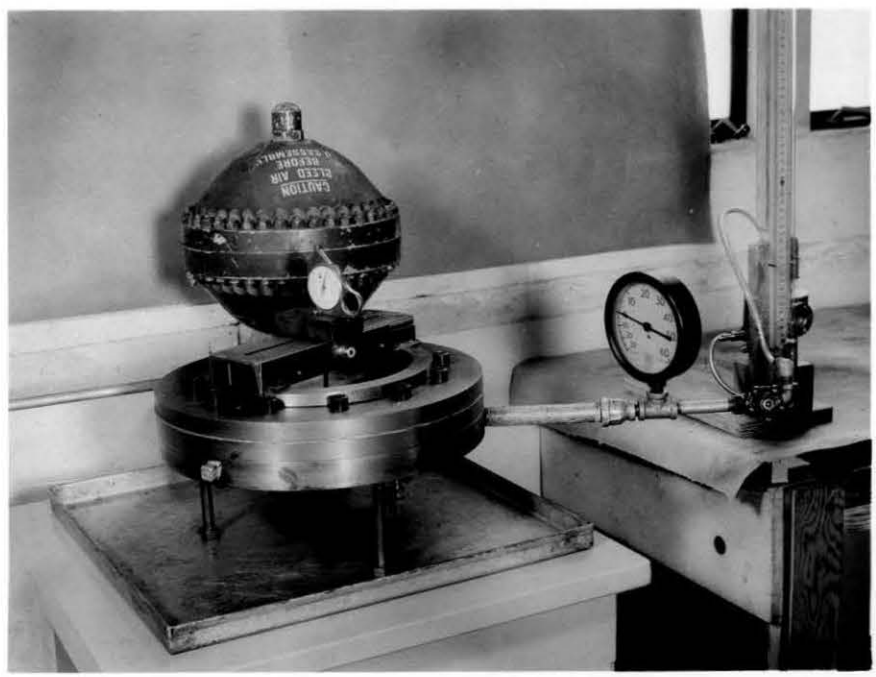

FIG. 13 - VIEW OF TESTING FIXTURE

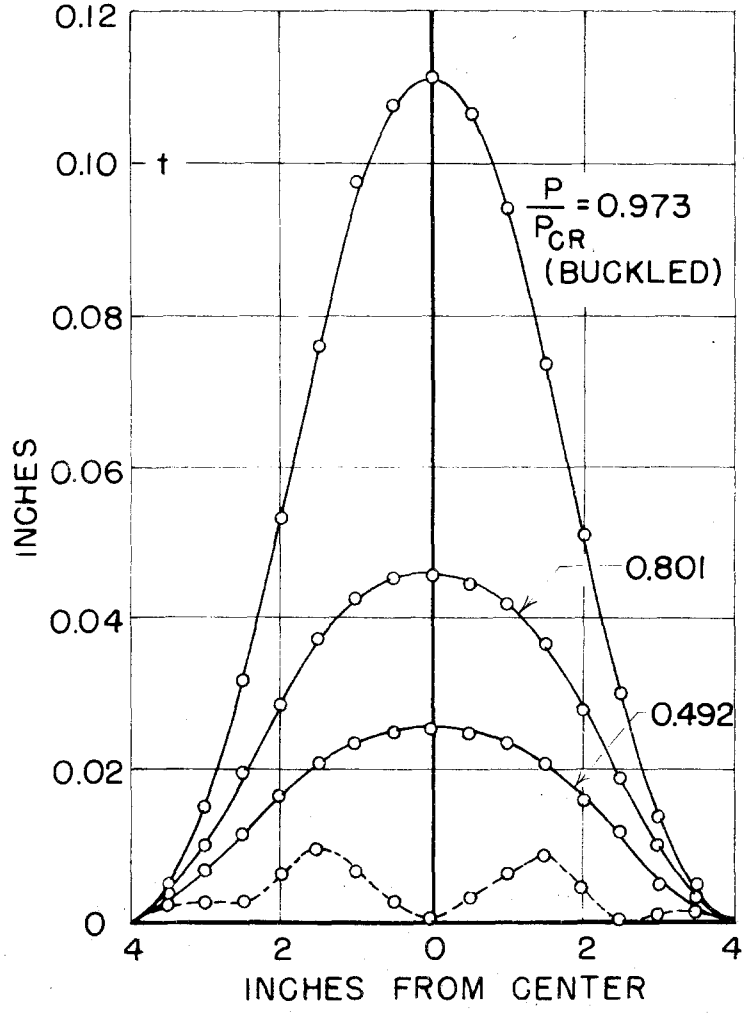

SPEC #1 $\lambda = 4.04$ $h = 0.251''$ $P_{CR} = 12.3$

DEFLECTION FROM INITIAL POSITION.

VARIATION OF INITIAL POSITION FROM A CIRCULAR ARC THRU CENTER.

OIL LOADING.

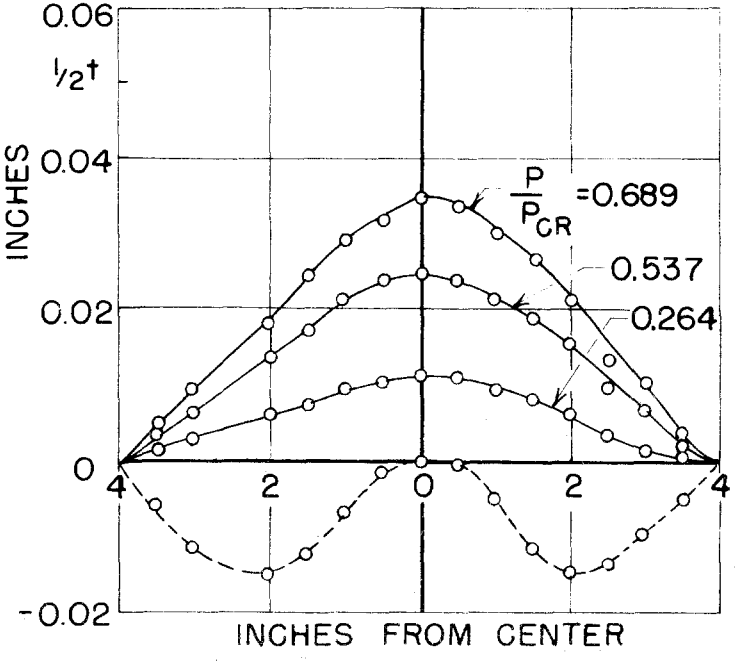

SPEC #5 $\lambda = 4.94$ $h = 0.376''$ $P_{CR} = 24.8$

FIG.14a-EXPERIMENTAL DEFLECTION SHAPES

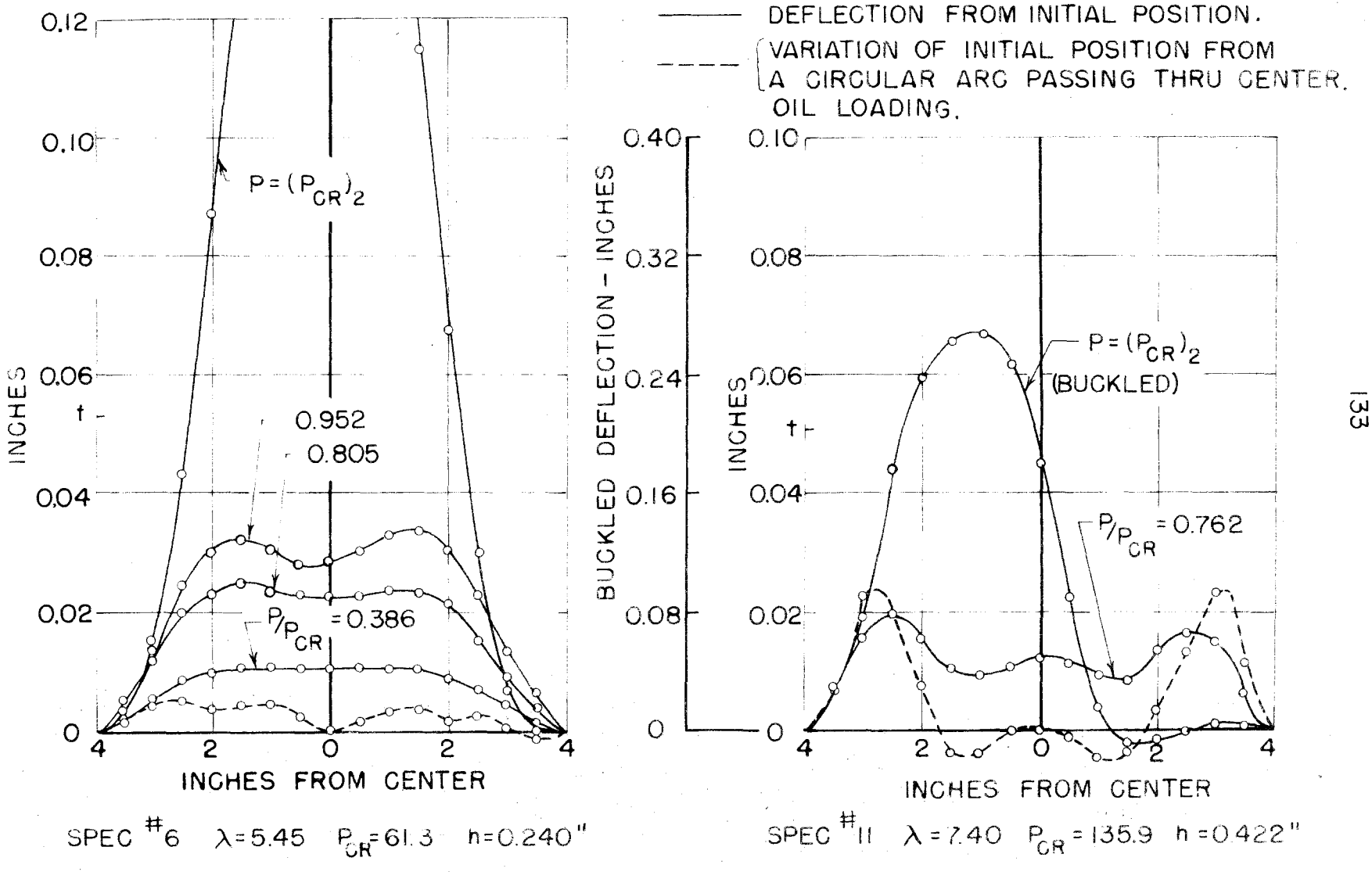

FIG. 14 b — EXPERIMENTAL DEFLECTION SHAPES

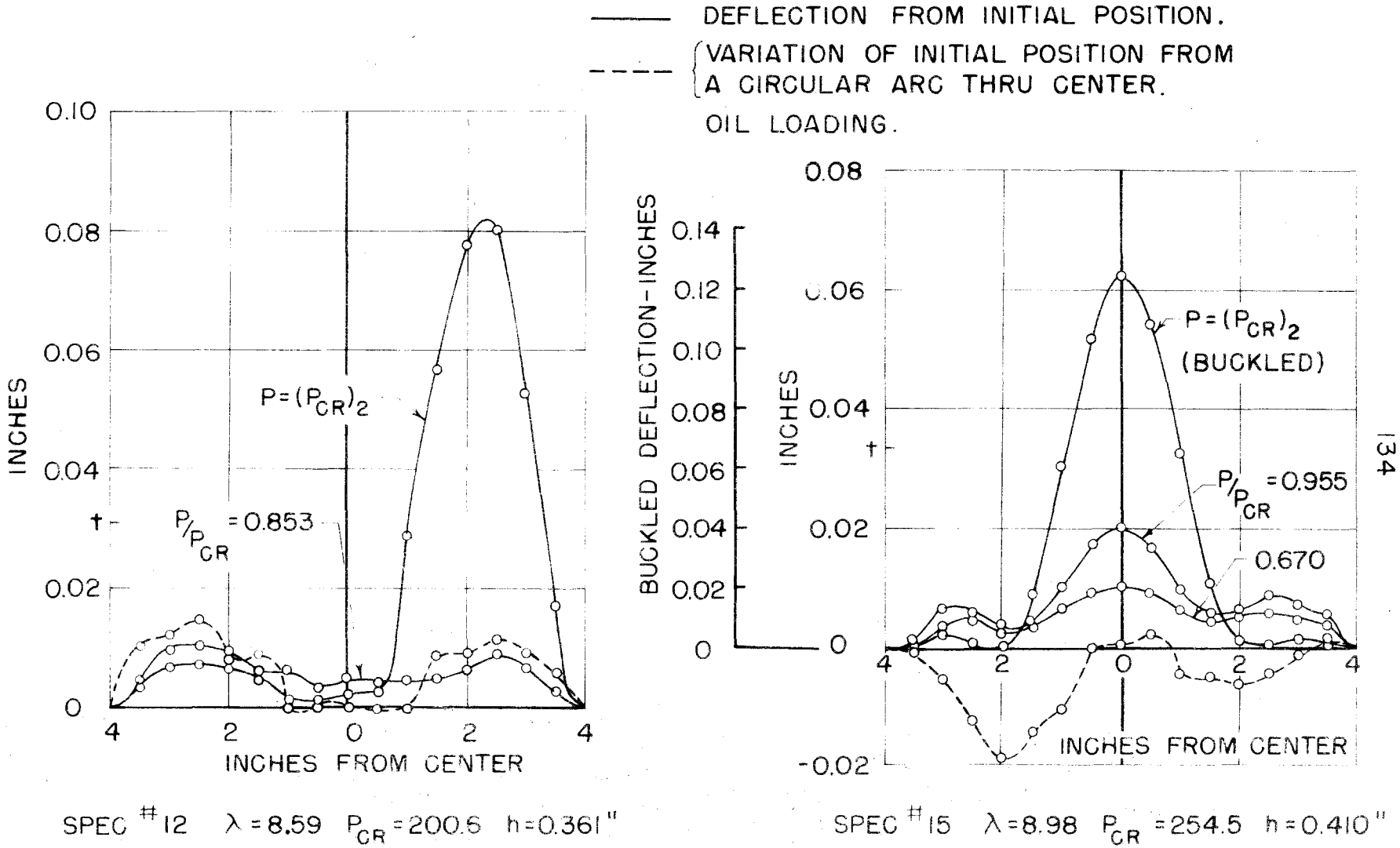

FIG.14c-EXPERIMENTAL DEFLECTION SHAPES

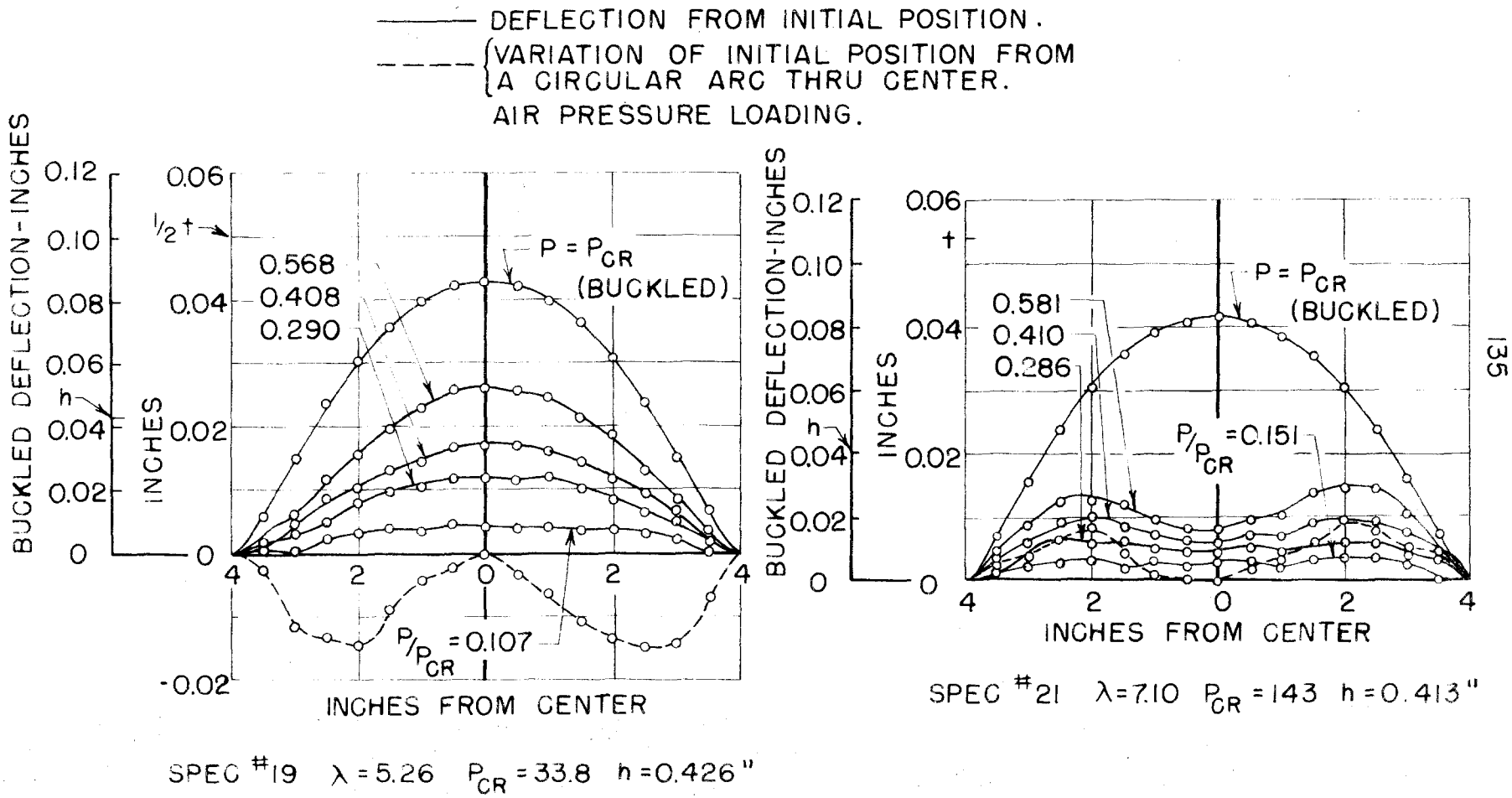

FIG. 14d-EXPERIMENTAL DEFLECTION SHAPES

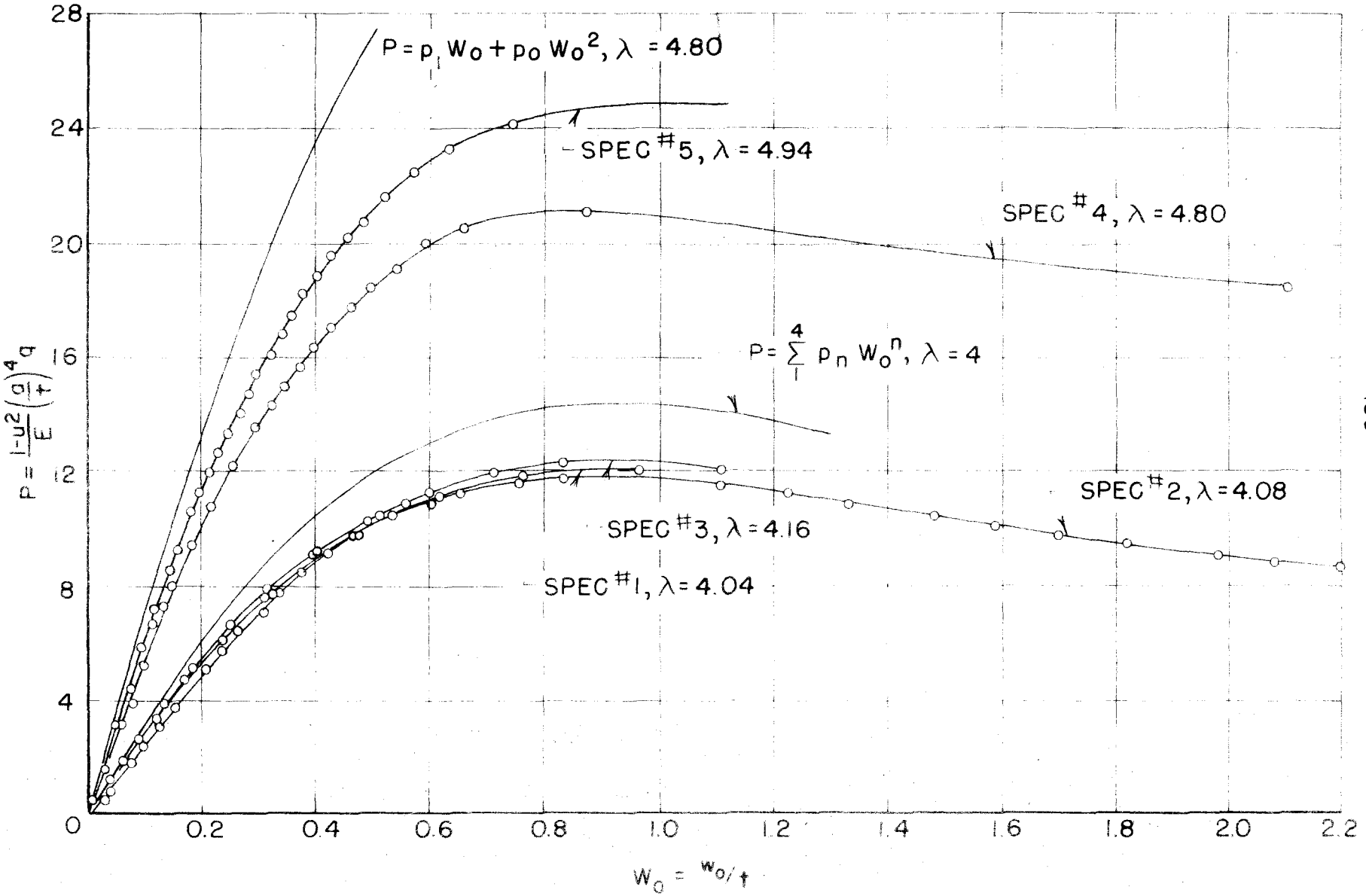

FIG. 15 - COMPARISON OF EXPERIMENTAL PRESSURE CENTER DEFLECTION CURVES WITH THEORETICAL RESULTS

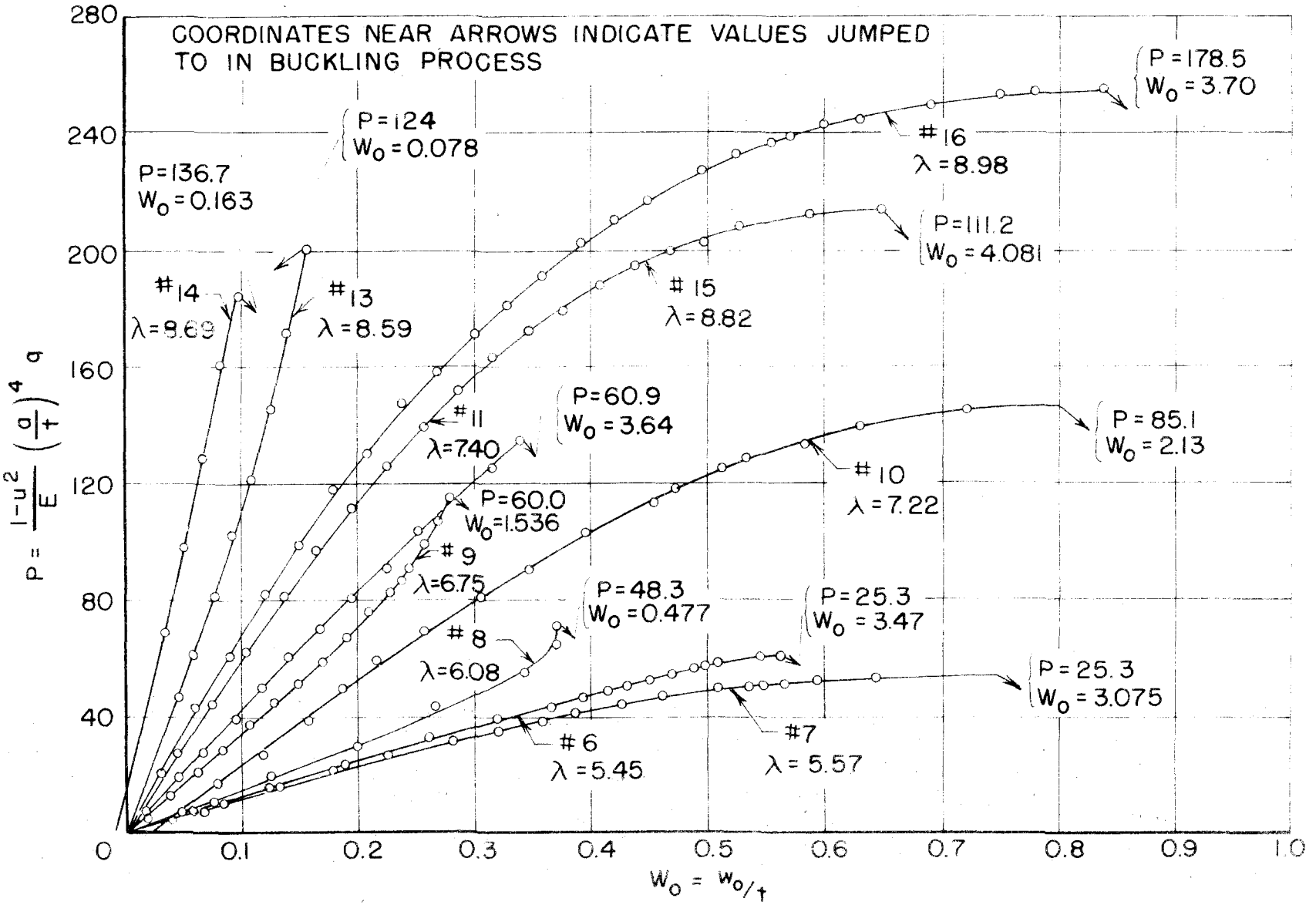

FIG. 16 - EXPERIMENTAL PRESSURE-CENTER DEFLECTION CURVES

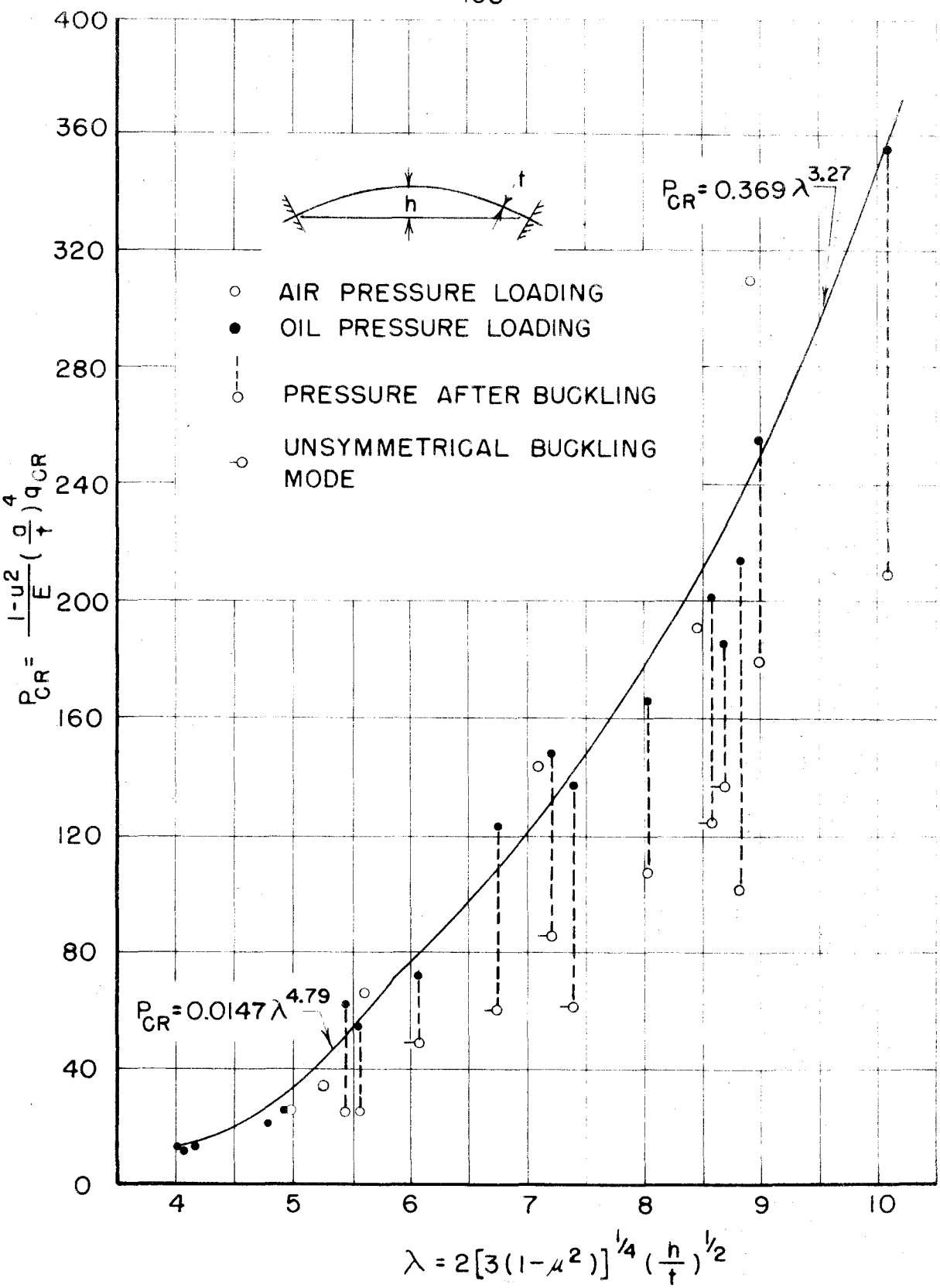

FIG. 17 – EXPERIMENTAL RESULTS

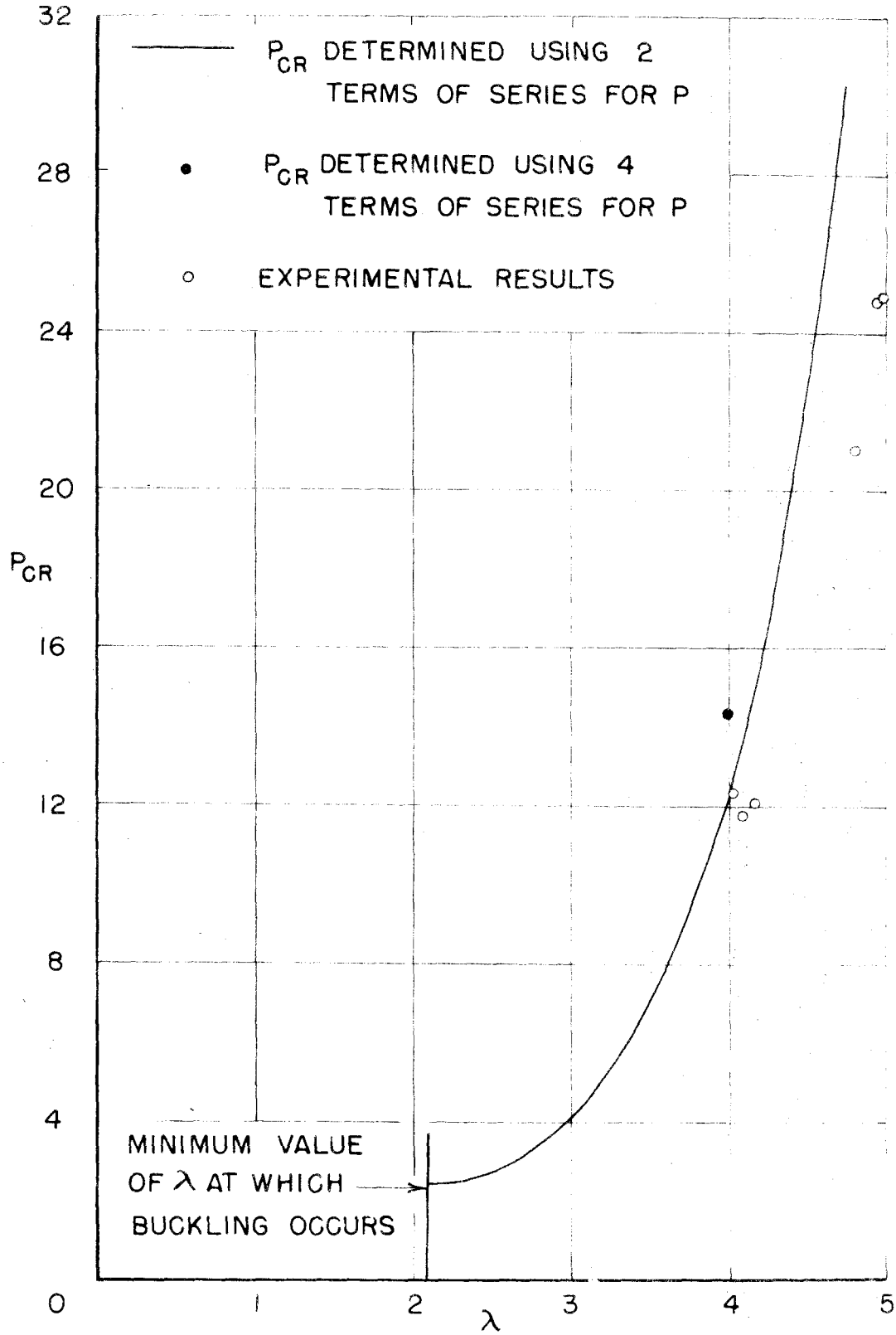

FIG. 18 – COMPARISON OF EXPERIMENTAL BUCKLING LOADS WITH THEORETICAL VALUES